Affine Arithmetic Based Methods for Power Systems Analysis Considering Intermittent Sources of Power

by

Juan Carlos Munoz Guerrero

A thesis
presented to the University of Waterloo
in fulfillment of the
thesis requirement for the degree of
Doctor of Philosophy
in
Electrical and Computer Engineering

Waterloo, Ontario, Canada, 2013

I hereby declare that I am the sole author of this thesis. This is a true copy of the thesis, including any required final revisions, as accepted by my examiners.

I understand that my thesis may be made electronically available to the public.

Abstract

Intermittent power sources such as wind and solar are increasingly penetrating electrical grids, mainly motivated by global warming concerns and government policies. These intermittent and non-dispatchable sources of power affect the operation and control of the power system because of the uncertainties associated with their output power. Depending on the penetration level of intermittent sources of power, the electric grid may experience considerable changes in power flows and synchronizing torques associated with system stability, because of the variability of the power injections, among several other factors. Thus, adequate and efficient techniques are required to properly analyze the system stability under such uncertainties.

A variety of methods are available in the literature to perform power flow, transient, and voltage stability analyses considering uncertainties associated with electrical parameters. Some of these methods are computationally inefficient and require assumptions regarding the probability density functions (pdfs) of the uncertain variables that may be unrealistic in some cases. Thus, this thesis proposes computationally efficient Affine Arithmetic (AA)-based approaches for voltage and transient stability assessment of power systems, considering uncertainties associated with power injections due to intermittent sources of power. In the proposed AA-based methods, the estimation of the output power of the intermittent sources and their associated uncertainty are modeled as intervals, without any need for assumptions regarding pdfs. This is a more desirable characteristic when dealing with intermittent sources of power, since the pdfs of the output power depends on the planning horizon and prediction method, among several other factors. The proposed AA-based approaches take into account the correlations among variables, thus avoiding error explosions attributed to other self-validated techniques such as Interval Arithmetic (IA).

The AA-based voltage stability method proposed in the thesis, computes the hull of PV curves associated with the assumed uncertainties, and is tested using two study cases, first, a 5-bus test system is used to illustrate the proposed technique in detail, and thereafter a 2383-bus test system to demonstrate its practical application. The results are compared with those obtained using conventional Monte Carlo Simulations (MCS) to verify the accuracy and computational burden of the proposed AA-based method, and also with respect to a previously proposed technique to estimate parameter sensitivities in voltage stability assessment. On the other hand, the proposed AA-based transient stability assessment method solves the set of Differential-Algebraic

Equations (DAEs) in affine form, using a trapezoidal integration approach which leads to the hull of the dynamic response of the system for large disturbances on the system. This approach is tested using a Single Machine Infinite Bus (SMIB) test system with simplified models, and a two-area test system with variable input powers from synchronous generators, and wind turbines based on Doubly Fed Induction Generators (DFIGs). In all study cases, MCS is used for comparison purposes.

The results obtained using the proposed AA-based methods for voltage and transient stability assessment depict a reasonably good accuracy at significantly lower computational costs when compared to those obtained using simulation based techniques. These AA-based methods can be used by system operators to efficiently estimate the system dynamic response and PV curves associated with the input-power uncertainties, and thus devise countermeasures in case of insecure operation.

Acknowledgments

First, I would like to dedicate my deepest appreciation and admiration to my supervisor Professor Claudio Cañizares for his continuous support, encouragement, trust, and guidance during the research and writing of this thesis. I would also like to acknowledge with much appreciation to my co-supervisor Professor Kankar Bhattacharya for all his support, advice, kindness and dedication. It has been a huge honor and enriching experience to conduct my research under their supervision.

I want to express my sincere gratitude to Professor Alfredo Vaccaro from the University of Sannio, for all his kind help and advice. I also want to acknowledge the following members of my comprehensive or examination committees for their valuable comments and input: Professor Srinivasan Keshav, from the Computer Science Department of the University of Waterloo, Professor Shesha Jayaram, and Professor Sheryas Sundaram, from the Electrical and Computer Engineering Department of the University of Waterloo. Also, thanks Professor Stephen Smith from the Electrical and Computer Engineering Department of the University of Waterloo, and Professor Venkataramana Ajjarapu from the Department of Electrical and Computer Engineering of the Iowa State University, for kindly agreeing to be part of the examination committee.

I would like to acknowledge the Natural Sciences and Engineering Research Council (NSERC) Canada, Hydro One, IBM Canada, ABB Corporate Research USA, and the Universidad de Los Andes in Venezuela for providing the funding necessary to carry out this research.

I want to gratefully and sincerely thank the following professors of the Engineering Faculty of the Universidad de Los Andes, for all their support and guidance during my studies: Ernesto Mora, Ricardo Stephen, Marisol Davila, Jose Contreras, Jaime Gonzalez, Pedro Mora, Jesus Velazco, Luz Moreno, Nelson Ballester, and Jean Carlos Hernandez. I also want to thank Mariela Monsalve, for her friendship and support.

I extend my gratitude to all my colleagues and friends in the Electricity Market Simulation and Optimization Laboratory (EMSOL), for their support and the pleasant work environment provided, special mention deserve Mauricio Restrepo, Daniel Olivares, Jose Daniel Lara, Behnam Tamimi and Nafeesa Mehboob for their friendship and willingness to help.

I also want to express my deeply gratitude to my lovely mother Eciodila and my wife Yeliana

for all the patience and love they offer to me, and the sacrifice they made to support me during my studies.

Special thanks and admiration go to my daughter Sharon Valentina for her love and enthusiasm that made me extremely happy in the ups and downs of this journey.

Finally, and most importantly, I would like to thank God who has guided me to make this thesis possible.

Dedication

This thesis is dedicated to the memory of my grandmother, Julia, and my grandfather, Ezio. Also this thesis is dedicated to my lovely family, my wife Yeliana, my mother Eciodila, my brother Jesus, and my sons Sharon Valentina and Juan Marcos.

Table of Contents

List of Tables

List of Figures

List of Abbreviations

AA	Affine Arithmetic
AESO	Alberta Electric System Operator
ARMA	Auto Regressive Moving Average
ATC	Available Transfer Capability
CBM	Capacity Benefit Margin
cdf	Cumulative Density Function
DAE	Differential-Algebraic Equations
DFIG	Doubly Fed Induction Generator
ETC	Existing Transmission Commitments
IA	Interval Arithmetic
MCR	Maximum Capacity Rating
MCS	Monte Carlo Simulations
NERC	North America Reliability Corporation
ODE	Ordinary Differential Equation
pdf	Probability Density Function
PIS	Population-based Intelligent Search
SF	Sensitivity Formula
SMIB	Single Machine Infinite Bus
TRM	Transmission Reliability Margin
TTC	Total Transfer Capability
WECS	Wind Energy Conversion Systems

Nomenclature

Indices

D	Index for dynamic variables, parameters, and functions
h	Index for approximation noise symbols
IC	Index indicating initial conditions
i, j	Bus indices
k, s	Index associated with differential-algebraic equations
m	Index for buses with intermittent sources of power
max	Index indicating maximum values
min	Index indicating minimum values
n	Index associated with trapezoidal integration method
nc	Index for buses with voltage control settings
nl	Index for load buses
o	Index indicating central values and reference values
PF	Index for power flow variables, parameters, and functions
r	Index indicating iteration number

ra Index for affine form $\widehat{u_A}$

rb Index for affine form $\widehat{u_B}$

rh Index for Chebyshev approximations

sa Index for saddle node bifurcation

sl Index for noise symbols in power flow analysis

Parameters

A_r Rotor blades swept area (m^2)

B Susceptance matrix (p.u.)

Da Damping coefficient (N.m.s/rad.)

ΔP_A Variation of injected active power (p.u.)

ΔP_G Direction of generator dispatch (p.u.)

ΔP_{G_A} Variation of generated power (p.u.)

ΔP_L Direction of the active power variations of load (p.u.)

ΔQ_A Variation of injected reactive power (p.u.)

ΔQ_L Direction of reactive power variations of load (p.u.)

Δt Time step (s)

ΔV_A Variation of voltage settings (p.u.)

ΔV_p Step size used in the parametrization technique (p.u.)

ε_A Noise symbols introduced by the approximation of non-affine operations

G Conductance matrix (p.u.)

H Synchronous generator inertia constant (p.u.-s)

H_m DFIG Rotor inertia (kWs/kVA)

K_a Excitation system controller gain

K_G Power share in the distributed slack bus approach

K_p Pitch angle controller gain

K_v DFIG Voltage controller gain

m_A Number of shared noise symbols of two affine forms

N Number of buses

na Number of noise symbols for the affine form $\widehat{u_A}$

nb Number of noise symbols for the affine form $\widehat{u_B}$

N_{DA} Number of differential-algebraic equations

N_{IG} Set of buses with intermittent sources of power

n_p Number of polynomials of the Chebyshev approximations

N_P Set of buses where the injected active power is specified (PV and PQ buses)

N_{PV} Set of buses with voltage control settings

N_{P_L} Set of buses considering active power load uncertainties

N_Q Set of PV buses where the injected reactive power is specified (PQ buses)

N_{Q_L} Set of buses considering reactive power load uncertainties

nu Number of noise symbols for the affine form $\widehat{u}$

ω_r DFIG Reference rotor speed (p.u.)

ω_s Synchronous speed (p.u.)

p_D Controllable parameters such as AVR set points (p.u.)

$\widehat{p}_D$ Affine form of p_D (p.u.)

p_{PF} Specified active and reactive powers, as well as terminal generator voltage set points (p.u.)

$\widehat{p}_{PF}$ Affine forms of p_{PF} (p.u.)

P_{X_f} Probability density function of the variable X_f

r_r Rotor resistance (p.u.)

r_s Stator reactance (p.u.)

t_c Fault clearing time (s)

t'_{do} Open-circuit transient time constant in direct axis (s)

t''_{do} Open-circuit sub-transient time constant in direct axis (s)

T_{ec} Time constant of static excitation controls (s)

t_f Final simulation time for time domain simulations (s)

t_{fault} Instant of fault (s)

T_p Pitch control time constant (s)

t'_{qo} Open-circuit transient time constant in quadrature axis (s)

t''_{qo} Open-circuit sub-transient time constant in quadrature axis (s)

T_r Power control time constant (s)

V_p Magnitude of the voltage used as a parameter (p.u.)

V_2 Magnitude of the infinite-bus voltage (p.u.)

V_{ref} Reference Voltage(p.u.)

X_d Direct axis reactance of synchronous generators (p.u.)

X'_d Direc axis transient reactance of synchronous generators (p.u.)

X''_d Direct axis sub-transient reactance of synchronous generators (p.u.)

X_q Quadrature axis reactance of synchronous generators (p.u.).

X'_q Quadrature axis transient reactance of synchronous generators (p.u.)

X''_q Quadrature axis sub-transient reactance of synchronous generators (p.u.)

x_m Magnetizing reactance (p.u.)

x_r Rotor reactance (p.u.)

x_s Stator reactance (p.u.)

X_T Transformer reactance (p.u.)

X_{12} Transmission line reactance (p.u.)

$\widehat{Y}$ Admittance matrix in affine form (p.u.)

$\bar{Y}$ Admittance matrix in phasorial form (p.u.)

Variables

A Matrix of coefficients for affine forms used in AA-based power flow analysis (p.u.)

A_L Matrix of coefficients for affine forms used to account for generator's limits (p.u.)

A_{vs} Matrix of coefficients for affine forms used in AA-based voltage stability assessment (p.u.)

α, β Coefficients of the Chebyshev approximations

b_{rh} Floating-point series coefficients of Chebyshev polynomials

C Auxiliary vector for linear programming formulation used in AA-based power flow analysis (p.u.)

C_L Auxiliary vector for linear programming formulation used to account for generator's limits (p.u.)

c_p Performance coefficient

C_{vs} Auxiliary vector for the linear programming formulation used in AA-based voltage stability assessment (p.u.)

$\widehat{\delta}$ Generator rotor angular position in affine form (electrical rad.)

$\Delta\widehat{F_A}$ Errors of the differential-algebraic equations in affine form

ΔF_H Equivalent approximation errors of non-affine operations for ΔF_A

$\Delta\lambda$ Variation of bifurcation parameter (p.u.)

$D_\lambda f_{PF}$ Jacobian of f_{PF} with respect to the bifurcation parameter (p.u.)

ΔP Mismatch of active power (p.u.)

ΔP_p Mismatch of active power in polar form (p.u.)

ΔP_r Mismatch of active power in rectangular form (p.u.)

ΔQ Mismatch of reactive power (p.u.)

ΔQ_p Mismatch of reactive power in polar form (p.u.)

ΔQ_r Mismatch of reactive power in rectangular form (p.u.)

$\Delta\theta$ Variation of bus voltage angle (p.u.)

ΔV Variation of bus voltage magnitude (p.u.)

$\Delta_{x_{PF}}$ Corrections of power flow variables (p.u.)

$D_{x_{PF}} f_{PF}$ Jacobian of f_{PF} with respect to power flow variables (p.u.)

$\Delta\widehat{x_D}$ Corrections of state variables in affine form (p.u.)

$\Delta\widehat{y}$ Corrections of algebraic variables in affine form (p.u.)

$\Delta\widehat{z}$ Corrections of the state and algebraic variables in affine form (p.u.)

Δz_H Equivalent approximation errors introduced by non-affine operations of state and algebraic variables (p.u.)

$\widehat{E}'_{d,q}$ Synchronous generator sub-transient internal voltages associated with damping windings in affine form (p.u.)

$\widehat{E}_{d,q}$ Synchronous generator transient internal voltages associated with field and rotor-core induced windings in affine form (p.u.)

$\widehat{E}_f$ Voltage associated with field and rotor-core induced currents in affine form (p.u.)

e Error measured with respect to MC simulations (%)

$\widehat{E}$ Generator voltage behind the generator transient reactance in affine form (p.u.)

ε Noise symbols associated with AA-based power flow analysis

ε^A Vector of noise symbols associated with approximation errors

ε_A Noise symbols associated with affine form $\widehat{u_A}$

ε_B Noise symbols associated with affine form $\widehat{u_B}$

εf Individual noise symbols associated with approximation errors of non-affine operations of $\Delta\widehat{F_A}$

εf_H Equivalent noise symbols associated with approximation errors of non-affine operations of $\Delta\widehat{F_A}$

ε_H Equivalent noise symbols associated with approximation errors of non-affine operations of $\Delta\widehat{z}$

ε_{IG} Noise symbols associated with intermittent sources of power

εj Individual noise symbols associated with approximation errors of non-affine operations of $\widehat{J}$

ε_L Vector of noise symbols to account for generators' limits associated with AA-based power flow analysis

ε_P Noise symbols associated with active power injections

ε_{P_L} Noise symbols associated with load active power

$\varepsilon_{PVa,b}$ Noise symbols associated with voltage control settings

ε_Q Noise symbols associated with reactive power injections

ε_{Q_L} Noise symbols associated with load reactive power

ε_u Noise symbols associated with affine form $\widehat{u}$

ε_{VS} Vector of noise symbols associated with AA-based voltage stability assessment

ε_ξ Independent noise symbol of the multiplication affine approximation

Fa Individual approximation error of non-affine operations for $\Delta\widehat{F}$

Hc Chebyshev polynomial approximation of sinusoidal functions

$\widehat{I}$ Synchronous generator current injections in affine form (p.u.)

$\overline{I}$ Synchronous generator current injections in phasorial form (p.u.)

$\widehat{I_d}$ Synchronous generator direct axis current in affine form (p.u.)

$\widehat{I_q}$ Synchronous generator quadrature axis current in affine form (p.u.)

i_{dr} DFIG rotor current in direct axis (p.u.)

$\widehat{i_{dr}}$ DFIG affine form of rotor current in direct axis (p.u.)

i_{qr} DFIG rotor current in quadrature axis (p.u.)

$\widehat{i_{qr}}$	DFIG affine form of rotor current in quadrature axis (p.u.)
i_{ds}	DFIG stator current in direct axis (p.u.)
$\widehat{i_{ds}}$	DFIG affine form of stator current in direct axis (p.u.)
i_{qs}	DFIG stator current in quadrature axis (p.u.)
$\widehat{i_{qs}}$	DFIG affine form of stator current in quadrature axis (p.u.)
$\widehat{Jc}$	Jacobian matrix in affine form
J_{aug}	Augmented Jacobian matrix
$\widehat{K}_{A,B}$	Centered affine forms
L	Vector of active and reactive power injections for AA-based power flow analysis (p.u.)
L_L	Vector of active and reactive power injections used to account generator's limit (p.u.)
L_{vs}	Vector of active and reactive power injections for AA-based voltage stability assessment (p.u.)
λ	Bifurcation parameter (p.u.)
$\widehat{\lambda}$	Bifurcation parameter in affine form (p.u.)
λ_p	tip speed ratio
μ	Maximum absolute error for univariate Chebyshev approximations
N_h	Set of noise symbols introduced by approximations of non-affine operations
ω_m	DFIG rotor speed (p.u.)
$\widehat{\omega}$	Synchronous generator rotor speed (p.u.)
$\widehat{\omega_m}$	DFIG rotor speed in affine form (p.u.)
$\widehat{\Psi}_{Ch}$	Chebyshev approximation for quadratic terms

P Injected active power generated (p.u.)

$\widehat{P}$ Injected active power generated in affine form(p.u.)

P^A Computed partial deviation of injected active power related to approximation errors (p.u.)

$\widehat{P_e}$ Generator electrical output power in affine form (p.u.)

P_G Active power generated (p.u.)

$\widehat{P_G}$ Active power generated in affine form (p.u.)

$P^{N_{IG}}$ Computed partial deviation of active power injections related to intermittent sources of power (p.u.)

$P^{N_{P_L}}$ Computed partial deviation of active power injections related to active power loads (p.u.)

$P^{N_{Q_L}}$ Computed partial deviation of active power injections related to reactive power loads (p.u.)

P_ω^{opt} Optimal active power extracted from the wind (p.u.)

P_L Active power loads (p.u.)

$\widehat{P_m}$ Generator mechanical input power in affine form (p.u.)

$P^{N_{PV}}$ Computed partial deviation of active power injections related to PV buses (p.u.)

Q Injected reactive power (p.u.)

$\widehat{Q}$ Injected reactive power in affine form (p.u.)

Q^A Computed partial deviation of reactive power injections related to approximation errors (p.u.)

Q_G Reactive power generated (p.u.)

Q_L Reactive power load (p.u.)

$Q^{N_{PV}}$ Computed partial deviation of reactive power injections related to PV buses (p.u.)

$Q^{N_{P_L}}$ Computed partial deviation of reactive power injections related to active power loads (p.u.)

$Q^{N_{Q_L}}$ Computed partial deviation of reactive power injections related to reactive power loads (p.u.)

q Matrix of errors introduced by approximations of non-affine operations in power flow AA-based analysis

qe Lumped approximation error associated with the affine forms of generator reactive power (p.u.)

qp Components of generator reactive power associated with uncertain active power injections (p.u.)

qq Components of generator reactive power associated with uncertain reactive power injections (p.u.)

q_L Matrix of errors introduced by approximations of non-affine operations to account for generator's limits (p.u.)

Q_L Reactive power loads (p.u.)

q_{vs} Matrix of errors introduced by approximations of non-affine operations in AA-based voltage stability assessment (p.u.)

R Resistance (p.u.)

R_{IC} Vector of central values for active and reactive power in AA-based power flow analysis (p.u.)

$R_{L_{IC}}$ Vector of central values for active and reactive power used to account generator's limits (p.u.)

$R_{vs_{IC}}$ Vector of central values for active and reactive power in AA-based voltage stability assessment (p.u.)

$\bar{S}$	Complex power in phasorial form (p.u.)
σ	Auxiliary variable for univariate Chebyshev approximations
Ψ_{ds}	Stator flux in direct axis (p.u.)
Ψ_{qs}	Stator flux in quadrature axis (p.u.)
t	Time (s)
θ	Bus voltage angles (rad.)
$\widehat{\theta}$	Bus voltage angles in affine form (rad.)
$\widehat{\theta_{Ia}}$	Current angles in affine form (rad.)
θ_p	Pitch angle (rad.)
u	Real variable
U	Variable used to represent the bounds of the product of two zero centered affine forms in the Chebyshev approximation approach
$\bar{u}$	Interval associated with the variable u
$\bar{u}_A$	Interval associated with the variable u_A
$\widehat{u_A}$	Variable u_A in affine form
$\bar{u}_B$	Interval associated with the variable u_B
$\widehat{u_B}$	Variable u_B in affine form
v	Wind speed (m/s)
V	Bus voltage magnitudes (p.u.)
$\widehat{V}$	Bus voltage magnitudes in affine form (p.u.)
$\overline{V}$	Bus voltages in phasorial form (p.u.)

$V_{a,b}$ Auxiliary variables used to modify voltage control settings (p.u.)

$\widehat{V_d}$ Synchronous generator terminal voltage in direct axis (p.u.)

v_{dr} DFIG direct axis rotor-voltage (p.u.)

$\widehat{v_{dr}}$ DFIG direct axis rotor-voltage in affine form (p.u.)

v_{ds} DFIG direct axis stator-voltage (p.u.)

$\widehat{v_{ds}}$ DFIG direct axis stator-voltage in affine form (p.u.)

V_I Imaginary components of bus voltages (p.u.)

$\widehat{V_I}$ Bus voltage imaginary components in affine form (p.u.)

v_m Mean wind speed (m/s)

V_{PQ} Variable associated with the voltage of the PQ-bus used as parameter (p.u.)

$\widehat{V_q}$ Synchronous generator quadrature axis terminal-voltage (p.u.)

v_{qr} DFIG quadrature axis rotor-voltage (p.u.)

$\widehat{v_{qr}}$ DFIG quadrature axis rotor-voltage in affine form (p.u.)

v_{qs} DFIG quadrature axis stator-voltage (p.u.)

$\widehat{v_{qs}}$ DFIG quadrature axis stator-voltage in affine form (p.u.)

V_R Real component of bus voltages (p.u.)

$\widehat{V_R}$ Real component of bus voltages in affine form (p.u.)

$\widehat{V_{ref}}$ Reference of voltage for voltage controllers in affine form (p.u.)

V_{ref} Reference of voltage for voltage controllers (p.u.)

$\widehat{\omega}$ Generator rotor angular speed in affine form (rad/s)

ω_L Left eigenvector associated with the zero eigenvalue of $D_{x_{PF}} f_{PF}$

x_D State variables (p.u.)

$\widehat{x_D}$ State variables in affine form (p.u.)

X_f Random variable

$X_{f_{a,b}}$ Bounds of the random variable X_f

x_f Integration variable

x_{PF} Bus voltage magnitudes, angles and other unknown variables such as generator reactive powers (p.u.)

$\widehat{x_{PF}}$ Affine forms for x_{pf} (p.u.)

y Algebraic variables such as static voltages and angles (p.u.)

$\widehat{y}$ Algebraic variables in affine form (p.u.)

Y_L Load admittance (p.u.)

$\widehat{Y_L}$ Load admittance in affine form (p.u.)

z Vector of state and algebraic variables (p.u.)

$\widehat{z}$ Vector of state and algebraic variables in affine form (p.u.)

z_{ch} Auxiliary variable for the Chebyshev polynomial expansion

Functions

F Bounded function twice differentiable and whose second derivative does not change sign within its domain

$\widehat{F_A}$ Set of algebraized DAEs in affine form

F^{ap} Chebyshev approximation of F

f_D	Set of differential equations
f_{PF}	Set of power flow equations
g	Set of algebraic equations
Hc	Chebyshev approximation function
h_{ode}	Invertible function
P_{X_f}	Probability density function of the random variable X_f
r_L	function of the line used in the univariate Chebyshev approximation of non-affine functions
T_{rh}	Chebyshev polynomials

Chapter 1

Introduction

1.1 Research Motivation

Renewable energy sources are increasingly penetrating electrical grids because of global warming concerns, volatility of fuel prices and their effect on conventional generation cost, and governmental financial incentives, such as the Green Energy Act in Ontario, Canada [1]. Large-scale renewable energy projects are being developed in several countries aimed at harnessing the potential of renewable energy sources and reducing CO_2 emissions according to established goals. For instance, the Ontario Power Authority (OPA) is planning the long-term supply mix, shown in Figure 1.1, which eliminates coal as a generation source, and increases wind, solar and bioenergy generation sources.

Globally, wind power is one of the fastest growing renewable energy sources; this is mainly motivated by improved wind turbine technologies and the short capital investment recovery period [2]. However, wind, as well as, solar generation exhibits intermittency of their output power, which imposes a huge challenge to power system planning, operation, and control due to the additional uncertainties involved [2–5]. In an attempt to predict the output power associated with these intermittent sources, solar and wind power forecast tools are used by system operators and planners [6–8]. However, the accuracy of these tools, particularly for wind power, depends on factors such as the quality of the prediction model, the level of the predicted power, the predic-

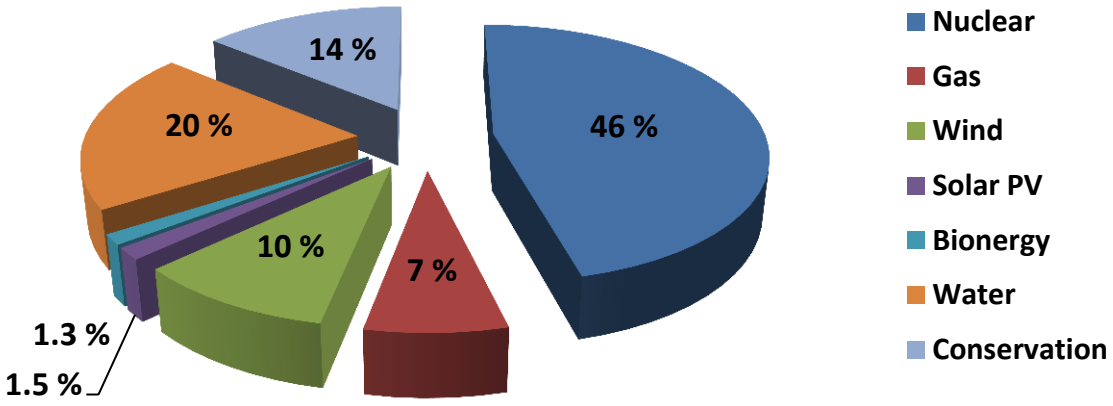

Figure 1.1: Long-term energy supply for Ontario in 2030 [9].

tion horizon, and spatial distribution of wind farms. Consequently, different prediction tools can lead to different expected productions and different probability density functions (pdfs) to model the uncertainty of the prediction error [6–8]. Similarly, the accuracy of solar power forecast methods are affected by factors such as the prediction horizon and the environmental conditions, among others. For these reasons, uncertainties associated with the power prediction are better expressed in terms of intervals instead of point estimates [6]. For instance, Figure 1.2 illustrates a 12 hours ahead aggregated wind power forecast corresponding to Alberta Electric System Operator (AESO); these forecasted values are based on near real-time meteorological data, and are given in terms of maximum, minimum and most likely values.

In order to maintain the power balance at any time instant, conventional power plants are normally used to cope with renewable power production uncertainties. As a result, conventional unit commitment and dispatch of generators are reformulated to account for these uncertainties by means of enough power reserve provisions [2], [4]. In this case, conventional generator outputs are adjusted up and down to compensate for the variability of intermittent energy sources. An alternative solution is the use of energy storage technologies which can smooth the output of intermittent energy sources [11]; however, technical and economical factors are a limitation for energy storage deployment, specially at transmission system levels.

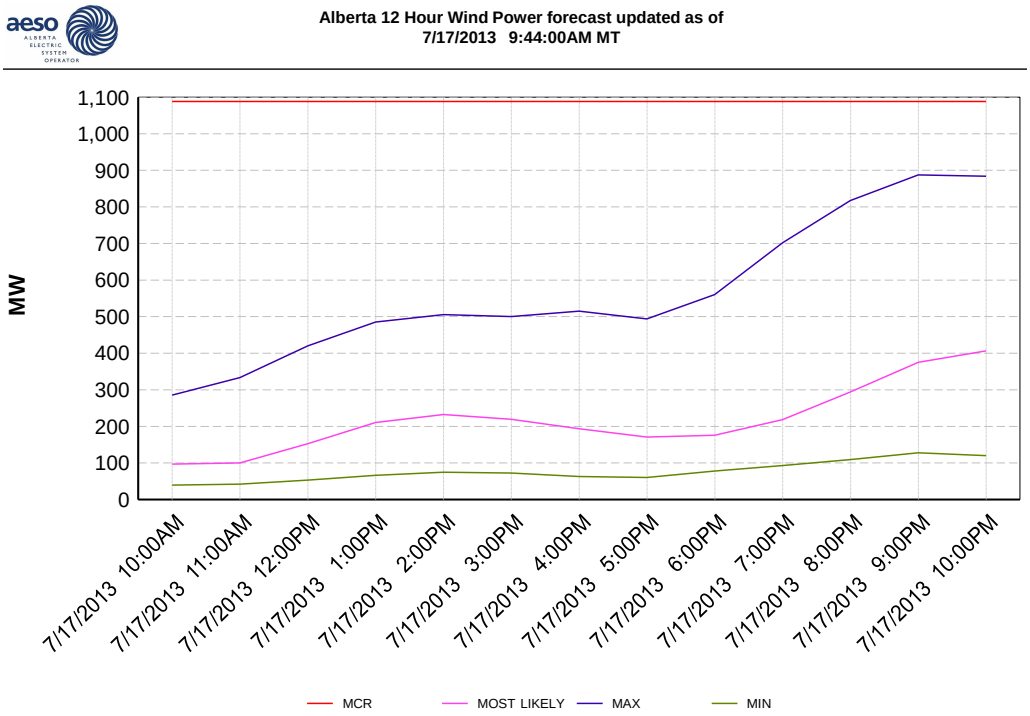

Figure 1.2: Wind power forecast example [10].

Depending on the penetration level of intermittent sources of power, the electricity grid may experience considerable and uncertain changes in power flows. These changes may lead to limit violations that affect system security [2]. Moreover, the location of renewable resources, which may be far from the main load centers, also affects the system limits, since these generation may have to be transported over long distances, leading to system congestion that have a direct impact on system stability margins [2, 3, 12, 13].

Besides the changing synchronizing forces that the system experiences due to the uncertain power flow variations associated with intermittent sources of power, the effective system inertia changes when a large amount of variable speed wind turbines and solar power is connected, which may affect the system transient stability. This change in the effective inertia will affect the angular acceleration of the synchronous generators when a disturbance occurs [13]. Also, the rate of frequency decay can be accelerated for generator trip events if proper controls are not implemented. Adequate analysis tools are thus required to properly analyze power system

stability when subjected to penetration of intermittent sources of power.

A variety of methods are available in the literature to perform power flow, transient, and voltage stability analyses considering uncertainties associated with electrical parameters [14–83]. Most of these methodologies are better suited for reliability and planning studies where detailed probabilistic methods are used; moreover, some of them require a high volume of computations, as in sampling based methods. A different approach based on Affine Arithmetic (AA), which does not rely on detailed probabilistic or sampling methods is proposed in [14] for power flow assessment considering uncertainties associated with the operating conditions. This approach is able to compute bounds of bus voltage magnitudes, angles and line flows when the generator output powers and load power levels are assumed to vary within established intervals. Therefore, the application of this technique to stability analysis is studied here in detail.

1.2 Literature Review

In this section, previously proposed techniques and tools aimed at assessing power flow, voltage stability and transient stability considering uncertainties are briefly discussed, highlighting their main advantages and disadvantages.

1.2.1 Stochastic Power Flow Analysis

Stochastic power flow assessment based on Monte Carlo Simulations (MCS) are reported in [15–17]. Although these methods allow simulating stochastic events with any level of complexity, they impose a large computational burden. Some analytical techniques are reported in the literature seeking to reduce the computational time associated with MCS [18–22]. These techniques use properties and theorems of probability to compute the pdfs of the desired variables based on the pdfs of the input data. Some simplifications such as linearization of the power flow equations and assuming a normal distribution for the stochastic variables are reported in [18]. Linearization of the power flow equations introduces errors in the pdf calculations; thus, considerable effort has been put into improving the accuracy of analytical approaches. For instance, in [19], a multilinearization technique is formulated to reduce the inaccuracies associated with

the linear approximation of the non-linear power flow equations. Furthermore, in [20], a second order approximation for the power flow equations together with a technique of moments is employed to improve the accuracy associated with linear approximation based analytical methods. Alternatively, in [21] and [22], the line flow pdfs are approximated by means of Gram-Charlier expansions together with cumulants for nodal powers. In general, these analytical methods are based on probabilistic theorems and elaborated computations that add some mathematical complexity when compared to MCS. Furthermore most of them are only accurate for particular inputs variable pdfs such as normal distributions.

As an alternative to analytical and MCS, in [23], the point estimate method is used to account for the uncertainties in the transmission line parameters, operating conditions, and topologies. This method exhibits a good accuracy and computational efficiency when compared with analytical and sampling approaches. Likewise, in [24], the point estimate method is applied considering unbalanced three-phase power systems and correlations between the input variables; in this paper, it is concluded that the proposed method performance in terms of computational time is better than the performance offered by MCS. Furthermore, in [25], a probabilistic optimal power flow proposed for a market environment, and based on the two-point estimate method, is found to be better suited for a relatively low number of stochastic variables, or alternatively, for stochastic variables with small standard deviations.

Methods that combine analytical and MCS are also reported in the literature. For instance, in [26], a sampling method based on latin hypercube and Cholesky decomposition is used together with MCS in order to reduce the computational cost attributed to conventional MCS. Similarly, in [27], a multilinearization technique is combined with MCS for the purpose of reducing the inaccuracies of linear approximation based analytical approaches.

As an alternative to the aforementioned methods, fuzzy power-flow methods are widely applied in stochastic power flow calculations [28–31]. In these methods, stochastic variables are modeled by means of fuzzy sets, which are associated with a membership function. The final output is a possibility distribution rather than a pdf.

Stochastic power flow based on self-validated methods such as IA and AA has also received attention in the literature. In [32], IA is applied to compute the power flow bounds of a five-bus test system when loads and generator power uncertainties are modeled using intervals; a Newton

operator is used to deal with the nonlinear equations. The authors observe that although the IA offers a better performance than MCS in terms of simulation time, it may produce excessively conservative results when the input interval sizes increase. Similarly, in [33], IA is used to solve the power flow problem by means of the Krawczyk method; the authors conclude that IA is an efficient technique to solve the power flow problem considering uncertainties. In [34], a radial power flow solution by means of IA is proposed for balanced systems. In this methodology, the load uncertainties are modeled as intervals, and a complex approach for the IA operations is used; the IA results are observed to be very close to MCS results in this case. Also, in [35], a radial power flow is solved by using IA combined with an interval constraint propagation technique in order to obtain narrower intervals; this technique is based on finding a restriction function that produces thinner intervals by a successive contraction process. Since IA-based methods are not able to account for correlations among variables, they may lead to error explosion, resulting in impractical bounds. Aimed at avoiding the error explosion attributed to IA-based methods, an AA-based approach for power flow assessment is proposed in [14]. Herein, analysis carried out considering a 50-bus test system, assuming uncertainties in the injected powers, demonstrate the accuracy of the method as compared to MCS and IA, reporting considerable improvements in computational efficiency when compared to MCS.

In [36], a fast approximation of the power flow solution bounds is assessed by sampling a reduced set of deterministic power flow solutions, based on a worst case analysis of the generation and load scenarios. These scenarios correspond to maximum generation and minimum load, maximum generation and maximum load, minimum generation and minimum load, and minimum generation and maximum load. The deterministic power flow solutions corresponding to these generation/load scenarios are then combined to determine an approximation of the hull boundary of the power flow solutions.

From the above described methods, sampling based approaches such as MCS have been widely used for power flow appraisal; they can manage complex and accurate probabilistic models at the cost of a considerable computational burden. Analytical methods are also an option aimed to be more computationally efficient than MCS; however, their accuracy is in general affected due to the simplifications needed to enable the use of probabilistic theorems. These simplifications are in some cases based on unrealistic representations of the stochastic nature of the input variables. For instance, for the particular case of wind power, the probability distri-

bution for the forecast errors depends on the considered time scale, among other factors; thus, assuming normal distributions for all time scales, as in most of the analytical methods, may lead to inaccurate results [6]. The AA-based method previously mentioned for power flow assessment considering uncertainties associated with loads and power injections does not require assumptions regarding the pdfs of the uncertain variables; furthermore, it is able to improve the computational efficiency when compared to MCS, while providing quite reasonable accuracy because correlations among variables are considered [14]. Therefore, this thesis proposes an improved AA-based power flow methodology, with a more efficient representation of generator reactive power limits.

1.2.2 Stochastic Voltage Stability Assessment

MCS have been used to model a variety of system complexities for voltage stability assessment [37], [38]. However, the high computational cost of MCS renders it unsuitable for certain applications. Thus, most of the effort in the literature has concentrated on reducing the computational cost of MCS while achieving acceptable accuracy. For instance, the two-point estimate method used in [39] computes the transfer capability associated with uncertainties of transmission line parameters and bus injections. This method computes approximations for the moments of the output variable, using only two probability concentrations for each uncertain input variable. However, in certain cases, for a relatively large number of uncertain input variables and/or large statistical dispersion of these variables, the two-point estimate method is not sufficiently accurate as compared to MCS [25]. Moreover, a higher order point estimate method is required for the cases where the pdfs of the input variables are not normal, which adversely affects the computational efficiency of the method. In this sense, one of the advantages of the proposed AA-based technique is its independence with respect to the pdfs associated with the uncertain variables, which are modeled as intervals with no assumptions regarding their probabilities.

Enumeration techniques are alternate approaches to MCS for online applications. For instance, in [40], an enumeration technique is used to compute the voltage stability indicators assuming uncertainties in the loads; the stability indicators are derived from the power flow equations based on various simplifications such as constant generator voltage magnitudes and phases. In [41], online risk indices are proposed to evaluate the system security from the perspective of

low voltage violation, overload, cascading overload, and long-term voltage stability.

Truncated Taylor series expansion methods are used in [42] to efficiently account for variations in the transfer capability due to variations in system parameters. A formula to compute reliability margins is derived, assuming conditions associated with the central limit theorem. According to this theorem, the uncertain parameters must be independent and their number be sufficiently large, in order to approximate the output variable as normally distributed. In the proposed AA-based method for voltage stability assessment, the uncertain input variables are not necessarily assumed to be statistically independent; in fact, correlations among uncertain variables are explicitly represented in the model.

In [43] and [44], the effect of system control parameters and system data on voltage stability margins is accounted for by means of linearization techniques and direct formulas. In [45], these formulas are used to efficiently estimate changes in saddle node bifurcations and limit induced bifurcations, due to changes in power system transactions in a market environment. These methods, based on sensitivity analysis and formulas, are able to efficiently estimate voltage stability indices due to system parameter variations, but within certain limits in which the assumed linearizations are valid. Moreover, they are not intended to compute full PV curves under uncertainties, which is the main contribution of the AA-based method proposed here.

Some research work is reported on the computation of loadability margins considering uncertainties associated with intermittent sources of generation. For instance, in [46], a stochastic response surface is used to estimate the pdf of the loadability margins considering stochastic generation variations attributed to renewable energy sources and assuming non-conforming loads. This method is able to reduce the computational burden of MCS by using a polynomial chaos expansion of a relatively low order. As the number of uncertain variables increase, the order of this polynomial chaos expansion may increase and hence improve the accuracy of the method. Alternatively, various papers are focused on finding maximum loadabilities in terms of load uncertainties. For example, in [47], the stochastic nature of loads is modeled using a hyper-cone model whose thickness represents the uncertainty of future loading and the vertex is the current operating point. This approach is focused on finding the worst case scenario for maximum loadabilities in terms of load uncertainties, while the AA-based method proposed in this thesis computes the bounds of PV curves and associated maximum loadabilities, considering uncertainties due to power injections. In [48], a cumulant method is used for assessment of saddle

node bifurcations considering uncertainties in load forecast. The method is used to solve the resultant stochastic non-linear programming formulation that leads to the estimation of the pdf for maximum loadability. The cumulant method requires information on the cumulants of the uncertain variables which may not be accurately available for uncertainties associated with intermittent sources of generation, where there is no general agreement on the pdf to best represent the forecasting errors [6, 7].

In order to overcome some of the limitations of sampling- and statistical-based methods, the use of soft-computing-based methodologies for uncertainty representation in voltage stability assessment has been proposed in the literature. In particular, the application of fuzzy set theory to represent uncertainties has been proposed in [49, 50]. In this paradigm, the input data are modeled by fuzzy numbers, which are special types of fuzzy sets. Defining the connection between interval analysis and fuzzy set theory is not a trivial task [51]. In [52], the ideas of fuzzy sets and interval analysis are both connected to a general topological theory. Similarly, in [53], it is argued that the theory of fuzzy information granulation, the rough set theory, and interval analysis can all be considered as subsets of a conceptual and computing paradigm of information processing called Granular Computing. An essential aspect of this paradigm is that its constituent methodologies are complementary and symbiotic, rather than competitive and exclusive. Based on these principles, the main contributions of the present thesis lie on the application of advanced interval based solution approaches to voltage stability analysis with data uncertainties.

More recently, computational intelligence based techniques have been proposed in both state selection (as an alternative to MCS) and in state evaluation (as an aid to MCS). The application of these techniques allows deploying directed intelligent search paradigms which are an alternative to the proportionate sampling approach characterizing standard MCS. Amongst these techniques, the most promising for the problem under study, is the PIS-based algorithm [54]. This algorithm tries to generate the dominant failure states and minimize the generation of success states. Thanks to this feature, fewer states need to be evaluated compared to standard MCS (where the majority of the states sampled are success states). The proposed AA-based approach is intrinsically different from this computing paradigm since it does not integrate either sampling based methods or evolutionary computation processes. By using the methodology presented in this thesis, a reliable estimation of the problem solution hull can be directly computed taking into account the parameter uncertainty interdependencies as well as the diversity of uncertainty

sources. The main advantage of this solution strategy is that it neither requires derivative computations nor interval systems, and hence are suitable, in principle, for large scale problems, where robust and computationally efficient solution algorithms are required.

Another general class of statistical methods aimed at empirically assessing the parametric confidence intervals of a sampling distribution are based on resampling theory. The most common technique in this class is the so called bootstrap method, a technique for using the data collected from a single experiment to simulate what the results might be, if the experiment was repeated by sampling (with replacement) data from the original dataset [55]. This paradigm has been recognized as a powerful tool for testing or avoiding parametric assumptions when computing confidence intervals in many engineering problems [56, 57]. Although the adoption of the bootstrap method is expected to be more effective, compared to standard MCS, especially in terms of computational efforts, it still requires repetitive simulations.

The detailed chronological nature of intermittent power sources can be considered using sequential MCS and time series models instead of analytical approaches or simple state-sampling MCS. For instance, in [58], an Auto Regressive Moving Average (ARMA) based technique is used to estimate the wind speed and the corresponding output power of a Wind Energy Conversion System (WECS) on an hourly basis. These hourly point estimates are used together with the random failure of generating units and load profiles to compute the hourly available system reserve using sequential MCS. The goal of this approach is the computation of reliability indices and generating capacity adequacy assessment over a long-term time frame. Since this method requires repetitive MCS for each time instant considered, it imposes a high computational burden. The proposed AA-based approach for voltage stability assessment can indeed consider the chronological issues associated with intermittent sources of power, since it uses intervals to model the uncertain output power of these intermittent and non-dispatchable sources, with no assumptions regarding their probabilities nor the associated time windows. For a different time window, a new estimate of the interval that properly reflects the uncertainty can be easily obtained. The larger the time window, the larger the interval of uncertainty, and vice versa. It is also important to point out that the proposed method is intended to efficiently compute the hull of PV curves associated with intermittent sources of power considering short operational time frames and it is not intended to compute reliability indices or evaluate generating adequacy capacity, as in [58] and other similar applications of sequential MCS.

Various probabilistic voltage stability studies are reported in the literature that use machine learning techniques. For instance, in [59], a trained radial basis function network is used to perform online appraisal of the probabilistic risk of voltage collapse given the loading condition and the settings for the reference voltages at PV buses; a radial basis function is trained by considering uncertainties in transmission line parameters and reference voltages for PV buses. In [60], probabilistic insecurity indices considering voltage stability restrictions are computed for several load levels considering reactive power redispatch and single- and double-line contingencies. This methodology uses artificial neural networks to evaluate the system voltage security margins; in addition, corrective actions aimed to improve the voltage security are introduced by evaluating the sensitivity of the probabilistic insecurity indices with respect to the reactive power control actions. The general shortcoming of machine learning based techniques is the relatively elevated number of training cases that may be needed in order to produce accurate results, which can add some level of complexity to the problem.

In this thesis, a new AA-based computing paradigm is proposed that is an alternative to sampling based approaches to represent the uncertainties of the power system state variables. This allows expressing the system equations in a more convenient formalism compared to the traditional and widely used linearization, frequently adopted in interval Newton methods. By using the proposed methodology, a reliable estimation of the problem solution hull can be computed taking into account the parameter uncertainty interdependencies, as well as the diversity of uncertainty sources, without requiring repetitive simulations and assumptions regarding pdfs.

1.2.3 Stochastic Transient Stability Assessment

Transient stability analysis for operation and planning purposes evaluates the capability of the power system to remain in synchronism when subjected to large and sudden system disturbances. To account for the uncertainties associated with power system variables, probabilistic methods for transient stability analysis have been widely proposed in the literature. Most of these methods account for the probabilities of different factors, such as the fault type and location, clearing time, operating conditions, fault duration, and reclosing times. Thus, various papers address the probabilistic transient stability problem by means of MCS. In [61], MCS are used together with transient energy functions for transient stability assessment considering uncertainties in

fault characteristics and the reliability of circuit breakers. In [62], MCS are employed to determine the probability of instability for a large-scale power system; probabilistic models for the load level, fault type, fault location, and successful reclosing time are developed by means of available system historical data. The accuracy of the probabilistic models is achieved because of the availability of the historical data for this particular system. In [63], a MCS-based approach is proposed where the equal area criterion is used to calculate the critical clearing times. In [64], a deterministic approach is combined with MCS in order to analyze the system security while reducing the computational time. Most of these MCS-based approaches are mainly focus on probabilistic transient stability assessment for medium and long term planning purposes. Furthermore, they require enough historical data to assess the pdfs of the uncertain variables. Considering that MCS involve a long computational burden, the proposed AA-based methodology for transient stability assessment significantly improves the computational efficiency, which may render it suitable for online applications.

Special attention has also been paid in the literature to conditional probability based methods. In [65], the probability indices for an 8-bus, 3-machine system are determined using the conditional probability theorem considering the probabilities of faults and assuming the load variations in three discrete levels; the critical clearing times are computed using Lyapunov methods. The main drawback of this approach is the difficulty in properly computing the transient energy functions and the stability regions for large scale systems. In [66], the conditional probability method is used for assessment of transient stability of a multimachine system considering uncertainties in the fault types, locations and clearing times, which are modeled using available historical data; however, the effect of the stochastic prefault conditions on transient stability indices is not addressed. In [67], conditional probability approach and the Bayes' theorem are used to compute the probability of instability based on the historical data for the occurrence of each considered event. In [68], the pdfs for the reclosing time and the fault duration are convolved to obtain the pdf of successful reclosing; uncertainties in fault type, fault location and loading levels are considered. In this paper, the conditional probability theorem is applied to calculate the stability probability indices with successful and unsuccessful reclosing. In an attempt to reduce the volume of computation associated with the calculation of critical clearing times, a fixed clearing time which is equal to the maximum clearing time given by its normal probability distribution is assumed in [69]; accordingly, the critical clearing times are only computed if

the system is unstable for a particular combination of stochastic events. These critical clearing times and the transient stability assessment are carried out by means of a corrected transient energy function strategy. For the evaluation of the instability indices, the uncertainties associated with fault characteristics are considered, but those linked to pre-fault conditions are not taken into account. In [70], the conditional probability approach is used to estimate the probability of stability indices in long term planning for a 10-bus system, considering wind power penetration; besides uncertainties in the fault characteristics and protection operation, uncertainties in operating conditions are accounted for in this case.

Similarly to MCS, conditional probability approaches are mainly applied to stability studies for medium and long term planning purposes. Even though the conditional probability approaches reduce the simulation times as compared to MCS, their accuracy relies on the available historical data in order to provide accurate statistics of the transient stability indices. In general, conditional probability based approaches exhibit some difficulties in properly modeling the pdfs of the uncertainties associated with the operating conditions. This is not an issue for the proposed AA-based methodology, where the uncertainties associated with the operating conditions are modeled as intervals.

Some research is reported on the application of machine learning techniques for probabilistic transient stability assessment aimed at improving the computational efficiency when compared to conventional MCS. For instance, in [71], a self organizing map neural network is used to reduce the size of the samples required in MCS; this map is built considering transient and voltage stability constraints. It is noted that the self-organizing map neural network is able to reduce the computational times compared to the conventional MCS. Alternatively to the use of artificial neural networks, in [72], a Bayes decision function is used to classify the level of security of the system states. The method of calculation of the Bayes decision function is based on the estimation of the mean and variances of chosen security groups, which are calculated from the characterization of feature vectors; finally, the Bayes decision function is used to classify new feature vectors according to the established security groups and compute transient stability security indices. In [73], the polynomial representation of the transient stability boundary region obtained in [74] by means of a machine learning technique is used together with a linearization approach to compute a risk-based index for dynamic security considering uncertainties in the operating conditions; this approach also reduces the computational time when compared to MCS.

These machine learning based techniques are designed to reduce the computational burden associated with MCS; however, their accuracy relies on the quality and number of cases used in the training stage, which may present a computational challenge. This training stage is not required in the proposed AA-based methodology for transient stability assessment, which represents an important advantage with respect to machine learning based techniques.

In [75], pdfs for the maximum relative rotor angles considering stochastic loads, stochastic clearing times, and a particular fault type and location are computed by means of the two-point estimate method. In this paper, the cumulative probabilities of individual relative rotor angles are computed in order to determine the probabilities of stability according to a predefined threshold. The basic idea is to reduce the number of samples of the stochastic variables to only two representative samples for each stochastic variable, which are then used to compute the individual relative maximum rotor angles for each generator by means of a transient simulation package. For pdfs other than normal pdfs, a higher order point estimate method is required, adversely affecting the computational efficiency of the two point estimate method, as discussed before. The AA-based methodology proposed in this work is intended to be independent of the pdfs assumed to model the uncertain input variables, resulting in a more flexible approach.

Analytical approaches to probabilistic transient stability assessment are also reported in the literature. In [76], a method to compute transient stability indices in terms of relevant system fixed parameters and statistical parameters is presented to determine an analytical expression for the critical clearing time. The nonlinear relationship between the critical clearing time and system load is approximated using a log-linear model whose parameters are computed by linear regression. Similarly, in [77], an analytical approach to probabilistic transient stability assessment considering uncertainties associated with fault clearing times and system loads, is proposed; this approach uses the potential energy boundary surface method to assess the transient stability. Likewise, in [78] the authors propose a methodology to calculate the pdf of the critical clearing time using a linear function with respect to the system load; the linear function is computed using the equal area criterion together with linearization techniques around an equilibrium point. These analytical approaches for transient stability assessment are mainly theoretical approaches; in practical power systems, these methods are mathematically difficult to implement. Thus, the accuracy of these analytical methods relies on the validity of the assumed simplifications; furthermore, the mathematical complexities of some of these probabilistic methods render them

unsuitable for applications to real size power systems. In this context, the proposed AA-based method for transient stability assessment is intended to avoid the need of elaborated probabilistic methods, while providing reasonable accurate results for the transient stability bounds, regardless of the system size.

As an alternative to sampling-and statistical-based methods, fuzzy set theory is applied in [79] to determine transient stability indices for a defined number of system conditions. Similarly, reachability analysis is used in [80, 81] to determine a bounded set of possible trajectories of the system state variables, when the system is perturbed by uncertainties which are modeled as bounded sets. Likewise, in [82], reachability analysis is used to generate the possible trajectories of multi area frequency dynamics, considering uncertainties associated with intermittent renewable sources. One of the advantages of reachability analysis based approaches is the modeling of the uncertain variables as bounded sets, without the need of assumptions regarding pdfs; however, the large errors attributed to interval operations and the difficulties associated with modeling of system discontinuities in reachability analysis may be an issue in some applications.

An IA-based method is applied in [83] to transient stability assessment considering uncertainties in the system parameters; the resultant interval differential equations are solved by means of an interval Taylor series method. It is noted that the proposed interval methodology may lead to excessively conservative results with relatively long simulation times. In fields other than power systems, a methodology to evaluate the impact of parameter variations in the transient and DC response of analog circuits using AA is proposed in [84], solving a set of Differential Algebraic Equations (DAEs) that models the analog circuit using an iterative approach.

Based on the aforementioned detailed literature review, the present thesis proposes the use of AA as a novel method for transient stability appraisal of power system with intermittent renewable sources. This method is more accurate than the IA-based methodology previously mentioned, since correlations among variables are considered. It is conceived to enclose the output variables according to intervals that yield reasonably fast and adequate output variable bounds when the input variables are modeled as intervals, without any assumptions regarding their probabilities.

1.3 Research Objectives

This thesis proposes novel methods for adequate voltage and transient stability assessment based on AA, aimed at reducing the computational burden associated with MCS-based methods, and avoiding the need of elaborated probabilistic methods and pdf assumptions. The proposed methods are conceived to be reliable and computational efficient tools for transient and voltage stability assessment of power systems with intermittent and renewable sources of power, representing a new computing paradigm, which is an alternative to sampling-based approaches. Therefore, the objectives of this thesis are the following:

- Improve the existing AA-based power flow analysis method, particularly with respect to the representation of generator reactive power limits.
- Develop a computationally efficient method based on AA for voltage stability assessment of power systems with intermittent renewable sources. This method is based on the computation of the bounds of PV curves, given the uncertainties associated with the power production of intermittent sources of power, which are modeled as intervals without any assumptions regarding their probabilities.
- Develop a computationally efficient method based on AA for transient stability assessment of power systems with intermittent renewable sources. This method is aimed at computing the hull of the transient stability time domain dynamic responses associated with the intervals that models the uncertainties of the power production.
- Validate the results of the proposed methods by comparison with respect to conventional probabilistic methods such as MCS-based approaches.
- Study the computational effort of the proposed methods using realistic test systems.

1.4 Thesis Outline

The rest of this thesis is organized as follows: Chapter 2 presents a review of relevant background, specially of power flow, voltage stability, and transient stability analyses. In addition,

self-validated numerical techniques are explained, with special attention to some of the available approaches to approximate non-affine operations. Also, MCS are explained in some detail, presenting and example of a stability analysis of a power grid with intermittent sources of power to demonstrate its relevant application in power systems.

Chapter 3 discusses the AA-based power flow analysis, and the results of the application of this method to three study cases. In Chapter 4, the proposed AA-based method for voltage stability assessment of power systems considering uncertainties associated with power injections is presented, discussing the results from applying it to small- and a large-size test systems.

Chapter 5 presents and discusses the proposed AA-based method for transient stability assessment of power systems considering uncertainties associated with power injections; results are discussed for two study cases using various generator models, including Doubly Fed Induction Generator (DFIG) based wind turbines. Finally, Chapter 6 presents the summary of the thesis, highlighting its contributions and possible future research work.

Chapter 2

Background Review

2.1 Introduction

In this chapter, fundamental concepts and solution techniques concerning power flow, voltage stability, and transient stability are briefly reviewed. In addition, a section is devoted to the discussion of self-validated IA and AA numerical techniques, with an special emphasis on the approaches used to approximate non-affine operations. Finally MCS are briefly discussed, and an example of the application of MCS to system stability analysis considering uncertain power injections due to wind generation is presented. The notation of all equations presented in this chapter, and the rest of the thesis, are defined at the beginning of this document in the nomenclature section.

2.2 Power System Analysis

Power systems contain a variety of components aimed at generating, transmitting and consuming the electrical power in an efficient an reliable manner. In order to properly design, plan, and operate a power system, analysis tools, which commonly rely on numerical methods, are employed. This section concentrates on the discussion of power flow, voltage stability and transient stability analysis tools, which are the main focus of this thesis.

2.2.1 Power Flow

Power flow studies are aimed at computing the steady-state voltage magnitudes and angles, as well as the complex powers across the elements that comprise a power grid. Power flows are the basic tools in power system analysis, and form the basis for stability analysis. The general formulation of the power flow problem is as follows [85]:

$$f_{PF}(x_{PF}, p_{PF}) = 0 \tag{2.1}$$

This vector equation represents a system of nonlinear equations referred to as the power flow equations, where x_{PF} represents the vector of bus voltage magnitudes, angles and other relevant unknown variables such as generator reactive powers, and p stands for the vector of specified active and reactive powers injected at each node, as well as terminal generator voltage set points.

A detailed representation of (2.1) in polar form is given by:

$$\Delta P_{P_i} = P_{G_i} - P_{L_i} - \sum_{j=1}^{N} V_i V_j [G_{ij} \cos(\theta_i - \theta_j) + B_{ij} \sin(\theta_i - \theta_j)] \quad \forall i = 1, ..., N \tag{2.2}$$

$$\Delta Q_{P_i} = Q_{G_i} - Q_{L_i} - \sum_{j=1}^{N} V_i V_j [G_{ij} \sin(\theta_i - \theta_j) - B_{ij} \cos(\theta_i - \theta_j)] \quad \forall i = 1, ..., N \tag{2.3}$$

Equations (2.2) and (2.3) can also be written in rectangular form as follows:

$$\Delta P_{r_i} = P_{G_i} - P_{L_i} - \sum_{j=1}^{N} V_{R_i}(V_{R_j} G_{ij} - V_{I_j} B_{ij}) + V_{I_i}(V_{I_j} G_{ij} + V_{R_j} B_{ij}) \quad \forall i = 1, ..., N \tag{2.4}$$

$$\Delta Q_{r_i} = Q_{G_i} - Q_{L_i} - \sum_{j=1}^{N} V_{I_i}(V_{R_j} G_{ij} - V_{I_j} B_{ij}) - V_{R_i}(V_{I_j} G_{ij} + V_{R_j} B_{ij}) \quad \forall i = 1, ..., N \tag{2.5}$$

In PV buses, the injected active power and bus voltage magnitude are specified, with the bus voltage angle and reactive power injection being the unknown variables to be calculated. In PQ buses, both the injected active and reactive powers are specified, and the voltage magnitude and

angle are unknown. Additionally, a slack bus has to be defined in order to provide a reference angle and balance the total power injections; active and reactive power injections are typically the unknown variables in this bus.

Because of the nonlinear characteristics of the power flow equations, these are usually solved using numerical techniques involving iterative methods, of which the Newton-Raphson method is the most commonly used. This method can be formulated with respect to equation (2.1) as follows:

- The solution method starts with an initial guess for the unknown variables. At each iteration, starting with the initial guess, then, this initial guess, the elements of the Jacobian matrix and the power mismatches are computed, and the following linear equation is used to compute the corrections of the unknown variables at an iteration r:

$$\frac{\partial f_{PF}(x_{PF}^{r-1}, p_{PF}^{r-1})}{\partial x_{PF}} \Delta x_{PF}^{r} = -f_{PF}(x_{PF}^{r-1}, p_{PF}^{r-1}) \tag{2.6}$$

- This process is repeated using the updated values of the unknown variables until the convergence criteria is met, or the maximum number of iterations is reached.

In the solution process, different strategies can be employed to account for the reactive power limits associated with generator buses. The most commonly used strategy is based on the switching of the bus type. According to this strategy, the generator reactive power limit violations are checked at each iteration. If a violation occurs, the corresponding generator cannot longer control the voltage at the corresponding bus and, thus, the PV bus is switched to PQ. Similarly, if the voltage recovers in the subsequent iterations, the PQ bus type is switched back to PV, and so on until a feasible solution is obtained without any limit violations.

As an alternative to the bus type switching strategy, the terminal voltage at generator buses can be treated as a variable, so that PV buses where reactive limits have been violated can be modified until no limit violations are observed, while still treating the bus as PV. This approach can be implemented either by modifying the terminal voltage whenever necessary in the iterative process, or by using an optimization approach, which is based on the representation of PV buses discussed in [86, 87], where the voltage at these buses is defined as:

$$V_{nc} = V_{o_{nc}} + V_{a_{nc}} - V_{b_{nc}} \qquad \forall nc \in N_{PV} \tag{2.7}$$

where:

$$\begin{cases} V_{a_{nc}} > 0, V_{b_{nc}} = 0 & \text{for} \quad Q_{G_{nc}} < Q_{G_{min_{nc}}} \\ V_{a_{nc}} = 0, V_{b_{nc}} > 0 & \text{for} \quad Q_{G_{nc}} > Q_{G_{max_{nc}}} \\ V_{a_{nc}} = V_{b_{nc}} = 0 & \text{for} \quad Q_{G_{max_{nc}}} \leq Q_{G_{nc}} \leq Q_{G_{min_{nc}}} \end{cases} \tag{2.8}$$

the first condition in (2.8) is a strict complementarity condition and guarantees that the minimum reactive power constraint of the generator is not violated; this is achieved by increasing the magnitude of the terminal voltage by means of the auxiliary variable $V_{a_{nc}}$ according to (2.7). Similarly, the second condition avoids violation of the upper reactive power limit by adjusting the magnitude of the auxiliary variable $V_{b_{nc}}$, which reduces the terminal voltage of the generator. When no reactive power limits are violated, the auxiliary variables in (2.7) are zero as in the third condition of (2.8), thus keeping the terminal voltage at its reference value $V_{o_{IC}}$. This model yields the following Mixed Complementarity Problem (MCP) [87]:

$$\begin{aligned} \min \quad & \tfrac{1}{2}\|\Delta P\|_2^2 + \tfrac{1}{2}\|\Delta Q\|_2^2 \\ \text{s.t.} \quad & (Q_{G_{nc}} - Q_{G_{min_{nc}}})V_{a_{nc}} = 0 \\ & (Q_{G_{nc}} - Q_{G_{max_{nc}}})V_{b_{nc}} = 0 \\ & Q_{G_{max_{nc}}} \leq Q_{G_{nc}} \leq Q_{G_{min_{nc}}} \\ & V_{nc} = V_{o_{nc}} + V_{a_{nc}} - V_{b_{nc}} \\ & V_{a_{nc}}, V_{b_{nc}} \geq 0 \\ & \forall nc \in N_{PV} \end{aligned} \tag{2.9}$$

2.2.2 Voltage Stability

Voltage stability deals with the ability of the power system to maintain acceptable voltage levels under normal operating conditions and after the system is perturbed by small or large disturbances [88]. Voltage stability can be associated with short-term or long-term phenomena. Short-term voltage stability is studied considering system dynamics, whereas long-term voltage stability is commonly studied by means of steady-state solution techniques. For instance, voltage collapse, which is usually associated with long-term phenomena, is commonly analyzed by power flow techniques and linearization of the system equations. Even though voltage stability is a dynamic process, steady-state analysis techniques are used to identify the absence of a long-term equilibrium in the post-contingency state, which leads to voltage instability [89]. This thesis is focused on this particular voltage stability phenomenon.

The maximum load that the system can withstand without experiencing a voltage collapse is commonly used to compute voltage-stability indices. This maximum loadability is associated with a saddle-node bifurcation or a limit-induced bifurcation point [90]. Saddle-node bifurcations refer to the operating point where the system state matrix becomes singular. This singularity of the system state matrix usually coincides with the singularity of the power flow Jacobian and thus, no power flow solution can be found using conventional power flow techniques. On the other hand, limit-induced bifurcations arise when generators reach their reactive power generation limits, thus losing voltage control capability.

Figure 2.1 illustrates saddle-node and limit-induced bifurcations for the 2-bus test system shown in Figure 2.2. Observe that limit-induced bifurcations tend to decrease the maximum loadability when compared to saddle-node bifurcations. In this example, limit-induced bifurcation are computed for two different values of the maximum generator reactive power associated with the generator connected at Bus 1, with $Q_{G_{max_1}} > Q_{G_{max_2}}$, yielding, as expected, a lower static load margin when the maximum generator reactive power limit is lower.

The most representative methods devised to compute the maximum loadability are the continuation power flow and direct methods, which are briefly discussed next.

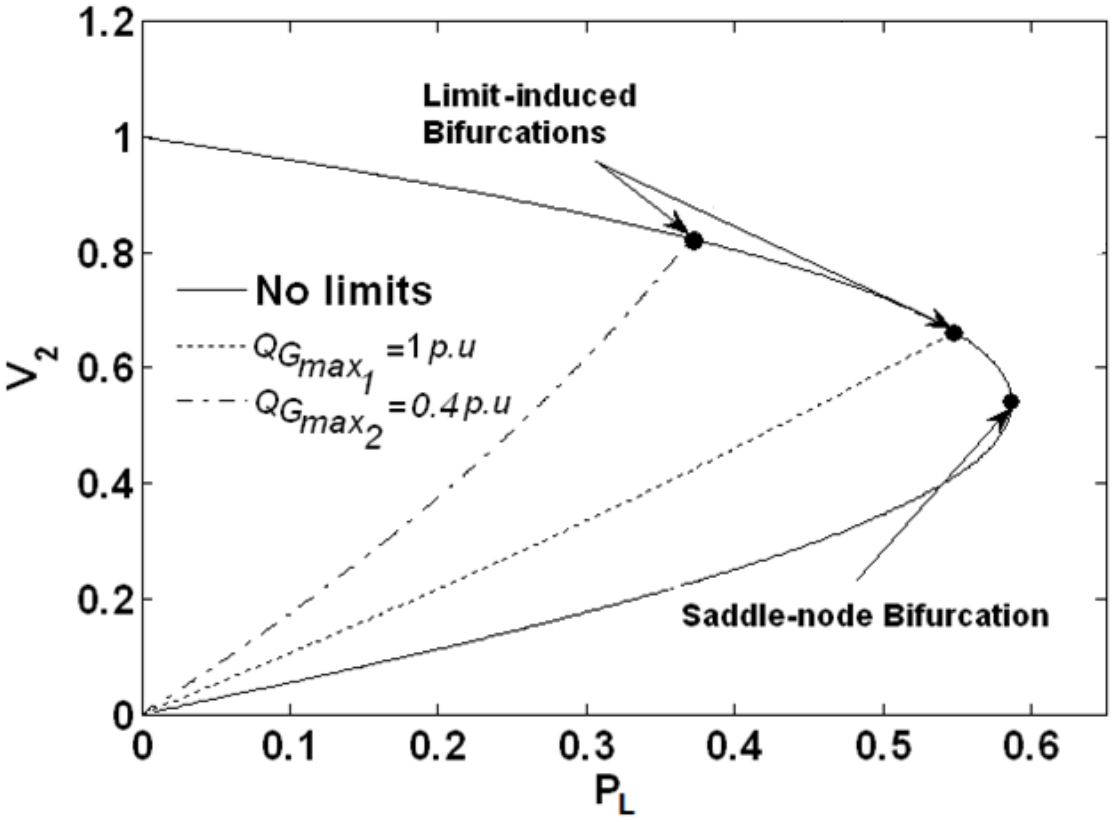

Figure 2.1: PV curves for 2-bus system.

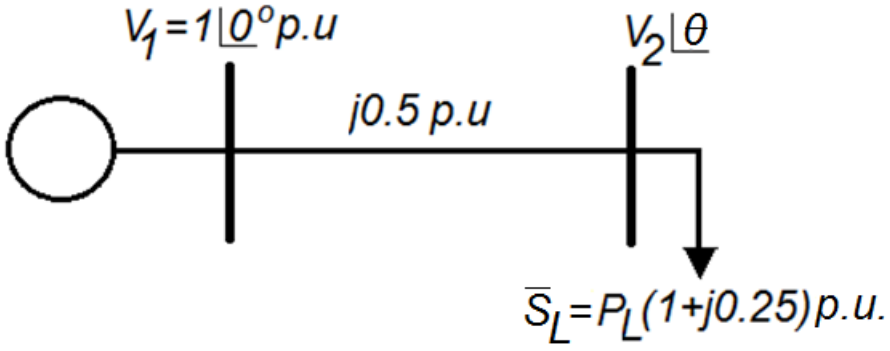

Figure 2.2: Two-bus system example.

Continuation Power Flow Method [90–93]

Continuation power flow methods are designed to overcome the difficulties associated with the computation of power flow solutions in the vicinity of the maximum loadability point. These difficulties are linked with the singularity of the power flow Jacobian matrix or the reactive power limits at this point. The general idea behind continuation power flow methods is the solution of the power flow equations given by:

$$f_{PF}(x_{PF}, p_{PF}, \lambda) = 0 \tag{2.10}$$

where the parameter λ is used to generate different scenarios for loads and generator outputs according to the following equations:

- For generator powers excluding the slack bus:

$$P_{Gi}(\lambda) = P_{Goi} + \lambda \Delta P_{Gi} \qquad \forall i = 1, ..., N-1 \tag{2.11}$$

- For generator powers including the slack bus (distributed slack bus):

$$P_{Gi}(\lambda) = P_{Goi} + (\lambda + K_G)\Delta P_{Gi} \qquad \forall i = 1, ..., N \tag{2.12}$$

- For load powers:

$$P_{Li}(\lambda) = P_{Loi} + \lambda \Delta P_{Li} \qquad \forall i = 1, ..., N \tag{2.13}$$

$$Q_{Li}(\lambda) = Q_{Loi} + \lambda \Delta Q_{Li} \qquad \forall i = 1, ..., N \tag{2.14}$$

The solution of (2.10) for different values of λ is obtained using two basic steps: predictor and corrector. In the predictor step, an approximate power flow solution for a small increase in the loading level is obtained from an initial operation point. Two methods are typically used to perform the predictor step: the tangent vector method and the secant method. The tangent vector method is based on the computation of an approximate solution for x and λ from a previous known solution in a direction that is tangent to the solution path. On the other hand, the secant method requires two previous solutions in order to compute the next approximate solution. In

the corrector step, the approximate solution obtained from the predictor step is used as an initial guess to solve the power flow equations plus an additional equation that allows to determine the value of λ, and facilitates convergence around the maximum loadability point. Two techniques that may be used in the corrector step are the perpendicular intersection technique and the parametrization technique. The perpendicular intersection technique, which is illustrated in Figure 2.3, uses a perpendicular vector at the approximated solution in order to define the required additional equation; to prevent convergence problems that may arise when a large predictor step is used, this method can be accompanied by a step cutting technique. In the parametrization technique, the convergence issues close to the maximum loading point are avoided by fixing a system variable such as the voltage magnitude at a specific load bus. Figure 2.4 illustrates the parametrization technique when a load voltage is fixed.

Conventional power flow methods are also used to compute the upper side of the PV curve. This technique depicted in Figure 2.5, used by many commercial packages, is based on a series of conventional power flows as the load is increased, together with a load step-cutting technique to obtain solutions in the vicinity of the maximum loading points [94].

Direct Methods

Direct methods rely on the direct computation of the maximum loadability point by means of an optimization approach. The general formulation for this optimization approach is as follows [86, 95]:

$$\begin{aligned} \max \quad & \lambda \\ \text{s.t.} \quad & f_{PF}(x_{PF}, p_{PF}, \lambda) = 0 \\ & x_{PF_{min}} \leq x_{PF} \leq x_{PF_{max}} \\ & p_{PF_{min}} \leq p_{PF} \leq p_{PF_{max}} \\ & \lambda \geq 0 \end{aligned} \tag{2.15}$$

The system controllable parameters p_{PF}, such as PV bus voltage set points, are considered as variables in this formulation in order to improve the maximum loadability.

If the controllable parameters p_{PF} are fixed, (2.15) can be reformulated to compute the max-

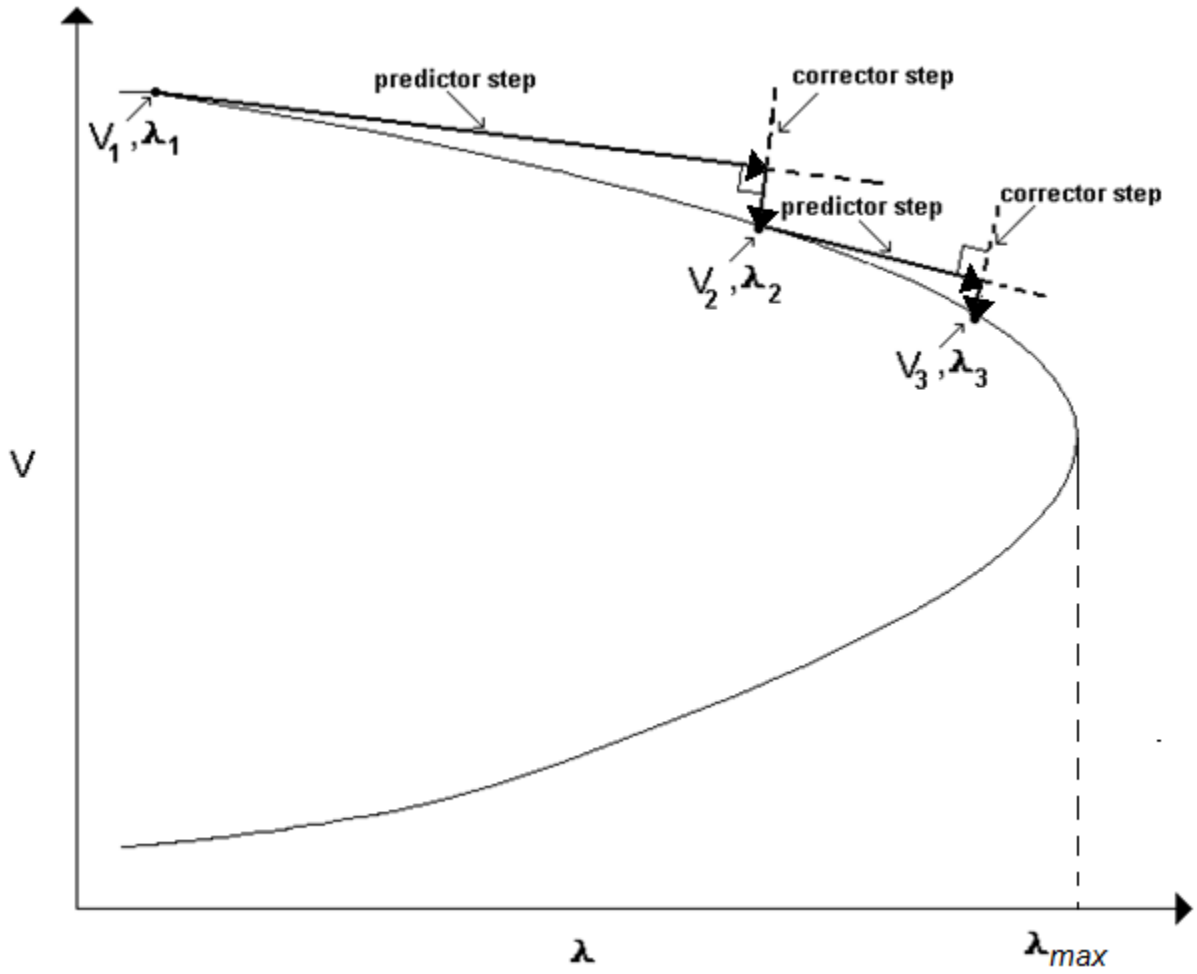

Figure 2.3: Perpendicular intersection technique for the correction step.

imum loadability due to saddle-node or limit-induced bifurcations [86, 95, 96].

The maximum loadability obtained using continuation power flow methods and direct methods may not be the same because of the particular treatment of voltage controlled buses used on each approach. In continuation power flow methods, the reference voltage at voltage-controlled buses are kept constant, unless a reactive power limit is violated. On the contrary, in typical direct methods, the voltage reference at voltage-controlled buses are allowed to change within limits [86, 96].

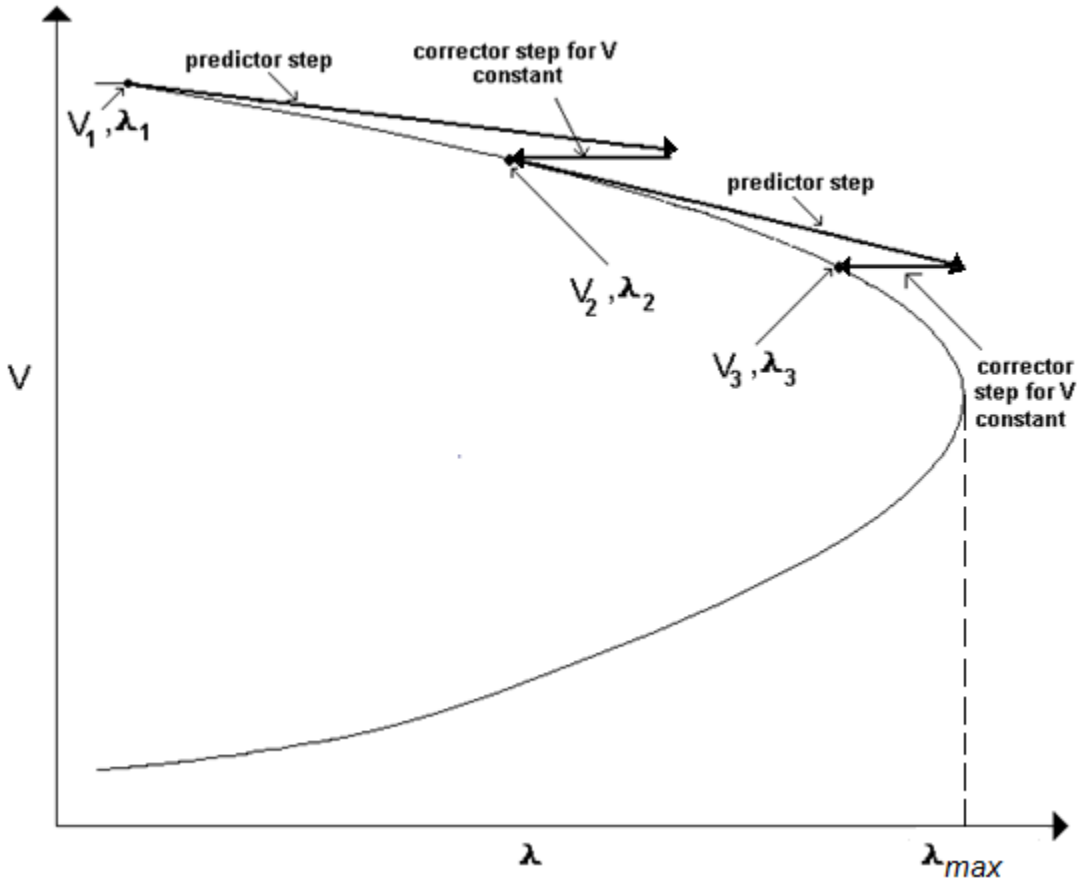

Figure 2.4: Parametrization technique for the correction step.

These and other tools are used by system operators and planners to guarantee the power system security, which is defined as the ability of the power system to withstand a set of realistic contingencies, without violating acceptable operating limits [97]. These contingencies may lead to changes in power flows and bus voltages that affect the system maximum loadabilities; thus, single-element and multiple-element contingencies are used by system planners and operators to guarantee the system well-being. Typically an N-1 contingency criterion is used to analyze the system and prevent insecure operation; this criterion states that for any single component failure of a system with n components, the system can still reliably operate. However, multiple

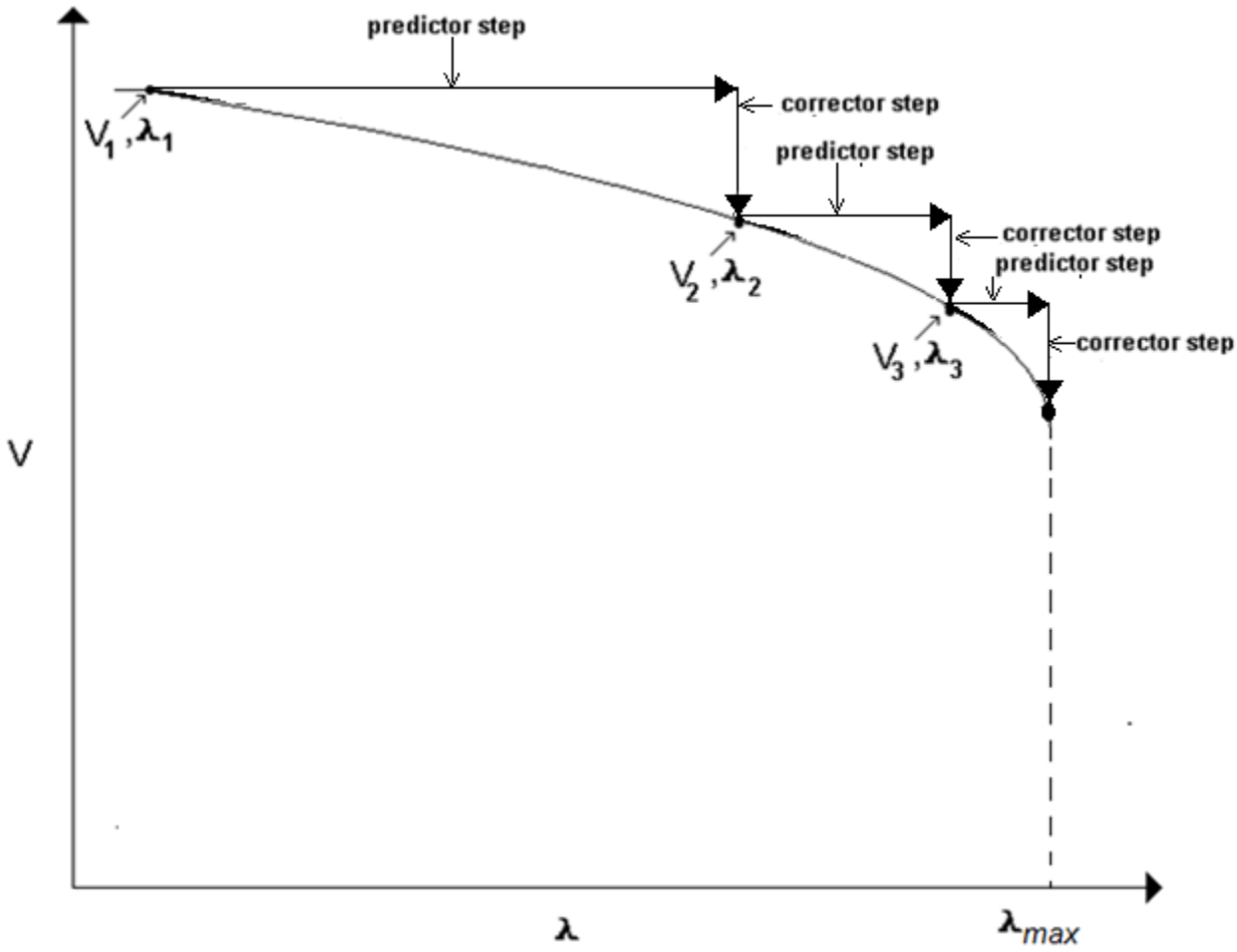

Figure 2.5: Conventional power flow technique.

contingencies that are likely to occur are also considered. One important concept used to securely operate the system is the Available Transfer Capability (ATC), which is described next:

Available Transfer Capability

Transfer capability refers to the ability of the power system to reliably transfer power between two areas [98]. These areas may be those formed by individual electric systems, power pools,

control areas, or subregions. The Available Transfer Capability is computed as follows [98]:

$$\text{ATC=TTC-TRM-ETC-CBM} \tag{2.16}$$

where:

- TTC or Total Transfer Capability is the maximum loadability of the system, defined as the minimum of the thermal, voltage or stability limits for the worst N-1 contingency.
- TRM or Transmission Reliability Margin takes into account uncertainties associated with other contingencies and is usually assigned a fixed value, as a percentage of the TTC, or computed using probabilistic methods.
- ETC or Existing Transmission Commitments denotes the current power transferred between the concerned areas.
- CBM or Capacity Benefit Margin is the reserve required by load-serving entities to meet their generation reliability requirements.

2.2.3 Transient Stability

Transient stability deals with ability of the power system to remain in synchronism when subjected to large and sudden disturbances [88]. The severity of this disturbance makes it impossible to linearize the system dynamic model equations; thus, in practical systems, numerical analysis techniques are commonly used to solve the corresponding nonlinear equations.

The general form for the nonlinear Differential Algebraic Equations (DAEs) that describe the system behavior is as follows [99–106]:

$$\dot{x_D}(t) = f_D(x_D, y, p_D, \lambda) \quad \text{for} \quad x_D(0) = x_{D_{IC}} \tag{2.17}$$

$$0 = g(x_D, y, p_D, \lambda) \quad \text{for} \quad y(0) = y_{IC} \tag{2.18}$$

where x_D represents the state variables such as generator internal angles and speeds; y refers to algebraic variables such as static load voltages and angles; p_D stands for controllable parameters

such as AVR set points; and λ represents uncontrollable parameters such as load levels. A different set of (2.17) and (2.18) is needed when a discrete variable change occurs, which corresponds to discontinuities in the algebraic variables associated with limits and external disturbances. For instance, when a transmission line is tripped, at the instant of line trip there is a discontinuity, with the algebraic variables showing instantaneous step changes, while the state variables remain unchanged.

The network model can be written in terms of algebraic equations for power balance or in terms of algebraic equations for current balance. The complex power balance model has the following form:

$$\overline{S}(x_D, y, p_D, \lambda) - \overline{V}\,\overline{Y}^*(x_D, y, p_D)\overline{V}^* = 0 \tag{2.19}$$

On the other hand, the current balance form is obtained by dividing both sides of the previous equation by $\overline{V}$, and taking the complex conjugate, which results in:

$$\overline{I}(x_D, y, p_D, \lambda) - \overline{Y}^*(x_D, y, p_D)\overline{V}^* = 0 \tag{2.20}$$

Depending on the study, the loads could be treated as constant power or constant impedance loads. The former is suitable for simulation times less than the under load tap changer time constants, and the latter is used for long-term stability studies where the effect of load tap changers is important.

There are different approaches for the numerical solution of these DAEs. These approaches are generally classified into two main groups, namely partitioned and simultaneous approaches, as described next.

Partitioned Approach [100–102]

The general procedure of the partitioned approach requires finding the exact solution of the algebraic equations and then using this solution to numerically integrate the differential equations. The solution of the differential equations is then used to solve the algebraic equations again and the cycle is repeated until the stopping criterion is met. In this procedure, there is a delay between

the algebraic equations and the differential equation solutions. In order to overcome this delay, an iterative partitioned approach is used, which is based on the reintegration of the differential equations at each time step until convergence of all variables is achieved. With the aim of reducing the computational cost that involves the exact solution of the algebraic equations at each reintegration step, extrapolated values for the solution of the algebraic equations are generally used. Moreover, further simplifications are achieved if a single iteration for the differential and algebraic equation solutions is taken per cycle.

The most evident advantage of the partitioned approach is the possibility of choosing different methods for solving the differential and the algebraic equations. Thus, the approach can be applied either to implicit or explicit integration methods. In the implicit integration methods, the differential equations are algebraized and then solved as a whole, while in the explicit integration methods, each differential equation is individually solved.

Simultaneous Approach [100–102]

In the simultaneous approach, all the equations, namely differential and algebraic equations are simultaneously solved. Therefore, a single numerical method is used together with an implicit integration method. The main advantage of the simultaneous approach is the elimination of the computation delay between the algebraic and the differential equations at the cost of a lower computational speed when compared to the partitioned approach. However, superior numerical stability is achieved.

Numerical Methods for Integration

The available numerical methods for solving the set of DAEs offer differing advantages and disadvantages in terms of complexity and numerical stability. Numerical stability is a measure of the ability of the method to avoid error accumulation over the whole process. These errors can originate from truncation, roundoff, finite time increments or specific errors introduced by the method itself. The impact of these errors on the accuracy of the final results is highly dependent on the system stiffness, which refers to the ratio of the maximum and minimum time constants of the model [100–102]. For systems with high stiffness, numerical integration methods with

low numerical stability produce inaccurate results, unless the integration time step is sufficiently small. If an integration method with a better numerical stability is used, the error propagation is not as much as for a method with lower numerical stability and, thus, the integration time step can be increased.

Some of the most common explicit integration methods used in transient stability analysis are the Euler methods, while one of the most common implicit integration method is the trapezoidal method. Since the trapezoidal method offers good numerical stability, it is used in this thesis to formulate the proposed AA-based transient stability method. This method is based on an approximated solution of the integrals by means of trapezoids whose areas can be readily calculated [99, 101]. A graphical representation of this method is depicted in Figure 2.6 where the definite integral between t_o and t_1 is approximated by the area of the corresponding trapezoid; the same applies for the definite integral between t_1 and t_2 and so on. Thus, the trapezoidal method yields the following numerical discrete solution for (2.17) and (2.18):

$$x_{D_n} - x_{D_{n-1}} - (\Delta t/2)(f_D(x_{D_{n-1}}, y_{n-1}, p_D, \lambda, t_{n-1}) + f_D(x_{D_n}, y_n, p_D, \lambda, t_n)) = 0 \tag{2.21}$$

$$g(x_{D_n}, y_n, p_D, \lambda) = 0 \tag{2.22}$$

In this case, the solution for x_{D_n} and y_n not only depends on the solution at the previous time instant $x_{D_{n-1}}$ and y_{n-1}, but also on x_{D_n} and y_n themselves. Thus, the Newton method is used to iteratively solve the resultant system of equations. This approach facilitates the handling of DAE models, since all nonlinear equations can be solved simultaneously.

2.3 Self-validated Numerical Methods for Uncertainty Analysis

Self-validated numerical methods are numerical methods that automatically keep track of the sources of error in such a way that the computed variables are bounded [107, 108]. These sources

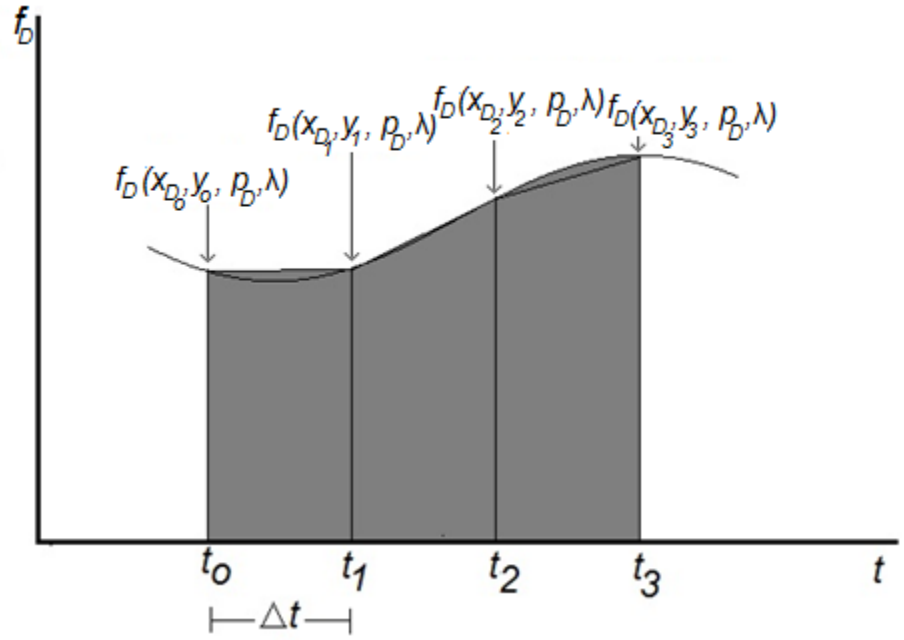

Figure 2.6: Trapezoidal method.

of error can be internal or external. The external sources of error typically correspond to measurement errors or uncertainties, while the internal sources of error are introduced within the computation itself, such as errors caused by truncated series, rounded arithmetic, finite steps, etc. The term self-validated refers to the fact that all sources of error are taken into account in the process of computing the variables, yielding guaranteed enclosures for these variables. These enclosures are obtained after computations are performed; thus, they are initially unknown. Two self-validated numerical methods are described next in this section, namely, Interval Arithmetic and Affine Arithmetic.

2.3.1 Interval Arithmetic

Interval Arithmetic defines the real variables as intervals of floating point numbers [107]. The main mathematical operations and functions can be applied to these intervals, resulting in new

intervals that enclose the output variables. The mathematical formulation for the intervals is as follows:

$$\bar{u} = [u_{min}\ , u_{max}] \qquad \{u \in R : u_{min} \leq u \leq u_{max}\} \tag{2.23}$$

The bounds u_{min} and u_{max} can be infinite.

The basic operations of addition, subtraction, multiplication, and division are straightforward in IA. these are based on finding the maximum and minimum values for the output intervals as follows:

$$\bar{u}_A + \bar{u}_B = [u_{A_{min}}, u_{A_{max}}] + [u_{B_{min}}, u_{B_{max}}] = [u_{A_{min}} + u_{B_{min}}, u_{A_{max}} + u_{B_{max}}] \tag{2.24}$$

$$\bar{u}_A - \bar{u}_B = [u_{A_{min}}, u_{A_{max}}] + [u_{B_{min}}, u_{B_{max}}] = [u_{A_{min}} - u_{B_{max}}, u_{A_{max}} - u_{B_{min}}] \tag{2.25}$$

$$\bar{u}_A \bar{u}_B = [u_{A_{min}}, u_{A_{max}}] \times [u_{B_{min}}, u_{B_{max}}] = [up_{min}, up_{max}] \tag{2.26}$$

where:

$$up_{min} = min\{u_{A_{min}}u_{B_{min}}, u_{A_{min}}u_{B_{max}}, u_{A_{max}}u_{B_{min}}, u_{A_{max}}u_{B_{max}}\}$$

$$up_{max} = max\{u_{A_{min}}u_{B_{min}}, u_{A_{min}}u_{B_{max}}, u_{A_{max}}u_{B_{min}}, u_{A_{max}}u_{B_{max}}\}$$

And:

$$\frac{\bar{u}_A}{\bar{u}_B} = \frac{[u_{A_{min}}, u_{A_{max}}]}{[u_{B_{min}}, u_{B_{max}}]} = [ud_{min}, ud_{max}] \tag{2.27}$$

where:

$$ud_{min} = min\left\{\frac{u_{A_{min}}}{u_{B_{min}}}, \frac{u_{A_{min}}}{u_{B_{max}}}, \frac{u_{A_{max}}}{u_{B_{min}}}, \frac{u_{A_{max}}}{u_{B_{max}}}\right\}$$

$$ud_{max} = max\left\{\frac{u_{A_{min}}}{u_{B_{min}}}, \frac{u_{A_{min}}}{u_{B_{max}}}, \frac{u_{A_{max}}}{u_{B_{min}}}, \frac{u_{A_{max}}}{u_{B_{max}}}\right\}$$

These operations can be coded for use in various applications, considering particular cases where the bounds for $\bar{u}_A$ or $\bar{u}_B$ are defined by infinite or zero values. The volume of computations for multiplication and division can be reduced by coding a routine that checks the signs of the bounds.

Some of the monotonic mathematic functions such as logarithms, exponential, and square roots are also simple to implement in IA. The only consideration that is usually required is the filtering of the input intervals according to the domains associated with each function. Particular attention should be paid to sinusoidal functions, which can be non-monotonic depending on the interval selected. For intervals where the function is non-monotonic, the local minimum and maximum have to be found, whereas, for monotonic intervals, the minimum and maximum are located at the end-points.

The main drawback of IA is the representation of the variables as independent intervals. This issue is commonly referred to as the dependency problem, and is the main factor leading to excessively conservative results, which can be impractical in many applications. This problem is accentuated when there is a long chain of operations involved. In this case, IA is prone to produce error explosion at the final calculation of the chain. Some measures can be useful in some cases to avoid error explosion; for instance, long operation chains can be rearranged in the most efficient way in order to produce thinner intervals, and, interval splitting can also be applied. However, these measures become more difficult to implement when the operation chain length increases.

2.3.2 Affine Arithmetic

Affine Arithmetic is a numerical analysis technique where the variables of interest are represented as affine combinations of data uncertainties and/or approximation errors. AA was proposed in [107, 108], and a similar approach was previously proposed in [109]. It is intended to reduce the excessively conservative width of the output intervals that arise in some cases by IA. This interval width reduction is achieved in AA by tracking the correlation between the computed quantities, which is not possible in IA. However, AA requires more complex operations and larger computational cost than IA [107, 108].

Affine forms are characterized by a linear equation which has the following general expression [107, 108]:

$$\widehat{u} = u_o + u_1\varepsilon_{u_1} + u_2\varepsilon_{u_2} + ... + u_{nu}\varepsilon_{u_{nu}} \tag{2.28}$$

The noise symbol coefficients $u_1, u_2, ..., u_{nu}$ are calculated as the partial derivatives of the variable u with respect to each of the independent components associated with the noise symbols $\varepsilon_{u_1}, \varepsilon_{u_2}, ..., \varepsilon_{u_{nu}}$. By definition, the noise symbols can vary within the interval [-1, 1].

In general, affine forms for the different variables under study can fully or partially share the noise symbols. This characteristic allows reduction of the width of the AA output intervals when compared to IA-based methods. However, AA-based techniques deal with the issue of approximating nonlinear functions by adding an independent noise symbol representing the error of the approximation. Since most of the applications in power system analysis deal with long chains of nonlinear operations such as multiplications and sinusoidal functions, the next sections focus on the approximation methods of the affine representation of these non-affine operations, presenting some basic affine operations.

Sum of Affine Forms

The summation or subtraction of two affine forms given by $\widehat{u}_A = u_{A_o} + u_{A_1}\varepsilon_{A_1} + u_{A_2}\varepsilon_{A_2} + ... + u_{A_{na}}\varepsilon_{A_{na}}$ and $\widehat{u}_B = u_{B_o} + u_{B_1}\varepsilon_{B_1} + u_{B_2}\varepsilon_{B_2} + ... + u_{B_{nb}}\varepsilon_{B_{nb}}$ is defined as:

$$\widehat{u} = \widehat{u}_A \pm \widehat{u}_B = u_{A_o} \pm u_{B_o} \pm \sum_{ra=1}^{na}(u_{A_{ra}}\varepsilon_{A_{ra}}) \pm \sum_{rb=1}^{nb}(u_{B_{rb}}\varepsilon_{B_{rb}}) \tag{2.29}$$

If the considered affine forms $\widehat{u}_A$ and $\widehat{u}_B$ share all the noise symbols, (2.29) can be simplified as follows:

$$\widehat{u} = \widehat{u}_A \pm \widehat{u}_B = u_{A_o} \pm u_{B_o} + \sum_{ra=1}^{na}\left[\left(u_{A_{ra}} \pm u_{B_{ra}}\right)\varepsilon_{A_{ra}}\right] \tag{2.30}$$

Multiplication of Affine Forms

The multiplication of two affine forms $\widehat{u}_A = u_{A_o} + u_{A_1}\varepsilon_{A_1} + u_{A_2}\varepsilon_{A_2} + ... + u_{A_{na}}\varepsilon_{A_{na}}$ and $\widehat{u}_B = u_{B_o} + u_{B_1}\varepsilon_{B_1} + u_{B_2}\varepsilon_{B_2} + ... + u_{B_{nb}}\varepsilon_{B_{nb}}$ is given by:

$$\widehat{u} = \widehat{u}_A\widehat{u}_B = u_{A_o}u_{B_o} + \sum_{rb=1}^{nb}(u_{A_o}u_{B_{rb}})\varepsilon_{B_{rb}} + \sum_{ra=1}^{na}(u_{B_o}u_{A_{ra}})\varepsilon_{A_{ra}} + \sum_{ra=1}^{na}\sum_{rb=1}^{nb}u_{A_{ra}}u_{B_{rb}}\varepsilon_{A_{ra}}\varepsilon_{B_{rb}} \tag{2.31}$$

This multiplication operation produces quadratic terms for the noise symbols which make u a non-affine form. This issue is solved by means of two commonly adopted approaches: the Chebyshev approximation and the trivial approximation [107, 108, 110, 111]. The Chebyshev approximation produces the highest accuracy with a high computational cost, while the trivial approximation is computationally efficient, but exhibits a higher error.

Chebyshev Approximation [110]

Chebyshev approximations for the multiplication of $\widehat{u}_A$ and $\widehat{u}_B$ are based on finding the best affine approximation for the quadratic terms $\sum_{ra=1}^{na}\sum_{rb=1}^{nb}u_{A_{ra}}u_{B_{rb}}\varepsilon_{ra}\varepsilon_{rb}$. This approximation, denoted by Ψ_{Ch}, can be written as:

$$\widehat{\Psi}_{Ch} = \frac{U_{max} + U_{min}}{2} + \frac{U_{max} - U_{min}}{2}\varepsilon_{\xi} \tag{2.32}$$

where U_{max} and U_{min} are the bounds of the product of the zero centered affine forms $\widehat{K}_A = \widehat{u}_A - u_{A_o}$ and $\widehat{K}_B = \widehat{u}_B - u_{B_o}$. The computation of U_{max} and U_{min} is not straightforward, as it requires the tracking of the extreme values across the edges and intersection points of a convex polygon, representing the bounded domain of the affine forms $\widehat{K}_A$ and $\widehat{K}_B$. Thus, Figure 2.7 shows an example of a convex polygon that bounds the joint combination of affine forms $\widehat{u}_A$ and $\widehat{u}_B$. The number of edges E is at most $2m_A + 4$; hence, the greater the number of shared noise symbols between $\widehat{u}_A$ and $\widehat{u}_B$, the longer is the computation time required to numerically obtain U_{min} and U_{max}.

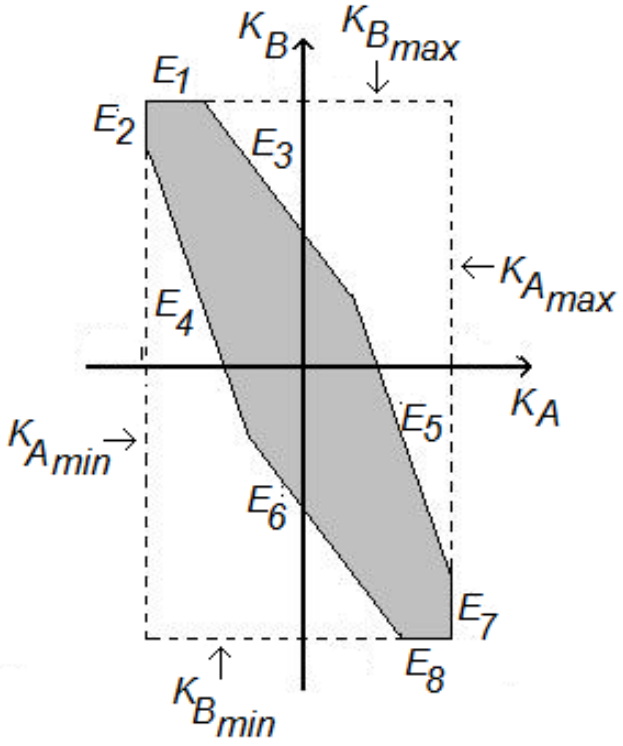

Figure 2.7: Convex polygon defining the bounds of $\widehat{K}_A$ and $\widehat{K}_B$ bounds for $m_A = 4$.

Trivial Affine Approximation

The trivial affine approximation is the most computationally efficient method to approximate the multiplication of two affine forms; however, it is not as accurate as the Chebyshev approximation. According to this method, the quadratic terms are conservatively approximated as follows [107, 108]:

$$\sum_{ra=1}^{na}\sum_{rb=1}^{nb} u_{A_{ra}} u_{B_{rb}} \varepsilon_{A_{ra}} \varepsilon_{B_{rb}} \simeq \left(\sum_{ra=1}^{na} \|u_{A_{ra}}\|\right)\left(\sum_{rb=1}^{nb} \|u_{B_{rb}}\|\right)\varepsilon_{\xi} \tag{2.33}$$

By substituting (2.33) into (2.31) one gets:

$$\widehat{u} = \widehat{u}_A \widehat{u}_B = u_{A_o} u_{B_o} + \sum_{rb=1}^{nb} (u_{A_o} u_{B_{rb}}) \varepsilon_{B_{rb}} + \sum_{ra=1}^{na} (u_{B_o} u_{A_{ra}}) \varepsilon_{A_{ra}} + \left(\sum_{ra=1}^{na} \|u_{A_{ra}}\| \right) \left(\sum_{rb=1}^{nb} \|u_{B_{rb}}\| \right) \varepsilon_{\xi} \quad (2.34)$$

As in the previously studied approximations, the new noise symbol ε_{ξ} is independent of the original noise symbols and can exhibit a maximum error four times greater than the error given by the Chebyshev approximation [107, 108].

Various approaches seeking to improve the accuracy of the trivial approximation are reported in [111]. For instance, the so called quadratic form is based on the inclusion of new quadratic noise symbols into the trivial affine approximation. These new quadratic noise symbols improve the accuracy of the approximations; however, the computational efficiency is reduced compared to the trivial affine approximation. Since the trivial affine approximation offers a good trade off between accuracy and computational cost, this approach is used in this thesis to approximate the multiplication of affine forms.

Chebyshev Orthogonal Polynomial-Based Approximations

Sine and cosine functions as well as other non-affine functions such as exponential functions are approximated in this thesis using a series of Chebyshev orthogonal polynomials as follows:

$$Hc(z_{ch}) = \sum_{rh=0}^{np} b_{rh} T_{rh}(z_{ch}) \quad (2.35)$$

where the Chebyshev polynomials $T_{rh}(z_{ch})$ are computed using the following recurrence relation [112]:

$$\begin{aligned} T_0(z_{ch}) &= 1 \\ T_1(z_{ch}) &= z_{ch} \\ T_{rh+1}(z_{ch}) &= 2 z_{ch} T_{rh}(z_{ch}) - T_{rh-1}(z_{ch}) \end{aligned} \quad (2.36)$$

The number of polynomials np in (2.35) are truncated, depending on the number of digit

accuracy. Thus, for 5-digit accuracy, as in this thesis, the error of the Chebyshev approximation is 10^{-5}. This error is attributed to the truncation of the Chebyshev series only. Because the polynomials of this approximation involves non-affine operations, additional errors are introduced [108]; therefore, the final affine forms of the sine and cosine operations exhibit errors greater than those attributed to the Chebyshev approximations only.

2.4 Monte Carlo Simulations

MCS refers to the repetitive evaluation of deterministic problems such as mathematical expressions or physical models by sampling random variables [113,114]. This method has been applied in many fields such as optimization, evaluation of definite integrals, estimation of statistical parameters, and in general, in problems where an analytical solution is intractable. One of the advantages of MCS is their ability to model system complexities subjected to many uncertainties, which are modeled using pdfs. The pdfs are sampled to evaluate deterministic models, and the obtained results are lumped in order to compute parameters such as mean and variance of the concerned variables, and/or obtain their corresponding pdfs, which provide information regarding the likeliness of a random variable to take on different values.

If a random variable is discrete, the pdf is referred to as discrete probability density function. In this case, the pdf of the different values of the discrete random variable are associated with a probability. On the other hand, if a random variable is continuous, the pdf is referred to as continuous probability density function, and the information regarding the probability of the random variable to lie within an interval is given by the integral of the associated pdf over this interval, as follows:

$$Prob[X_{fa} \leq X_f \leq X_{fb}] = \int_{X_{fa}}^{X_{fb}} P_{X_f}(x_f)\, dx_f \tag{2.37}$$

Besides the mean, variance and other statistical parameters, a qualitative analysis of the pdfs can be achieved computing their skewness and excess kurtosis. The skewness of a pdf is a measure of its asymmetry with respect to its mean value, and the excess kurtosis represents a measure of its peakiness.

Conventional MCS are used in this thesis as benchmark for comparison purposes, since by definition, it does not produce any spurious trajectories, and for a large enough number of trials, the union of the uncertainty region described by MCS is a very close approximation of the correct problem solution. To demonstrate its application in this thesis, an example of MCS for system stability analysis is presented next, based on the Power System Analysis Toolbox (PSAT) [115], which is used to perform stability studies with variable wind power generator in the IEEE 14-bus system shown in Figure 2.8. This benchmark system, described in detail in [116], comprises two synchronous generators connected at Buses 1 and 2, and three synchronous condensers connected at Buses 3, 6 and 8. The synchronous generator at Bus 2 is replaced by an aggregated DFIG-based wind turbine as shown in Figure 2.9, the transformers from 480 V to 25 kV, and from 25 kV to 69 kV, as well as the impedance of the collector system in a wind farm for better modelling accuracy. A brief description of the DFIG model and associated controls as well as the relevant system data can be found in [117]. For all simulations, the loads are modeled using exponential recovery models.

The wind speed distribution is modeled using the typical Rayleigh pdf used for these purposes, which is expressed in terms of the wind speed v and mean wind speed v_m as follows [118]:

$$P_{X_f}(v) = \frac{2v}{1.128 v_m e^{\frac{v}{1.128 v_m}^2}} \tag{2.38}$$

Figure 2.10 (a) shows the wind's pdf for a mean wind speed of 10 m/s. This function is used to approximate the stochastic nature of the considered wind speed. Figure 2.10 (b) shows the turbine output power as a function of the wind speed. The rated wind speed is 15 m/s, while the cut-in and cut-out wind speeds are 5 m/s and 25 m/s, respectively. When the wind speed is above the rated speed, the pitch angle controller comes into effect in order to maintain the output power constant at its rated value. Moreover, for wind speeds above the cut-out wind speed (which is not very likely according to Figure 2.10 (a)), the wind turbine is prevented from generating power in order to avoid any damage; and for wind speeds under 5 m/s, the wind power output is null.

Three study cases are presented and discussed here:

- In Case A, the maximum loadability variations of the above described system for the wind farm with terminal voltage control are assessed by using MCS.

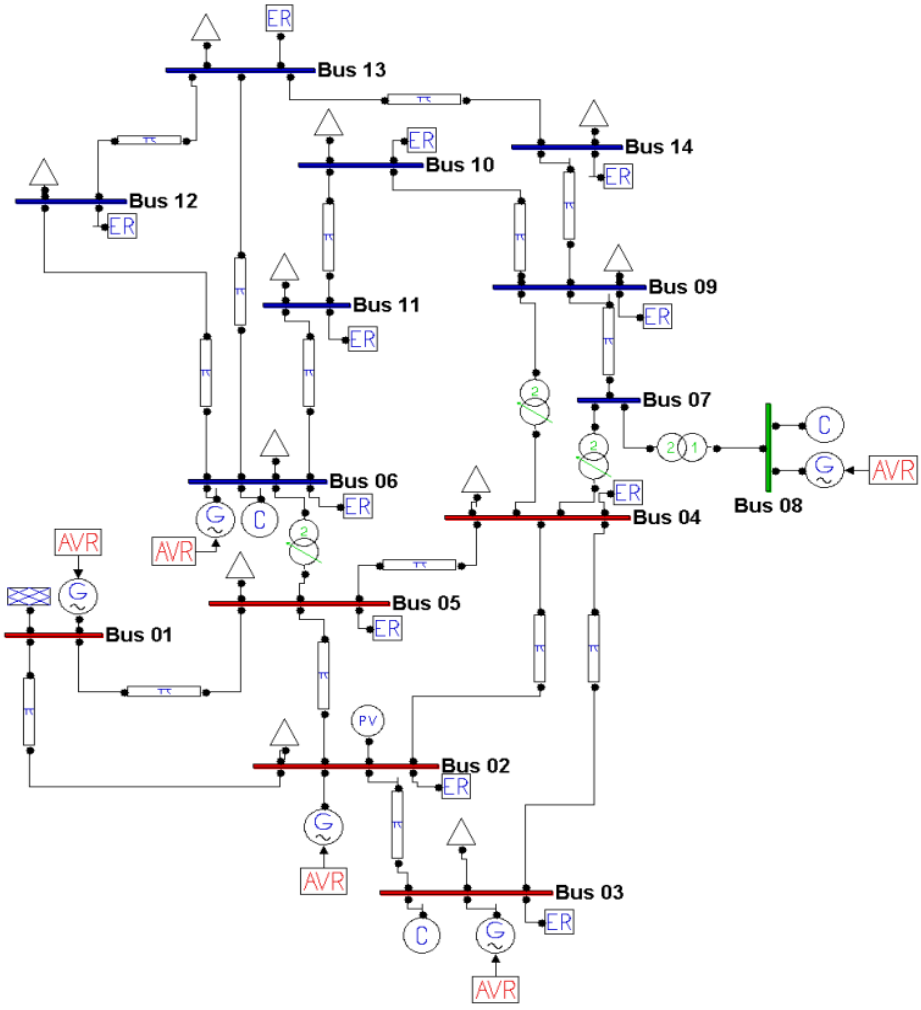

Figure 2.8: IEEE 14 bus system in PSAT.

- In Case B, MCS are used to compute the maximum system loadability variations for the wind farm with constant power factor mode.
- In Case C, the variations in the damping ratio of the dominant mode are assessed using MCS for the wind farm with terminal voltage control.

Normal and contingency operating conditions are considered in the above described cases. The

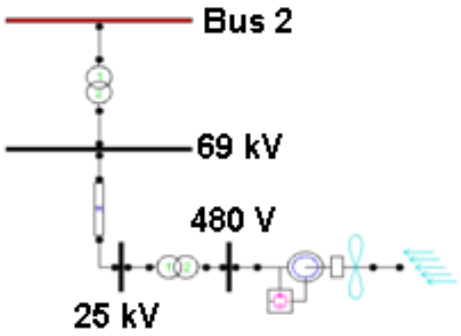

Figure 2.9: DFIG collector system in PSAT.

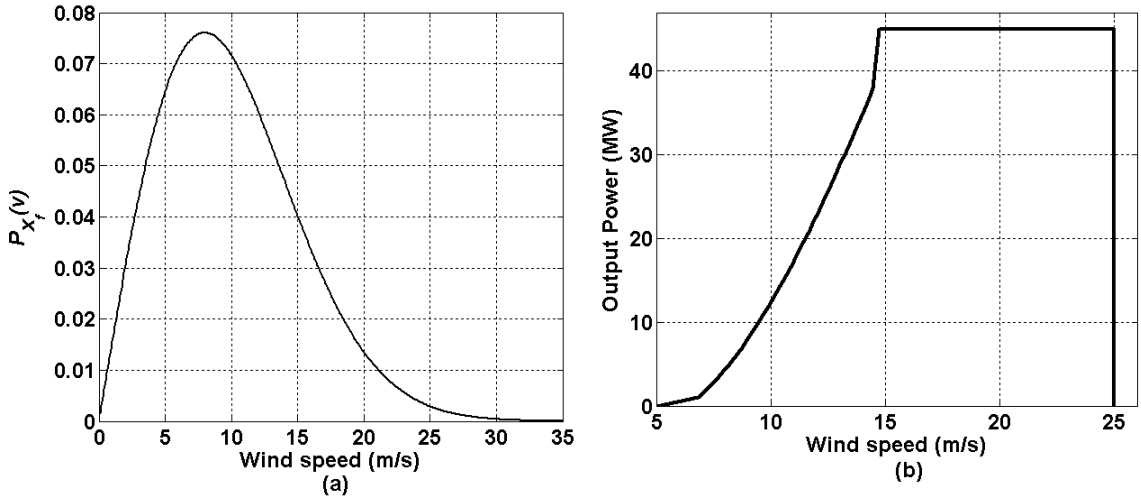

Figure 2.10: (a) Wind speed pdf and corresponding (b) power output characteristics of a wind turbine.

transmission line connected between Buses 2 and 4 is disconnected to simulate a contingency.

Case A:

The static load margins obtained using PV curves for the wind turbine in terminal voltage control mode are bounded by a minimum value of 424.92 MW and a maximum value of 431.46 MW, when the wind speed varies according to the specified pdf. The probabilities associated with

loading margins within these bounds are depicted in Figures 2.11 (a) and (b). The occurrence of these static load margins are associated with the probabilities of having a wind speed below the cut-in speed and above the cut out speed, and the probability of having a wind speed within the rated and cut-out speeds, respectively. When the line 2-4 is tripped, the static load margins lie in the interval of 387.88 MW and 383.32 MW for wind power output variations within 45 MW and 0 MW. The probabilities associated with loading margins within these bounds are illustrated in Figures 2.11 (c) and (d).

The observed pdf's peaks are due to the relatively high probabilities associated with having either zero output power for the wind farm (left peak) or nominal output power (right peak). This is mainly due to the Rayleigh pdf assumed to model the wind speed stochastic behavior, since according to this pdf, there exists a relatively high probability of having a wind speed below the cut-in wind speed or above the cut-out wind speed, and also a high probability associated with having a wind speed within the nominal speed and the cut-out wind speed. These heavy tailed distributions lead to a high kurtosis, which is 74.1e5 and 22.9e6 for normal and contingency conditions, respectively.

The mean and standard deviations for the maximum loadability in normal operating condition are 427.66 MW and 2.63 MW, respectively, with a skewness of 0.384. This positive skewness indicates that the distribution is more stretched on the side above the mean. For contingency conditions, the mean and standard deviations are 385.31 MW and 1.82 MW, respectively; the skewness in this case is 0.23, and thus the distribution is more stretched on the side above the mean.

Case B:

When the DFIG is operated at constant power factor mode, the static load margins in normal operating condition are within the interval given by [419.30, 424.11] MW, which is smaller than the system with voltage control wind turbine, as expected. Moreover, the static load margin interval is reduced even further under contingency conditions to the interval [378.7, 382.4 MW].

The pdfs and cdfs in this case are very similar to those shown in 2.11.

Case C:

Figure 2.12 (a) depicts the cdf of the dominant mode damping ratio under normal operating conditions for a loading level of 331.5 MW. Participation factors associated with this dominant mode, correspond to the AVR of the synchronous generator connected at Bus 1. When the wind power output varies within 0 MW and 45 MW, the dominant-mode damping ratio is bounded by the interval given by [1.12, 3.3]%; in this case, the probability of occurrence of a damping ratio lower or equal than 3% is approximately 0.82. On the other hand, the damping ratios under contingency conditions vary within the interval [0.59, 2.6]%; from Figure 2.12 (b), the probability of occurrence for a damping ratio lower than 2% is approximately 0.77.

Figure 2.13 (a) shows the trajectories for the dominant-mode damping ratios associated with the AVR of the synchronous generator connected at Bus 1. As the wind power output level increases, the damping ratio improves not only for normal operating conditions, but also for contingency conditions. Figure 2.13 (b) shows the eigenvalues associated with the rotor speed of the synchronous generator connected at Bus 1. In this case, the damping ratio decreases when the wind power output level rises; however, the minimum damping ratio is sufficiently large to assure system stability.

2.5 Summary

The basic tools for power flow, long-term voltage stability, and transient stability analysis have been briefly discussed in this chapter. Particularly, for voltage stability assessment, different strategies commonly used for the computation of the maximum loadability were presented, namely, direct methods and continuation power flow techniques. Also, the definitions associated with ATC computation were briefly discussed.

Relevant aspects concerning the formulation and solution of the DAEs that describe the system dynamics were also addressed in this chapter; specifically, the trapezoidal method was briefly described, this method offers good numerical stability and thus, is considered in this thesis for the formulation of the AA-based transient stability assessment.

Self-validated numerical methods for uncertainty analysis were presented as well. Specifically, the main characteristics of IA and AA were pointed out. It was explained that IA is characterized by its simplicity and low computational cost; however, its inability to properly represent the dependency among variables may lead to excessively conservative results making it impractical. On the other hand, AA was shown to represent the correlations among variables, which may lead to better results than IA; however, non-linear operations and functions in AA have to be approximated by means of affine forms, which affect its accuracy. In this regard, some of the available techniques intended to approximate non-affine operations and functions were discussed.

Finally, MCS were briefly discussed, and their application to voltage and transient stability assessment of a test system considering uncertainties associated with wind power generation was demonstrated.

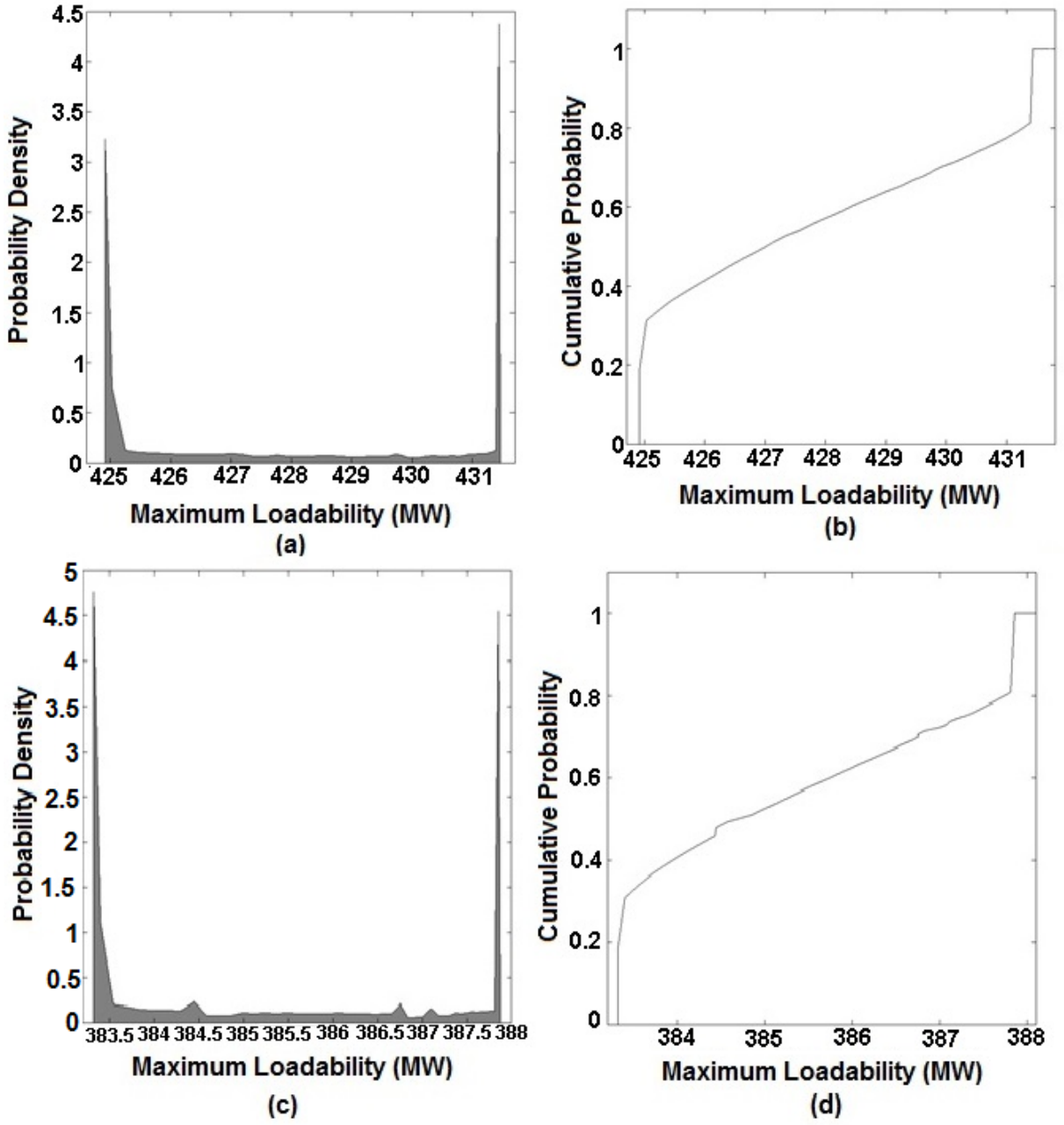

Figure 2.11: Pdfs and cdfs for the static load margins when the wind farm is operating in voltage control mode: (a) pdf and (b) cdf in normal operating conditions. (c) pdf and (d) cdf for a contingency.

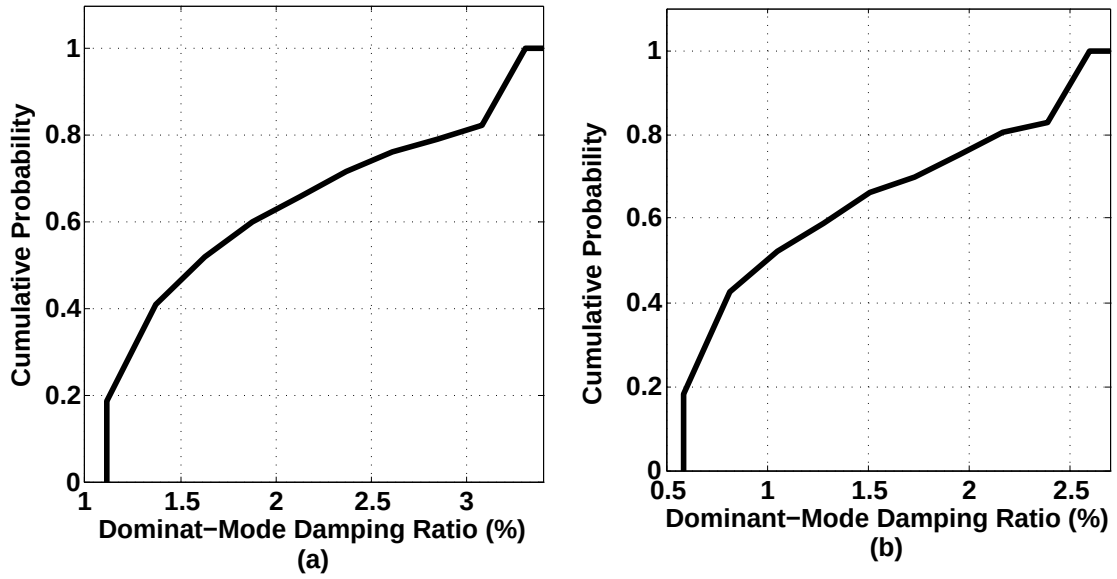

Figure 2.12: Cdfs of dominant-mode damping ratio for the DFIG wind turbine operating in voltage control mode: (a) normal operating conditions and (b) contingency conditions.

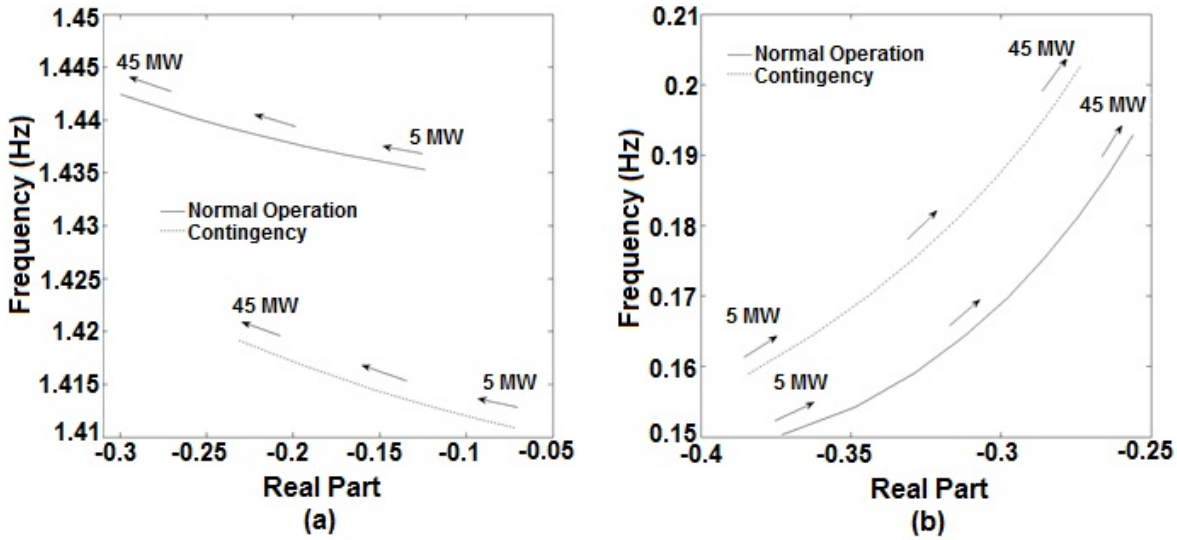

Figure 2.13: Eigenvalues for synchronous generator at Bus 1 for different wind power outputs when the DFIG is operated in voltage control mode: (a) AVR relevant modes and (b), rotor speed relevant modes.

Chapter 3

Affine Arithmetic Based Power Flow Assessment

3.1 Introduction

This chapter discusses the formulation of the AA-based power flow analysis method based on [14], proposing a novel modeling of reactive power limits. The power flow equations are formulated in both rectangular and polar form for comparison purposes, and simulations are carried out using the IEEE-30 Bus test system, and assuming uncertainties associated with loads and generation, which are modeled as intervals.

3.2 Problem Formulation

AA is used in [14] to solve the power flow problem considering uncertainties in the load and generation levels. According to this approach, the initial affine approximation for bus voltage magnitudes and angles can be written as follows:

- In polar form [14]:

$$\widehat{V_i} = V_{o_i} + \sum_{j \in N_P} \left.\frac{\partial V_i}{\partial P_j}\right|_o \Delta P_{A_j} \varepsilon_{P_j} + \sum_{j \in N_Q} \left.\frac{\partial V_i}{\partial Q_j}\right|_o \Delta Q_{A_j} \varepsilon_{Q_j} \qquad \forall i \in N_P \tag{3.1}$$

$$\widehat{\theta_i} = \theta_{o_i} + \sum_{j \in N_P} \left.\frac{\partial \theta_i}{\partial P_j}\right|_o \Delta P_{A_j} \varepsilon_{P_j} + \sum_{j \in N_Q} \left.\frac{\partial \theta_i}{\partial Q_j}\right|_o \Delta Q_{A_j} \varepsilon_{Q_j} \qquad \forall i \in N_P,\ N_Q \tag{3.2}$$

- In rectangular form (new):

$$\widehat{V_{Ri}} = V_{R_{o_i}} + \sum_{j \in N_P} \left.\frac{\partial V_{R_i}}{\partial P_j}\right|_o \Delta P_{A_j} \varepsilon_{P_j} + \sum_{j \in N_Q} \left.\frac{\partial V_{R_i}}{\partial Q_j}\right|_o \Delta Q_{A_j} \varepsilon_{Q_j} \qquad \forall i \in N_P,\ N_Q \tag{3.3}$$

$$\widehat{V_{Ii}} = V_{I_{o_i}} + \sum_{j \in N_P} \left.\frac{\partial V_{I_i}}{\partial P_j}\right|_o \Delta P_{A_j} \varepsilon_{P_j} + \sum_{j \in N_Q} \left.\frac{\partial V_{I_i}}{\partial Q_j}\right|_o \Delta Q_{A_j} \varepsilon_{Q_j} \qquad \forall i \in N_P,\ N_Q \tag{3.4}$$

The number of noise symbols in (3.1) to (3.4) depends on the number of uncertainties to be analyzed. For instance, if only uncertainties of generation outputs are considered, the number of noise symbols will be restricted to the number of generators. It is important to point out that correlations amongst generators, as in the case of close-by wind farms, can be easily represented in (3.1) to (3.4) by means of a single noise symbol associated with the correlated variations of power of these wind farms. The coefficients of the noise symbols, given by the derivatives of voltage magnitudes and angles with respect to the injected active and reactive power, can be calculated by using the Jacobian matrix or numerical sensitivity studies. These derivatives are evaluated at the central values of the active and reactive powers injected at PQ buses and the active powers injected at PV buses, which are defined as follows:

$$P_{o_i} = \frac{P_{G_{max_i}} - P_{L_{max_i}} + P_{G_{min_i}} - P_{L_{min_i}}}{2} \qquad \forall i \in N_P \tag{3.5}$$

$$Q_{o_i} = \frac{Q_{G_{max_i}} - Q_{L_{max_i}} + Q_{G_{min_i}} - Q_{L_{min_i}}}{2} \qquad \forall i \in N_Q \tag{3.6}$$

The prediction intervals used to model the uncertainty associated with the predicted values can be obtained by using non-parametric approaches, which do not need any assumptions regarding the pdf of forecast errors and thus, are very appropriate to compute the intervals of the

uncertainties associated with intermittent renewable energy sources [119]. These intervals are associated with a confidence level; thus, depending on this confidence level, parts of the possible outcomes of the uncertain variables are necessarily neglected. Parametric approaches can also be used to compute the bounds associated with the forecasting uncertainty [120]; however, these methods rely on assumptions regarding the pdfs of the forecasting errors that may be unrealistic in some cases. Since in this thesis, the uncertain variables are modeled as prediction intervals, the expected predictions are not relevant.

Numerical sensitivity studies are used in this thesis to obtain an approximation of the derivatives in (3.1) to (3.4), using a small perturbation of the system around the central values of the uncertain parameters and then solving the standard power flow problem to compute the corresponding changes in the respective variables. This requires as many power flow solutions as uncertain variables, which in the case of large wind and solar power plants, are not many. Computing the changes to approximate derivatives leads to more accurate results than using the Jacobian matrix, where the derivatives are evaluated at the central values.

The numerical sensitivity approach yields initial approximations for the affine forms of the power flow variables. In order to compute the final affine forms and their associated bounds, the initial affine approximations obtained using the sensitivity approach are corrected based on the solution of the Linear Programming (LP) problems described later in this Chapter. These LP problems account for the physical restrictions imposed by the power flow equations, generator limits, as well as the bounds of the noise symbols. Also, aimed at accounting for the nonlinearities of the power flow equations, additional noise symbols are introduced by the approximation of non-affine operations [107]. Thus, the resultant final affine forms are different to the initial approximations obtained using the sensitivity approach.

The active and reactive power affine forms $\widehat{P_i}$ and $\widehat{Q_i}$ are obtained by replacing the voltage and angle affine forms given in (3.1) and (3.2) in the following equations:

$$\widehat{P_i} = \sum_{j=1}^{N} \widehat{V_i}\widehat{V_j}\left[G_{ij}\cos(\widehat{\theta_i} - \widehat{\theta_j}) + B_{ij}\sin(\widehat{\theta_i} - \widehat{\theta_j})\right] \quad \forall i \in N_P \tag{3.7}$$

$$\widehat{Q_i} = \sum_{j=1}^{N} \widehat{V_i}\widehat{V_j}\left[G_{ij}\sin(\widehat{\theta_i} - \widehat{\theta_j}) - B_{ij}\cos(\widehat{\theta_i} - \widehat{\theta_j})\right] \quad \forall i \in N_Q \tag{3.8}$$

Alternatively, the power flow equations in rectangular coordinates can be written as follows:

$$\widehat{P}_{r_i} = \sum_{j=1}^{N} \left(\widehat{V}_{R_i} \left(\widehat{V}_{R_j} G_{ij} - \widehat{V}_{I_j} B_{ij} \right) + \widehat{V}_{I_i} \left(\widehat{V}_{I_j} G_{ij} + \widehat{V}_{R_j} B_{ij} \right) \right) \quad \forall i \in N_P \tag{3.9}$$

$$\widehat{Q}_{r_i} = \sum_{j=1}^{N} \left(\widehat{V}_{I_i} \left(\widehat{V}_{R_j} G_{ij} - \widehat{V}_{I_j} B_{ij} \right) - \widehat{V}_{R_i} \left(\widehat{V}_{I_j} G_{ij} + \widehat{V}_{R_j} B_{ij} \right) \right) \quad \forall i \in N_Q \tag{3.10}$$

The affine forms for the active (3.7) or (3.9), and reactive powers (3.8) or (3.10) exhibit the following compact form, after all affine functions operations and approximations:

$$A\varepsilon = C \tag{3.11}$$

$$C = L - (R_o + q) \tag{3.12}$$

The maximum and minimum values of C are given by the corresponding maximum and minimum values of active and reactive power injections as follows:

$$C_{max} = L_{max} - R_o + |q| \tag{3.13}$$

$$C_{min} = L_{min} - R_o - |q| \tag{3.14}$$

where:

$$L_{max} = \begin{bmatrix} P_{max} \\ Q_{max} \end{bmatrix} \tag{3.15}$$

$$L_{min} = \begin{bmatrix} P_{min} \\ Q_{min} \end{bmatrix} \tag{3.16}$$

$$P_{max} = P_{G_{max}} - P_{L_{min}} \tag{3.17}$$

$$P_{min} = P_{G_{min}} - P_{L_{max}} \tag{3.18}$$

$$Q_{max} = Q_{G_{max}} - Q_{L_{min}} \tag{3.19}$$

$$Q_{min} = Q_{G_{min}} - Q_{L_{max}} \tag{3.20}$$

Equation (3.11) is a linear system, which can be solved for ε by means of the two following LP problems:

$$\begin{aligned} \min \quad & \sum \varepsilon_{sl_{min}} \\ \text{s.t.} \quad & -1 \leq \varepsilon_{sl_{min}} \leq 1 \\ & C_{min} \leq A\varepsilon \leq C_{max} \\ & \forall sl \in N_P,\ N_Q \end{aligned} \tag{3.21}$$

$$\begin{aligned} \max \quad & \sum \varepsilon_{sl_{max}} \\ \text{s.t.} \quad & -1 \leq \varepsilon_{sl_{max}} \leq 1 \\ & C_{min} \leq A\varepsilon \leq C_{max} \\ & \forall sl \in N_P,\ N_Q \end{aligned} \tag{3.22}$$

The values obtained for $\varepsilon_{sl_{min}}$ and $\varepsilon_{sl_{max}}$ from these solutions are used in (3.1) and (3.2), or alternatively in (3.3) and (3.4), to calculate the minimum and maximum voltage magnitudes and angles, respectively. A contraction domain technique is proposed in [14] to produce narrower intervals for the voltage and angle bounds. According to this formulation, the two optimization approaches are consecutively repeated and the coefficients for the voltage and angle affine forms are contracted at each iteration until convergence is achieved.

After the voltage and angle bounds are computed, the interval of maximum and minimum reactive powers generated at the PV buses and slack bus can be calculated as follows, in order to verify any limit violations,

$$Q_{G_{max_i}} = qp_{o_i} + \sum_{sl \in N_p} qp_{i_{sl}} \varepsilon_{sl_{max}} + \sum_{sl \in N_q} qq_{i_{sl}} \varepsilon_{sl_{max}} + |qe_i| \varepsilon_{h_i} + Q_{L_{max_i}} \qquad \forall i = 1, ...N_{PV} + 1 \quad (3.23)$$

$$Q_{G_{min_i}} = qp_{o_i} + \sum_{sl \in N_p} qp_{i_{sl}} \varepsilon_{sl_{min}} + \sum_{sl \in N_q} qq_{i_{sl}} \varepsilon_{sl_{min}} - |qe_i| \varepsilon_{h_i} + Q_{L_{min_i}} \qquad \forall i = 1, ...N_{PV} + 1 \quad (3.24)$$

In case of a limit violation, the associated bus or buses are treated as PQ buses as in standard power flow methods, and the methodology explained before is repeated until no more limit violations are observed. A similar procedure can be used to compute the generator active power interval at the slack bus.

3.3 Improved Reactive Power Limit Representation

According to the AA-based power flow approach proposed in [14] and previously described, the power flow equations are initially solved without limits, and in case of a limit violation, the associated bus or buses are treated as PQ buses as in standard power flow methods, applying again the procedure to compute the affine forms for voltages and angles; this is repeated until no more limit violations are observed. A different approach is proposed in this thesis to account for generator reactive power limits, based on the following polar formulation of voltages and angles in affine form [121, 122]:

$$\widehat{V_i} = V_{o_i} + \sum_{m \in N_{IG}} \left. \frac{\partial V_i}{\partial P_{G_m}} \right|_o \Delta P_{G_A m} \varepsilon_{IG_m} + \sum_{nc \in N_{PV}} \left. \frac{\partial V_i}{\partial V_{nc}} \right|_o \Delta V_{A_{nc}} \left(\varepsilon_{PVa_{nc}} - \varepsilon_{PVb_{nc}} \right) + \sum_{nl \in N_{P_L}} \left. \frac{\partial V_i}{\partial P_{L_{nl}}} \right|_o \Delta P_{L_A nl} \varepsilon_{P_{L_{nl}}} + \sum_{nl \in N_{Q_L}} \left. \frac{\partial V_i}{\partial Q_{L_{nl}}} \right|_o \Delta Q_{L_A nl} \varepsilon_{Q_{L_{nl}}} \qquad \forall i = 1, .., N \quad (3.25)$$

$$\widehat{\theta_i} = \theta_{o_i} + \sum_{m \in N_{IG}} \left.\frac{\partial \theta_i}{\partial P_{G_m}}\right|_o \Delta P_{G_A m} \varepsilon_{IG_m} + \sum_{nc \in N_{PV}} \left.\frac{\partial \theta_i}{\partial V_{nc}}\right|_o \Delta V_{A_{nc}} \left(\varepsilon_{PVa_{nc}} - \varepsilon_{PVb_{nc}}\right) + \sum_{nl \in N_{P_L}} \left.\frac{\partial \theta_i}{\partial P_{L_{nl}}}\right|_o \Delta P_{L_A nl} \varepsilon_{P_{L_{nl}}}$$
$$+ \sum_{nl \in N_{Q_L}} \left.\frac{\partial \theta_i}{\partial Q_{L_{nl}}}\right|_o \Delta Q_{L_A nl} \varepsilon_{Q_{L_{nl}}} \qquad \forall i = 1, .., N \tag{3.26}$$

where, the noise symbols ε_{PVa} and ε_{PVb} are introduced to account for the reactive power limits of generators, and thus avoid the need for PV-PQ bus switching. This approach is based on the representation of PV buses discussed in Chapter 2, which yields the following formulation:

$$V_{pv_{nc}} = V_{o_{pv_{nc}}} + \Delta V_{A_{nc}} \left(\varepsilon_{PVa_{nc}} - \varepsilon_{PVb_{nc}}\right) \tag{3.27}$$

where:

$$\begin{aligned} &0 < \varepsilon_{PVanc} < 1, \varepsilon_{PVb_{nc}} = 0 \quad \text{for} \quad Q_G < Q_{G_{min}} \\ &\varepsilon_{PVa_{nc}} = 0, 0 < \varepsilon_{PVb_{nc}} < 1 \quad \text{for} \quad Q_G > Q_{G_{max}} \qquad \forall nc \in N_{PV} \\ &\varepsilon_{PVa_{nc}} = 0, \varepsilon_{PVb_{nc}} = 0 \qquad \text{for} \quad Q_{G_{max}} \leq Q_G \leq Q_{G_{min}} \end{aligned} \tag{3.28}$$

the noise symbols $\varepsilon_{PVa_{nc}}$ and $\varepsilon_{PVb_{nc}}$ in (3.27) act as the auxiliary variables $V_{a_{nc}}$ and $V_{b_{nc}}$ in (2.7) to keep the reactive power within limits. The effect of the variation of the voltage specified at PV nodes due to these noise symbols is accounted for in (3.25) and (3.26) by means of the partial derivatives of the bus voltages and angles with respect to the voltage reference set points at PV buses. This approach is implemented using the Linear Programming (LP) formulations described in detail at the end of this section.

The coefficients of the noise symbols in (3.25) and (3.26), given by the partial derivatives of voltage magnitudes and angles with respect to the injected active power and reference voltages at voltage controlled buses, can be calculated from a "base" power flow solution and the numerical sensitivity analysis described in Section 3.2. Since the derivatives of the initial affine forms are approximated by computing the changes in the respective variables using small perturbations, ill-defined derivatives, that arise when reactive power limits are reached at a power flow solution corresponding to the central values, can be avoided. The central values are defined as follows:

$$P_{G_o m} = \frac{P_{G_{max_m}} + P_{G_{min_m}}}{2} \qquad \forall m \in N_{IG} \tag{3.29}$$

$$P_{L_o nl} = \frac{P_{L_{max_{nl}}} + P_{L_{min_{nl}}}}{2} \qquad \forall nl \in N_L \tag{3.30}$$

$$Q_{L_o nl} = \frac{Q_{L_{max_{nl}}} + Q_{L_{min_{nl}}}}{2} \qquad \forall nl \in N_L \tag{3.31}$$

The active and reactive power affine forms $\widehat{P_i}$ and $\widehat{Q_i}$ are obtained by replacing the voltage and angle affine forms given in (3.25) and (3.26), in (3.7) and (3.8), resulting in the following equations, after after all affine function operations and approximations given in [107, 108]:

$$\begin{aligned}\widehat{P_i} = P_{i_o} + \sum_{m \in N_{IG}} P_{i,m}^{N_{IG}} \varepsilon_{IG_m} + \sum_{nl \in N_{P_L}} P_{i,nl}^{N_{P_L}} \varepsilon_{P_{L_{nl}}} + \sum_{nl \in N_{Q_L}} P_{i,nl}^{N_{Q_L}} \varepsilon_{Q_{L_{nl}}} + \sum_{nc \in N_{PV}} P_{i,nc}^{N_{PV}} \varepsilon_{PV_{a_{nc}}} \\ - \sum_{nc \in N_{PV}} P_{i,nc}^{N_{PV}} \varepsilon_{PV_{b_{nc}}} + \sum_{h \in N_h} P_{i,h}^{A} \varepsilon_{A_h} \qquad \forall i = 1, .., N\end{aligned} \tag{3.32}$$

$$\begin{aligned}\widehat{Q_i} = Q_{i_o} + \sum_{m \in N_{IG}} Q_{i,m}^{N_{IG}} \varepsilon_{IG_m} + \sum_{nl \in N_{P_L}} Q_{i,nl}^{N_{P_L}} \varepsilon_{P_{L_{nl}}} + \sum_{nl \in N_{Q_L}} Q_{i,nl}^{N_{Q_L}} \varepsilon_{Q_{L_{nl}}} + \sum_{nc \in N_{PV}} Q_{i,nc}^{N_{PV}} \varepsilon_{PV_{a_{nc}}} \\ - \sum_{nc \in N_{PV}} Q_{i,nc}^{N_{PV}} \varepsilon_{PV_{b_{nc}}} + \sum_{h \in N_h} Q_{i,h}^{A} \varepsilon_{A_h} \qquad \forall i = 1, .., N\end{aligned} \tag{3.33}$$

These equations may be written in compact form as follows:

$$A_L \varepsilon_L = C_L \tag{3.34}$$

$$C_L = L_L - (R_{L_o} + q_L) \tag{3.35}$$

where:

$$A_L = \begin{bmatrix} P_{1,1}^{N_{IG}} & \cdots & P_{1,N_{IG}}^{N_{IG}} & P_{1,1}^{N_{P_L}} & \cdots & P_{1,N_{P_L}}^{N_{P_L}} & P_{1,1}^{N_{Q_L}} & \cdots & P_{1,N_{Q_L}}^{N_{Q_L}} & P_{1,1}^{N_{PV}} & \cdots & P_{1,N_{PV}}^{N_{PV}} & -P_{1,1}^{N_{PV}} & \cdots & -P_{1,N_{PV}}^{N_{PV}} \\ \vdots & \vdots & \vdots & \vdots & \vdots & \vdots & \vdots & \vdots & \vdots & \vdots & \vdots & \vdots & \vdots & \vdots & \vdots \\ P_{N-1,1}^{N_{IG}} & \cdots & P_{N-1,N_{IG}}^{N_{IG}} & P_{N-1,1}^{N_{P_L}} & \cdots & P_{N-1,N_{P_L}}^{N_{P_L}} & P_{N-1,1}^{N_{Q_L}} & \cdots & P_{N-1,N_{Q_L}}^{N_{Q_L}} & P_{1,1}^{N_{PV}} & \cdots & P_{1,N_{PV}}^{N_{PV}} & -P_{N-1,1}^{N_{PV}} & \cdots & -P_{N-1,N_{PV}}^{N_{PV}} \\ Q_{1,1}^{N_{IG}} & \cdots & Q_{1,N_{IG}}^{N_{IG}} & Q_{1,1}^{N_{P_L}} & \cdots & Q_{1,N_{P_L}}^{N_{P_L}} & Q_{1,1}^{N_{Q_L}} & \cdots & Q_{1,N_{Q_L}}^{N_{Q_L}} & Q_{1,1}^{N_{PV}} & \cdots & Q_{1,N_{PV}}^{N_{PV}} & -Q_{1,1}^{N_{PV}} & \cdots & -Q_{1,N_{PV}}^{N_{PV}} \\ \vdots & \vdots & \vdots & \vdots & \vdots & \vdots & \vdots & \vdots & \vdots & \vdots & \vdots & \vdots & \vdots & \vdots & \vdots \\ Q_{N-1,1}^{N_{IG}} & \cdots & Q_{N-1,N_{IG}}^{N_{IG}} & Q_{N-1,1}^{N_{P_L}} & \cdots & Q_{N-1,N_{P_L}}^{N_{P_L}} & Q_{N-1,1}^{N_{Q_L}} & \cdots & Q_{N-1,N_{Q_L}}^{N_{Q_L}} & Q_{N-1,1}^{N_{PV}} & \cdots & Q_{N-1,N_{PV}}^{N_{PV}} & -Q_{N-1,1}^{N_{PV}} & \cdots & -Q_{N-1,N_{PV}}^{N_{PV}} \end{bmatrix}$$

$$\varepsilon_L = \begin{bmatrix} \varepsilon_{IG_1} \\ \vdots \\ \varepsilon_{IG_{N_{IG}}} \\ \varepsilon_{P_{L_1}} \\ \vdots \\ \varepsilon_{P_{L_{N_{P_L}}}} \\ \varepsilon_{Q_{L_1}} \\ \vdots \\ \varepsilon_{Q_{L_{N_{Q_L}}}} \\ \varepsilon_{PV_{a,1}} \\ \vdots \\ \varepsilon_{PV_{a,N_{PV}}} \\ \varepsilon_{PV_{b,1}} \\ \vdots \\ \varepsilon_{PV_{b,N_{PV}}} \end{bmatrix} \qquad L_L = \begin{bmatrix} \left[P_{G_{min_1}} - P_{L_{max_1}}\right], \left[P_{G_{max_1}} - P_{L_{min_1}}\right] \\ \vdots \\ \left[P_{G_{min_{N-1}}} - P_{L_{max_{N-1}}}\right], \left[P_{G_{max_{N-1}}} - P_{L_{min_{N-1}}}\right] \\ \left[Q_{G_{min_1}} - Q_{L_{max_1}}\right], \left[Q_{G_{max_1}} - Q_{L_{min_1}}\right] \\ \vdots \\ \left[Q_{G_{min_{N-1}}} - Q_{L_{max_{N-1}}}\right], \left[Q_{G_{max_{N-1}}} - Q_{L_{min_{N-1}}}\right] \end{bmatrix}$$

$$R_{L_o} = \begin{bmatrix} P_{1_o} \\ \vdots \\ P_{N_o} \\ Q_{1_o} \\ \vdots \\ Q_{N_o} \end{bmatrix} \qquad q_L = \begin{bmatrix} P^A_{1,1} & \cdots & P^A_{1,Nh} \\ \vdots & \vdots & \vdots \\ P^A_{N-1,1} & \cdots & P^A_{N-1,Nh} \\ Q^A_{1,1} & \cdots & Q^A_{1,Nh} \\ \vdots & \vdots & \vdots \\ Q^A_{N-1,1} & \cdots & Q^A_{N-1,Nh} \end{bmatrix} \begin{bmatrix} \varepsilon_{A_1} \\ \vdots \\ \vdots \\ \vdots \\ \vdots \\ \varepsilon_{A_{N_h}} \end{bmatrix}$$

To obtain the maximum and minimum values of the noise vector ε in (3.34), the following LP problems need to be solved:

$$\begin{aligned} \min \quad & \sum \varepsilon_{IG_{min_m}} + \sum \varepsilon_{P_{L_{min_{nl}}}} + \sum \varepsilon_{Q_{L_{min_{nl}}}} + \sum \varepsilon_{PVa_{min_{nc}}} + \sum \varepsilon_{PVb_{min_{nc}}} \\ \text{s.t.} \quad & -1 \leq \varepsilon_{IG_{min_m}}, \varepsilon_{P_{L_{min_{nl}}}}, \varepsilon_{Q_{L_{min_{nl}}}} \leq 1 \\ & 0 \leq \varepsilon_{PVa_{min_{nc}}}, \varepsilon_{PVb_{min_{nc}}} \leq 1 \\ & C_{L_{min}} \leq A_L \varepsilon_{L_{min}} \leq C_{L_{max}} \\ & \forall m \in N_{IG}, \forall nc \in N_{PV} \end{aligned} \tag{3.36}$$

$$\begin{aligned} \max \quad & \sum \varepsilon_{IG_{max_m}} + \sum \varepsilon_{P_{L_{max_{nl}}}} + \sum \varepsilon_{Q_{L_{max_{nl}}}} + \sum \varepsilon_{PVa_{max_{nc}}} + \sum \varepsilon_{PVb_{max_{nc}}} \\ \text{s.t.} \quad & -1 \leq \varepsilon_{IG_{max_m}}, \varepsilon_{P_{L_{max_{nl}}}}, \varepsilon_{Q_{L_{max_{nl}}}} \leq 1 \\ & -1 \leq \varepsilon_{PVa_{max_{nc}}}, \varepsilon_{PVb_{max_{nc}}} \leq 0 \\ & C_{L_{min}} \leq A_L \varepsilon_{L_{max}} \leq C_{L_{max}} \\ & \forall m \in N_{IG}, \forall nc \in N_{PV} \end{aligned} \tag{3.37}$$

The values of $\varepsilon_{IG_{min}}, \varepsilon_{P_{L_{min}}}, \varepsilon_{Q_{L_{min}}}, \varepsilon_{PVa_{min}}, \varepsilon_{PVb_{min}}$, and $\varepsilon_{IG_{max}}, \varepsilon_{P_{L_{max}}}, \varepsilon_{Q_{L_{max}}}, \varepsilon_{PVa_{max}}, \varepsilon_{PVb_{max}}$ obtained by solving these simple LP problems are used in (3.25) and (3.26) to compute the maximum and minimum bus voltages and angles. Notice that the objective functions in (3.36) and (3.37) are mathematically formulated to contract the vector ε according to the physical restrictions imposed by the power flow equations and the bounds of the noise symbols; thus, there is no particular physical meaning attributed to the objective functions. Since (3.36) corresponds to a minimization problem, and the bounds of $\varepsilon_{PVa_{min_{nc}}}$ and $\varepsilon_{PVb_{min_{nc}}}$ are restricted to the interval [0,1], these variables will tend to zero unless there is any reactive power limit violation. Similarly,

because in (3.37) the objective function is formulated as a maximization problem, and the bounds of $\varepsilon_{PVa_{max_{nc}}}$ and $\varepsilon_{PVa_{max_{nc}}}$ are restricted to the interval [-1,0], these noise symbols tend to zero, unless a reactive power limit is violated. On the other hand, the noise symbols $\varepsilon_{IG_{min_m}}$, $\varepsilon_{IG_{max_m}}$, $\varepsilon_{P_{L_{min_{nl}}}}$, $\varepsilon_{P_{L_{max_{nl}}}}$, $\varepsilon_{Q_{L_{min_{nl}}}}$, $\varepsilon_{Q_{L_{max_{nl}}}}$ which are related to the intermittent power injections, are allowed to vary within the interval [-1,1], which is the hull assigned to affine arithmetic variables.

3.4 Example

The IEEE-30 bus benchmark system shown in Figure 3.1 is utilized for testing the solution of the AA-based power flow equations. There are two synchronous generators connected at Buses 1 and 2 and four synchronous condensers connected at Buses 5, 8,11, 13, respectively, and the system base load is 283.4 MW and 126.2 MVAR. The following three study cases are considered:

- Case A: The generators output power and all the loads are allowed to vary within a range of ±35% with respect to their central values in order to stress the system. The power flow equations are solved using both, rectangular and polar representation of the power flow equations. Generator reactive power limits are not taken into account in this case.
- Case B: The generator output power and all the loads for Case A are allowed to vary within a range of ±10% with respect to their central values. Generator reactive power limits are not taken into account in this case.
- Case C: The generator reactive power limits are considered and the generator output powers and all the loads are allowed to vary within a range of ±15% with respect to their central values. The maximum reactive power of the generator at Bus 2 is set to 50 MVA, and the maximum reactive powers of the generators at Buses 5 and 8 are set to 40 MVA.

In the three cases described above, and the rest of this thesis, MCS are used for comparison purposes because of their flexibility and simplicity. Moreover, for a large enough number of trials, the union of the uncertainty region described by MCS is a very close approximation of the correct problem solution. In these MCS, a uniform pdf is used to represent the uncertainties in power injections, since it is the most appropriate pdf used to yield solution intervals [14].

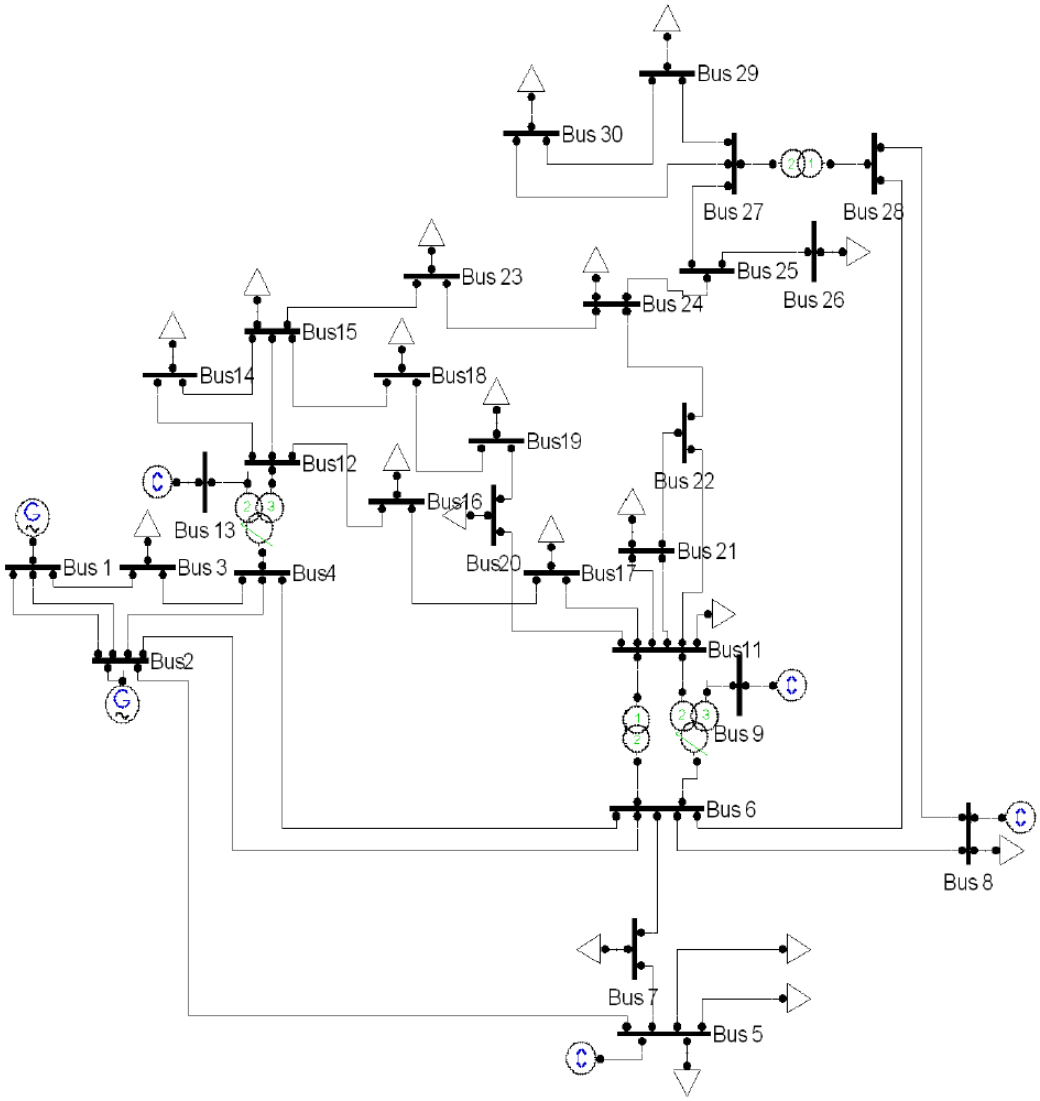

Figure 3.1: IEEE 30 bus system in PSAT.

The Trivial Affine Approximation is used to deal with the multiplications of affine forms, and the sine and cosine functions are approximated by using the Chebyshev Orthogonal Polynomial approach.

3.4.1 Case A

Figures 3.2 (a) and 3.2 (b) depict the upper and lower bounds of bus voltages and angles, respectively, when the power flow equations are formulated in rectangular form. The maximum discrepancies of the AA solution with respect to MCS results are 1.94% for the voltage magnitudes and 16.2% for the voltage angles. The computational time is 6.38 s for the AA-based method and 154.9 s for MCS (5000 iterations to guarantee convergence).

Aimed at illustrating the differences between the initial affine forms obtained using the sensitivity approach, and the final affine forms obtained by solving the LP maximization problem, the initial and final affine forms of the real part of the bus voltage magnitude at bus 30, truncated at the fifth noise symbol, are presented as example:

- Initial affine form:

$$\widehat{V}_{R_{30}} = 0.9498 + 0.0007\varepsilon_{L_1} - 0.0004\varepsilon_{L_2} - 0.0001\varepsilon_{L_3} - 0.0003 * \varepsilon_{L_4} - 0.0033 * \varepsilon_{L_5}...$$

- Final affine form:

$$\widehat{V}_{R_{30}} = 0.9498 + 0.0007\varepsilon_{L_1} - 0.0004\varepsilon_{L_2} - 0.0068e - 2\varepsilon_{L_3} - 0.0002 * \varepsilon_{L_4} - 0.0022 * \varepsilon_{L_5}...$$

Notice that the initial affine form has been corrected, resulting in a different final affine form.

The bounds for the bus voltages and angles when the polar form representation is used to formulate the power flow equations are depicted in Figures 3.3 (a) and 3.3 (b), respectively. In this case, the maximum errors obtained from the AA-based method with respect to MCS are 2.27% and 37.12% for bus voltage magnitudes and angles, respectively. Note that the rectangular coordinates representation exhibits a better accuracy than the polar form representation; this can be attributed to the relatively high volume of multiplications associated with the expansion of sinusoidal functions in the Chebyshev Orthogonal Polynomial approach. The computational time is 17.90 s in this case.

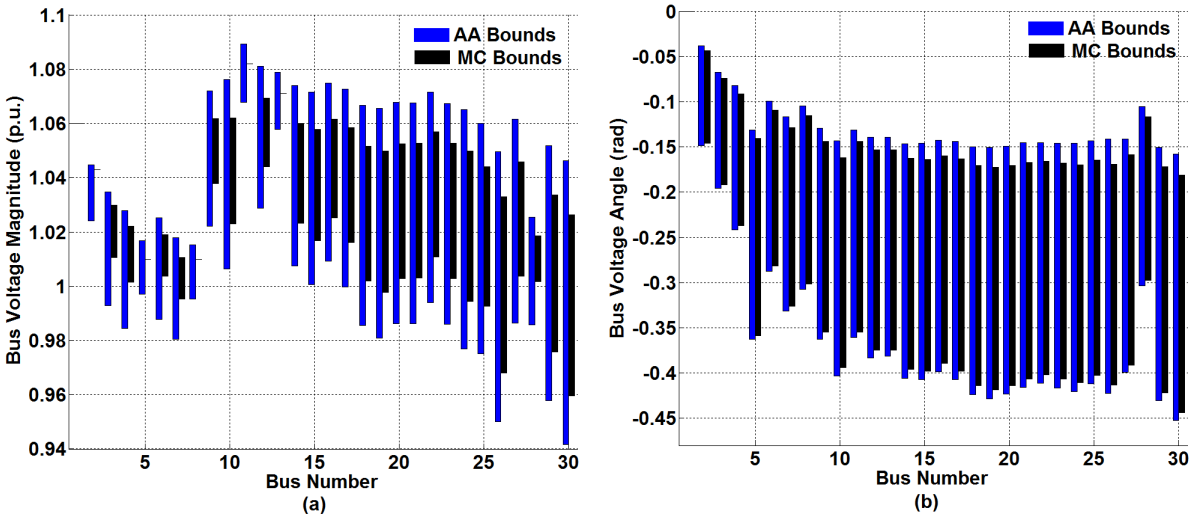

Figure 3.2: Case A with rectangular coordinates: (a) bus voltage magnitudes, and (b) bus voltage angles.

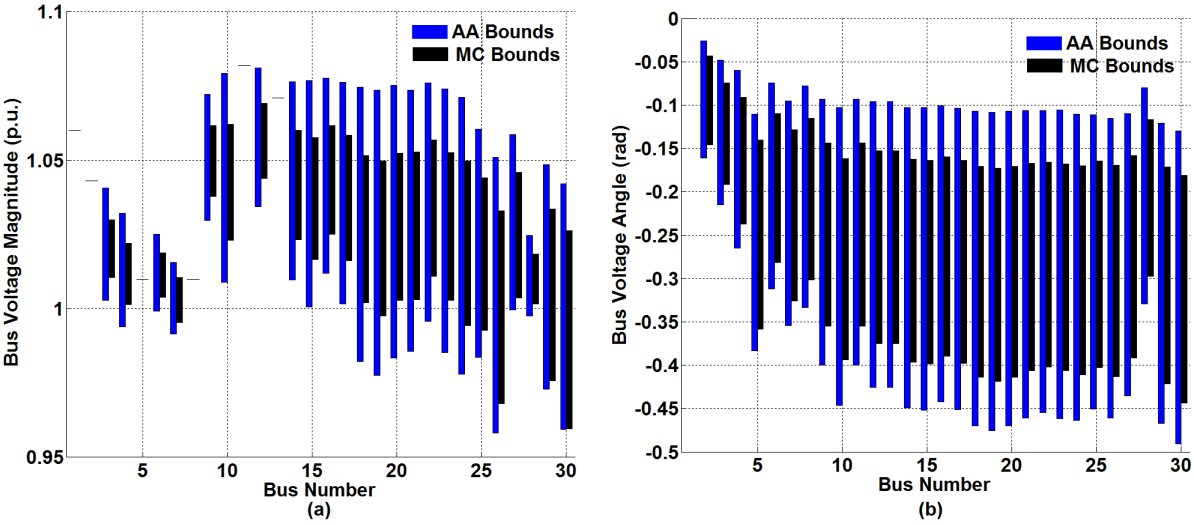

Figure 3.3: Case A with polar coordinates: (a) bus voltage magnitudes, and (b) bus voltage angles.

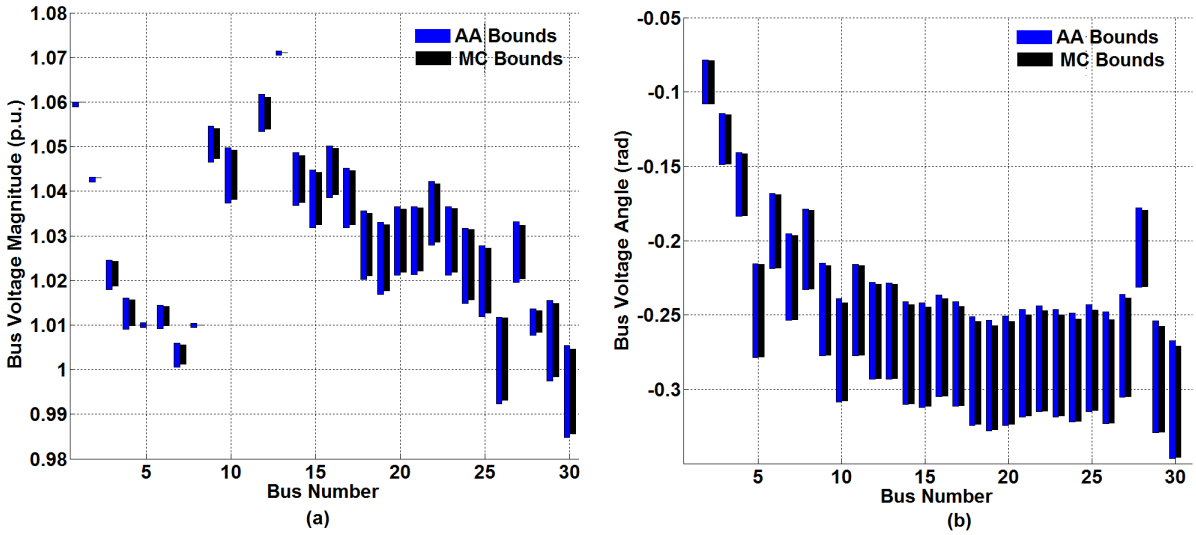

Figure 3.4: Case B with rectangular coordinates: (a) bus voltage magnitudes, and (b) bus voltage angles.

3.4.2 Case B

Observe in Figures 3.4 (a) and 3.4 (b) that the bus voltages and angles obtained with the AA-based method are almost superimposed on those obtained with MCS. Indeed, the maximum errors for the voltage magnitudes and angles are 0.23% and 2.06%, respectively, which is a significant improvement compared to Case A. The computational time is 2.51 s for the AA-based method and 166.4 s for MCS. Figures 3.5 (a) and 3.5 (b) depicts the results obtained using the polar form representation of power flow equations. In this case, the maximum error for the voltage magnitudes and angles are 1.84% and 18.0%, respectively, with a computational time of 3.75 s. These reduced errors are mainly due to the fact that the intervals of uncertainty have been reduced by over 1/3 with respect to Case A.

3.4.3 Case C

Figures 3.6 (a) and 3.6 (b) depict the bus voltage magnitude and angle bounds, respectively, when generator reactive power limits are considered, and the improved reactive power limit

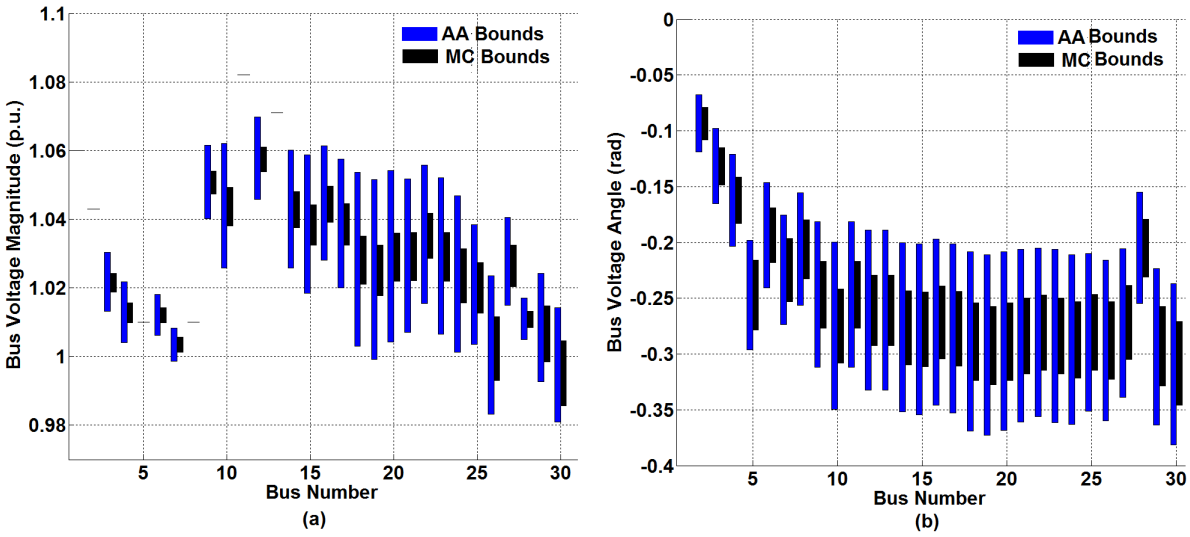

Figure 3.5: Case B with polar coordinates: (a) bus voltage magnitudes, and (b) bus voltage angles.

representation is used. The maximum discrepancy of the AA-based method results with respect to MCS is 5.2%, which shows good accuracy. The Computational time in this case is 4.55 s, which is approximately half the computational time obtained when the bus type switching strategy is used to account for generator reactive power limits (8.98 s). The computational time of MCS is 126.16 s.

Figure 3.7 shows bounds for reactive power in synchronous generators. Observe that the synchronous generator connected at Bus 2, and the synchronous condensers connected at Buses 5 and 8 reach their upper reactive power limits.

The accuracy of the proposed AA based methods is affected by the approximation of non-affine operations, the size of the intervals that model the uncertain variables, the number of uncertain variables, and the size of the system being analyzed. As demonstrated in the simulations, for relatively small sizes of the intervals that model the uncertain variables, the bounds obtained using MCS and AA are very close; however, when the size of these intervals increases, the error also increases.

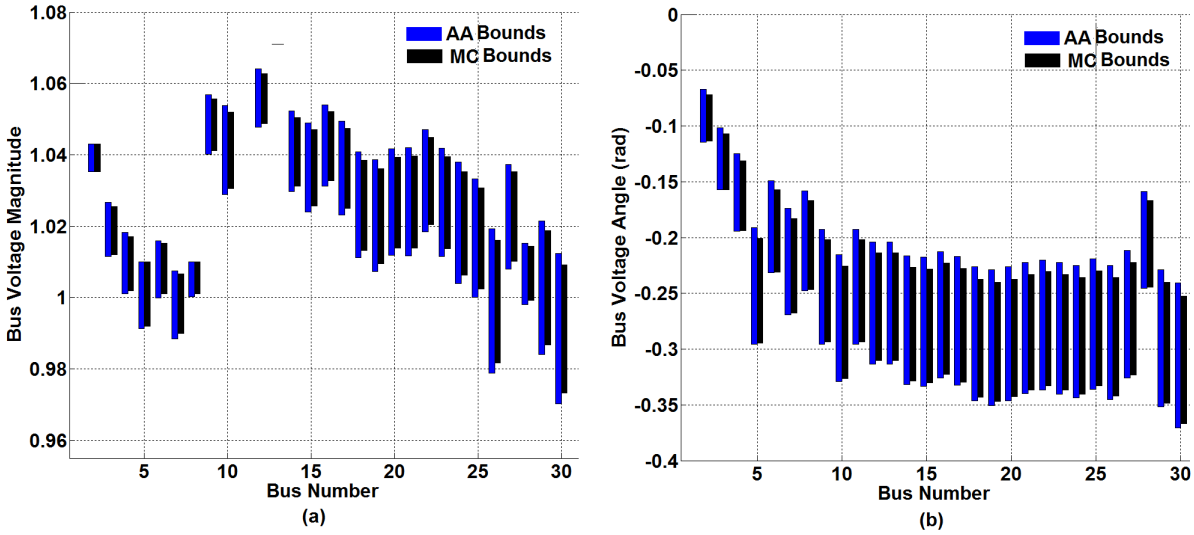

Figure 3.6: Case C with polar coordinates: (a) bus voltage magnitudes, and (b) bus voltage angles.

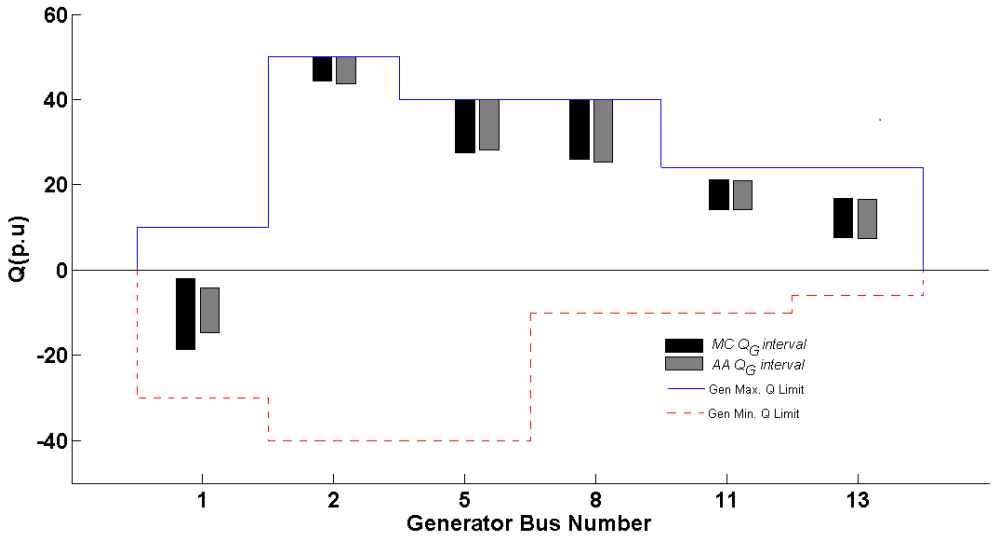

Figure 3.7: Generator reactive power intervals in Case C.

3.5 Summary

In this chapter, the AA-based power flow analysis was discussed in both polar and rectangular form, and various study cases were presented to compare the performance of different solution approaches.

A novel and more efficient way to deal with reactive power limits was also introduced. The impact of the input affine intervals width on the AA-based power flow method accuracy was investigated, concluding that the AA-based power flow method exhibits a reasonable accuracy and is more computationally efficient than MCS. Furthermore, this method automatically bounds the output variables according to the intervals that model the uncertain input variables, without the need to make assumptions regarding the pdf of the uncertainties. The use of rectangular-coordinate equations in the AA-based power flow problem was also studied, demonstrating to be significantly more accurate than the polar-coordinate equations approach. The basic principles of this AA-based power flow approach is used in this thesis to formulate the AA-based voltage stability methods, which is discussed next.

Chapter 4

Affine Arithmetic Based Voltage Stability Assessment

4.1 Introduction

In this chapter, the proposed AA-based method for voltage stability assessment of power systems considering uncertainties associated with operating conditions is discussed.The power flow equations in affine form, based on the more efficient representation of generator reactive power limits, are used to formulate the AA-based method for voltage stability assessment, which yields the hull of the PV curves associated with the assumed uncertainties. A parametrization approach which allows obtaining feasible solutions for the whole hull of PV curves is presented and discussed. Finally, the proposed method is tested using two study cases: first, a 5-bus test system is used to illustrate the proposed technique in detail, and thereafter, a 2383-bus test system is studied to demonstrate its practical application. The results are compared with those obtained using MCS to verify the accuracy and computational burden of the proposed AA-based method, and also with respect to a previously proposed technique to estimate the impact of parameter variations in voltage stability assessment.

4.2 Problem Formulation

The bus voltage magnitude and angle equations given by (3.25) and (3.26) are reformulated in this section to consider only uncertainties due to intermittent sources of power as follows:

$$\widehat{V_i} = V_{o_i} + \sum_{m \in N_{IG}} \frac{\partial V_i}{\partial P_{G_m}}\bigg|_o \Delta P_{G_{A}m} \varepsilon_{IG_m} + \sum_{nc \in N_{PV}} \frac{\partial V_i}{\partial V_{nc}}\bigg|_o \Delta V_{A_{nc}} \left(\varepsilon_{PVa_{nc}} - \varepsilon_{PVb_{nc}}\right) \qquad \forall i = 1, .., N \tag{4.1}$$

$$\widehat{\theta_i} = \theta_{o_i} + \sum_{m \in N_{IG}} \frac{\partial \theta_i}{\partial P_{G_m}}\bigg|_o \Delta P_{G_{A}m} \varepsilon_{IG_m} + \sum_{nc \in N_{PV}} \frac{\partial \theta_i}{\partial V_{nc}}\bigg|_o \Delta V_{A_{nc}} \left(\varepsilon_{PVa_{nc}} - \varepsilon_{PVb_{nc}}\right) \qquad \forall i = 1, .., N \tag{4.2}$$

In the proposed AA-based voltage stability method, (2.11) can be written for dispatchable generators, excluding the slack bus, as follows:

$$\widehat{P}_{G_i}(\lambda) = P_{G_{oi}} + \widehat{\lambda} \Delta P_{Gi} \qquad \forall i = 1, .., N-1 \tag{4.3}$$

Similarly, the load equations can be written as:

$$\widehat{P}_{L_i}(\lambda) = P_{L_{oi}} + \widehat{\lambda} \Delta P_{Li} \qquad \forall i = 1, .., N \tag{4.4}$$

$$\widehat{Q}_{L_i}(\lambda) = Q_{L_{oi}} + \widehat{\lambda} \Delta Q_{Li} \qquad \forall i = 1, .., N \tag{4.5}$$

where:

$$\widehat{\lambda} = \lambda_o + \sum_{m \in N_{IG}} \frac{\partial \lambda}{\partial P_{G_m}}\bigg|_o \Delta P_{G_{A}m} \varepsilon_{IGm} + \sum_{nc \in N_{PV}} \frac{\partial \lambda}{\partial V_{nc}}\bigg|_o \Delta V_{A_{nc}} \left(\varepsilon_{PVa_{nc}} - \varepsilon_{PVb_{nc}}\right) \tag{4.6}$$

Notice that the loading parameter λ is now in affine form, and thus is written as a function of the uncertainty of the output power of intermittent generators. This uncertainty is modeled as intervals that represent the maximum and minimum power injections associated with the simulation time period as follows:

$$P_{G_m} = \left[P_{G_{o}m} - \Delta P_{G_{A}m}, P_{G_{o}m} + \Delta P_{G_{A}m}\right] \qquad \forall m \in N_{IG} \tag{4.7}$$

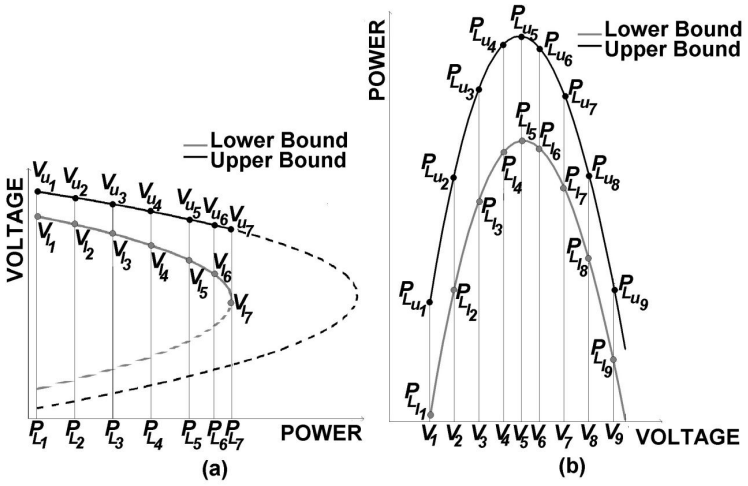

Figure 4.1: PV curves: (a) using the load power as the parameter; (b) using a PQ-bus voltage magnitude as the parameter.

or equivalently in AA:

$$\widehat{P}_{G_m} = P_{G_{o}m} + \Delta P_{G_{A}m}\varepsilon_{IGm} \qquad \forall m \in N_{IG} \tag{4.8}$$

For a different period of time, a different interval for the uncertain power injections may be needed; for instance, ΔP_{G_A} may be chosen according to the forecasting error associated with the concerned planning horizon. On the other hand, $\Delta V_{A_{nc}}$ may be decided so that there is a sufficient margin for the variation of the reference voltage setting of PV buses in order to keep generator's reactive power within limits. In this thesis, $\Delta V_{A_{nc}}$ has been assumed to be a 10% of the pre-established reference voltage control settings for all study cases.

For the computation of the central values and the upper and lower bounds of the PV curves, a parametrization technique is used in this thesis. Figure 4.1 (a) illustrates the problems when the load power is used as a parameter to compute the lower and upper parts of the PV curves. It is noted that varying the load by varying the power from P_{L1} to P_{L7}, and computing the respective upper voltages V_{u1} to V_{u7} and lower voltages V_{l1} to V_{l7} based on AA or MCS can only be done until the lower bound of the PV curve reaches the maximum loading point given by P_{L7}. Beyond this point, the dotted parts of the PV curves cannot be readily computed. To overcome this problem, the voltage magnitude at a PQ bus is chosen as the parameter, as in Figure 4.1(b), based

on a parametrization approach [90–93]. Notice that the voltage magnitude at the chosen PQ bus varies from V_1 to V_9, and for each of these voltages, the associated lower power loads P_{Ll1} to P_{Ll9} and upper power loads P_{Lu1} to P_{Lu9} can be readily computed. The PQ-bus voltage of the bus that exhibits the largest variation in voltage magnitude with respect to load variations is used as the parameter. The affine form for the voltage of this bus can be written as:

$$\widehat{V}_{PQ} = V_p \tag{4.9}$$

where V_p is updated for the computation of the PV curves as follows:

$$V_p = V_p - \Delta V_p \tag{4.10}$$

The step size ΔV_p varies depending on the proximity to the maximum loadability; thus, the closer to this maximum, the smaller the step size. The proximity to maximum loadability is detected by computing the difference between the former and the current loading factor interval $\widehat{\lambda}$; the lower this difference, the closer the system is to a saddle node bifurcation. Notice that for computations beyond the maximum loadability, the loading factor starts decreasing, and thus, it is straightforward to detect when the maximum loadability has been reached.

In standard PV computations, the parametrization approach is implemented by augmenting the power flow equations by one equation, which refers to the value assigned to the voltage magnitude chosen as the parameter. Thus, the set of equations to be solved is:

$$\begin{bmatrix} f_{PF}(\theta, V, \lambda) \\ V_{PQ} - V_p \end{bmatrix} = 0 \tag{4.11}$$

which is solved using a Newton approach, as follows:

$$\begin{bmatrix} f_{PF}(\theta^r, V^r, \lambda^r) \\ V_{PQ} - V_p \end{bmatrix} = -J_{aug^r} \begin{bmatrix} \Delta\theta^r \\ \Delta V^r \\ \Delta\lambda^r \end{bmatrix} \tag{4.12}$$

$$\begin{bmatrix} \theta^{r+1} \\ V^{r+1} \\ \lambda^{r+1} \end{bmatrix} = \begin{bmatrix} \theta^{r} \\ V^{r} \\ \lambda^{r} \end{bmatrix} + \begin{bmatrix} \Delta\theta^{r} \\ \Delta V^{r} \\ \Delta\lambda^{r} \end{bmatrix} \tag{4.13}$$

where r refers to the iteration number. These equations are iteratively solved until convergence is attained.

The proposed PV-curve computation approach is based on the following AA form of power flow equations:

$$\widehat{P}_{G_i} - P_{L_{oi}} - \widehat{\lambda}\Delta P_{Li} - \widehat{P}_i = 0 \qquad \forall i = 1, ..., N \tag{4.14}$$

$$\widehat{Q}_{G_i} - Q_{L_{oi}} - \widehat{\lambda}\Delta Q_{Li} - \widehat{Q}_i = 0 \qquad \forall i = 1, ..., N \tag{4.15}$$

plus the additional equation corresponding to the parametrization approach:

$$\widehat{V}_{PQ} - V_p = 0 \tag{4.16}$$

where $\widehat{P}_i$ and $\widehat{Q}_i$ are written according to (3.7) and (3.8), and $\widehat{P}_{G_i}$ is given by (4.3) for dispatchable generators, excluding the slack bus. In case of non-dispatchable generators, $\widehat{P}_{G_i}$ is modeled as an interval which represents the uncertainties associated with the output power, as in (4.8).

Equations (4.14) and (4.15) exhibit the following compact form, after all affine function operations and approximations:

$$A_{vs}\varepsilon_{vs} = C_{vs} \tag{4.17}$$

$$C_{vs} = L_{vs} - (R_{vs_o} + q_{vs}) \tag{4.18}$$

where:

$$R_{vs_o} = \begin{bmatrix} P_{1_o} + \lambda_o(\Delta P_{L_1} - \Delta P_{G_1}) \\ \vdots \\ P_{N_o} + \lambda_o(\Delta P_{L_n} - \Delta P_{G_n}) \\ Q_{1_o} + \lambda_o(\Delta Q_{L_1} - \Delta Q_{G_1}) \\ \vdots \\ Q_{N_o} + \lambda_o(\Delta Q_{L_n} - \Delta Q_{G_n}) \end{bmatrix}$$

and A_{vs}, ε_{vs}, C_{vs}, L_{vs}, and q_{vs} have the form of the matrices used in (3.34) and (3.35), neglecting

the load uncertainties.

Using a similar approach to the one previously described to account for generator reactive power limits, the LP formulation for the proposed AA-based voltage stability assessment is obtained by substituting C_L by C_{vs} and A_L by A_{vs} in (3.36) and (3.37) and ignoring the noise symbols for load variations $\varepsilon_{P_{L_{min}}}$, $\varepsilon_{P_{L_{max}}}$ and $\varepsilon_{Q_{L_{min}}}$, $\varepsilon_{Q_{L_{max}}}$. The values for $\varepsilon_{IG_{min}}$, $\varepsilon_{PVa_{min}}$, $\varepsilon_{PVb_{min}}$, and $\varepsilon_{IG_{max}}$, $\varepsilon_{PVa_{max}}$, $\varepsilon_{PVb_{max}}$ obtained by solving the resultant LP formulations are used in (4.6) to compute the loadability interval $\widehat{\lambda}$. Figure 4.2 depicts the algorithm used to compute the PV-curve intervals. The stopping criteria for this algorithm is decided based on the number of solution points of the hull of the PV curves beyond the maximum loadabilities.

4.3 Simulation Results

To test the proposed AA-based methodology for voltage stability assessment, two test systems are considered. The first is a 5-bus test system [85], which allows a thorough test and demonstration of the proposed methodology without the complexities associated with system size. The second corresponds to a portion of the Polish system and comprises 2383 buses [123], allowing to test and demonstrate the proposed approach in a realistic system. To validate and compare the results obtained with the proposed AA-based technique, PV curves are computed using an MCS approach, assuming uniform distribution for the non-dispatchable generators intervals, and are thus treated as the benchmark for comparison purposes. The convergence of MCS was determined by assuming a tolerance of 0.0001 in the change of the expected value. The sensitivity formula proposed in [44] is also used to compute the maximum loadability intervals for comparison purposes.

4.3.1 5-Bus Test System

This system comprises two generators which supply a base load of 440 MW. One of these generators is assumed to be an intermittent power source, while the second is assumed to be dispatchable, and is the system slack bus. For the computation of PV curves, the load directions in (4.14) and (4.15) are: $\Delta P_{L_i} = P_{L_{o_i}}$, and $\Delta Q_{L_i} = Q_{L_{o_i}}$.

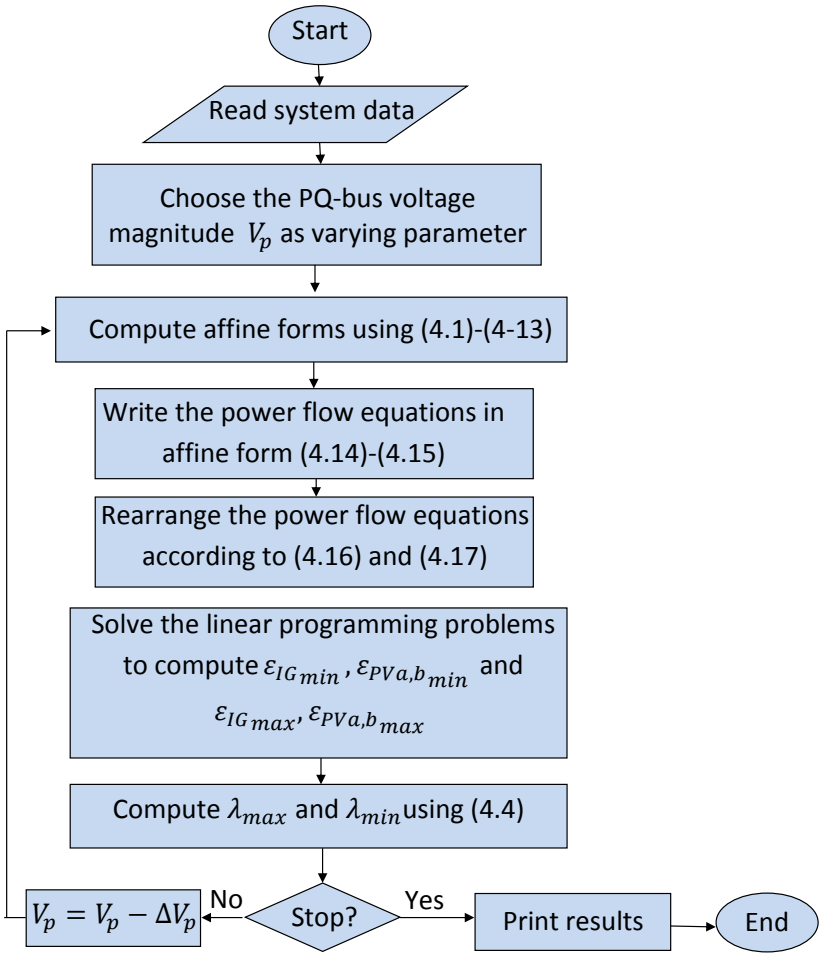

Figure 4.2: Algorithm for the AA-based PV curve computation method.

Table 4.1 shows the effect of increasing the size of the interval that models the uncertain variable on the computed maximum and minimum load changes. For comparison purposes, MCS, and the sensitivity formula (SF) results are also depicted (MCS required 50 samples to converge). Notice that as the margin of variation associated with the uncertain power injection increases, the error for the upper bound of the maximum loadabilities using AA and SF also increases, with the error corresponding to the AA-based method being slightly lower than the error computed using the SF approach. Also, notice that the lower bound for the maximum

Table 4.1: Comparison of load changes using different approaches for the 5-bus test system.

		Margin (%)			
		5	15	25	35
MCS	$\Delta L_{max}(MW)$	335.46	336.67	337.52	338.05
AA	$\Delta L_{max}(MW)$	335.47	336.97	338.47	339.97
	$e(\%)$	0.003	0.090	0.280	0.566
SF	$\Delta L_{max}(MW)$	335.55	337.16	338.77	340.38
	$e(\%)$	0.026	0.146	0.369	0.688
MCS	$\Delta L_{min}(MW)$	333.93	332.15	330.04	327.61
AA	$\Delta L_{min}(MW)$	333.67	331.57	329.51	327.45
	$e(\%)$	-0.082	-0.172	-0.162	-0.049
SF	$\Delta L_{min}(MW)$	333.94	332.33	330.72	329.11
	$e(\%)$	0.003	0.055	0.204	0.456

loadability is pessimistic for the AA-based approach and optimistic for the SF approach, which is an advantage of the proposed approach.

Figure 4.3 shows the PV curves obtained using MCS and the proposed AA-based method for a 30% margin variation of the uncertain variable. Notice that the AA-based approach allows to efficiently compute the upper and lower bounds of the PV curves, providing information regarding the hull of voltage profiles. No other technique proposed in the literature is capable of quickly generating such curves, which could be used by power system operators, as standard PV curves are used now [90] (e.g. to determine voltage profiles as the maximum system loadability is approached).

4.3.2 2383-Bus Test System

The system comprises 323 generators and 4 synchronous condensers supplying a base load of 24558 MW. A total of 50 generators, with total capacity of 7677.2 MW (31% of the total system generation capacity) are assumed to be intermittent power sources, with 15% margin variations. The size and number of uncertainties of this system allows evaluating the performance of the proposed AA-based voltage stability assessment for practical systems. As in the previous example, the following load and dispatch directions are assumed: $\Delta P_{L_i} = P_{L_{o_i}}$, $\Delta Q_{L_i} = Q_{L_{o_i}}$ and $\Delta P_{G_i} = P_{G_{o_i}}$ $\forall i$.

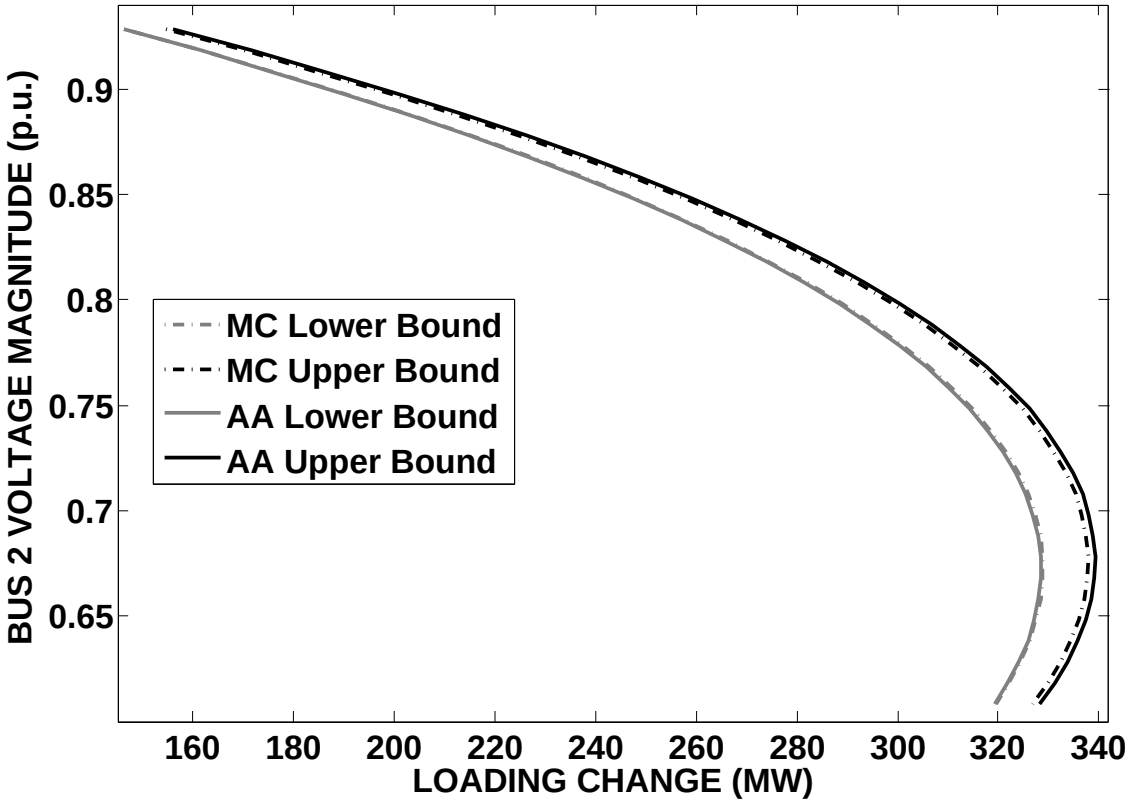

Figure 4.3: PV curves for the IEEE 5-bus test system.

The PV curves depicted in Figure 4.4 are computed using the proposed AA-based method and MCS for normal operating conditions. The probability distribution of the uncertain variables in MCS are assumed to be uniform distributions, requiring 2000 samples to attain convergence. Observe again that the proposed AA-based approach yields slightly pessimistic results.

Table 4.2 shows the bounds for load changes obtained using MCS, the proposed AA-based method, and the SF approach for the worst single line trip and single generator trip. Because of the difficulties encountered in the computation of the Jacobian matrices, the SF formula was approximated using the following equation:

$$\left.\frac{d\lambda}{dp}\right|_o \approx \left.\frac{\Delta\lambda}{\Delta p}\right|_o \tag{4.19}$$

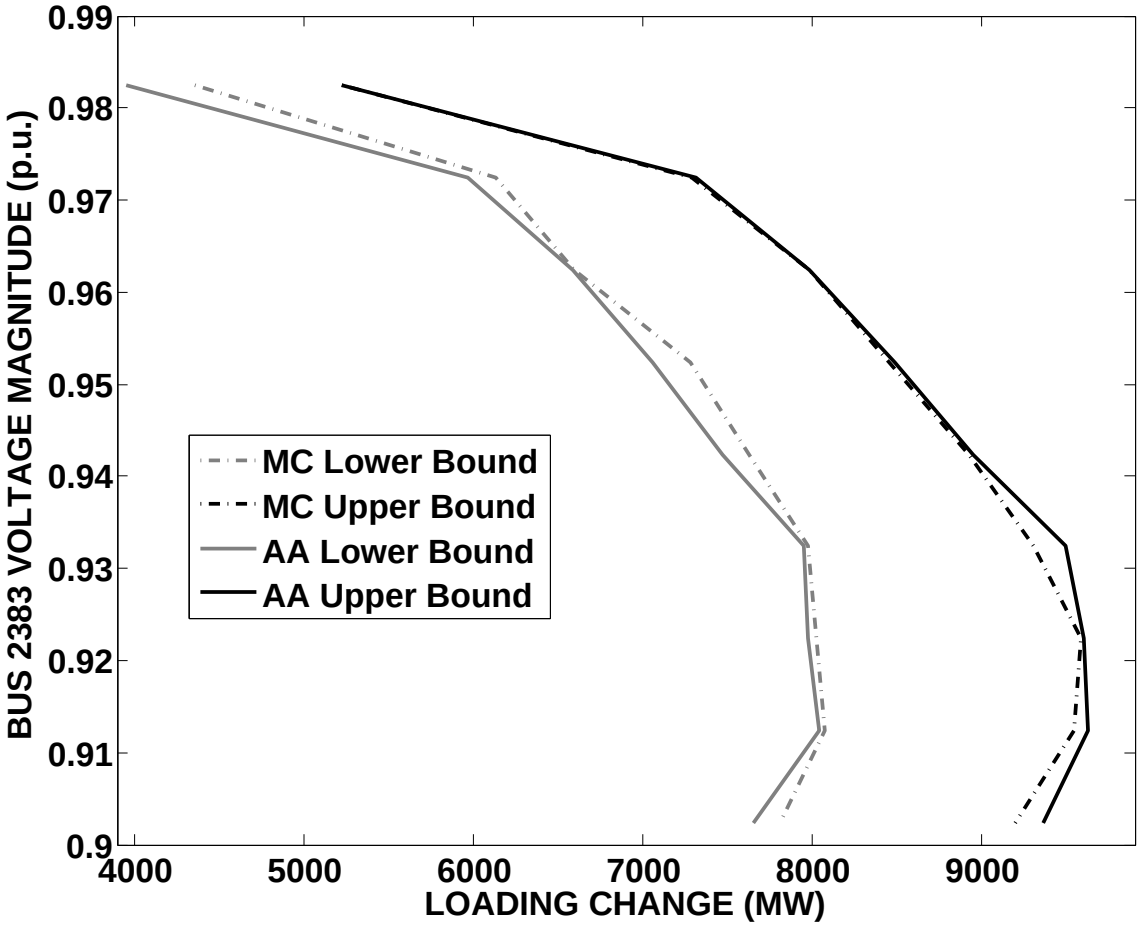

Figure 4.4: PV curves for the 2383-bus test system.

with Δp small enough to have a good approximation. It is observed that the worst contingency occurs when Line 67-138 is tripped. Observe that the errors in the values obtained using the proposed AA-based technique are lower than those obtained with the SF approach; furthermore, there are no underestimation of the margins by the AA-based method, as opposed to those obtained using the SF technique. In this case, the ATC for transmission line 31-32, which is the most loaded line in the system, computed using (2.16) and assuming CBM=0, varies within the intervals [31.83, 78.72] MW, [29.17, 82.56] MW, and [26.18, 85.31] MW, for MCS, the AA-based method, and the SF approach, respectively; this results in a maximum error for the AA-

based approach of 8.37%, while the maximum error for the SF approach is 17.77%. Notice that the difference between the loading changes computed using MCS and the AA-based approach tends to increase as the size of the system and number of uncertain variables increases. This result is to be expected, because, as the number of uncertain variables and operations increase, the approximation errors of the non-affine operations become larger.

Table 4.2: Comparison of load changes using different approaches for the 2383-bus test system.

		Normal	Line 67-138 trip	Gen Gen 131 trip
MCS	$\Delta L_{max}(MW)$	9585	4160	6532
AA	$\Delta L_{max}(MW)$	9622	4300	6577
	$e(\%)$	0.39	3.37	0.69
SF	$\Delta L_{max}(MW)$	9702	4400	6410
	$e(\%)$	1.22	5.77	-1.87
MCS	$\Delta L_{min}(MW)$	8072	2452	5120
AA	$\Delta L_{min}(MW)$	8038	2355	5111
	$e(\%)$	-0.42	-3.96	-0.18
SF	$\Delta L_{min}(MW)$	7958	2246	5176
	$e(\%)$	-1.41	-8.4	1.09

These simulations, based on MATLAB, were carried out on a computer with 8 GB of RAM and a processor of 3.40 GHz. The proposed AA-based approach was computationally more efficient than MCS, being 1.96 times faster (0.889 s vs 1.744 s) and 11 times faster (270.7 s vs 2975.7 s) for the 5-bus and the 2383-bus test system, respectively. These simulation times are referred to the system in normal operating conditions, without contingencies.

It is important to point out that the proposed AA-based methodology computes ATCs considering uncertainties attributed to intermittent sources of power for a system topology. Hence, based on the N-1 contingency criterion, the AA-based method was repeatedly applied for each contingency to compute the ATC. Note that the uncertainty associated with equipment outages (e.g. lines and transformers) can also be modeled using the proposed AA-based computing paradigm. According to a mathematical approach widely adopted in circuit analysis literature, the equipment outages can be described by proper variations of the admittance matrix elements, defining the parameters of the equipment equivalent circuits using proper intervals (e.g. $R_i = [R_{min}, R_{max}] = [R, 1e6]$, where $R_i = 1e6$ corresponds to the i-th equipment out of service).

4.4 Sources of Error

The main sources of error of the proposed AA-based method for voltage stability assessment are as follows:

- Errors introduced by sinusoidal function approximations: In this thesis, sinusoidal functions are written in terms of Chebyshev polynomial approximations for 5-digit accuracy. This approximation, given by (2.35), comprises a finite number of polynomials whose coefficients are floating-points. The number of polynomials Np are truncated depending on the number of digits accuracy. For 5-digit accuracy, as in this thesis, the Chebyshev approximation error is 10^{-5} because of the truncation of the Chebyshev series approximation only. Since the polynomials of this approximation involves non-affine operations, additional truncation approximation errors are introduced [107]. Therefore, the final affine forms of the sine and cosine operations exhibit approximation errors greater than those attributed to the Chebyshev approximations only. Therefore, increasing the number of digits of the Chebyshev approximation beyond 5 digits does not improve the overall accuracy of the sine and cosine affine approximations.

- Errors due to the size of the intervals that model the uncertain variables: The greater the size of the interval that models the uncertain variables, the greater the error. This is expected, since the initial coefficients of the affine forms are obtained using a sensitivity analysis approach. Thus, the greater the deviation of the central value of the affine forms with respect to their minimum and maximum values, the greater the error of the initial coefficients of the affine forms.

- Errors due to the number of uncertain variables and size of the system: The greater the number of uncertain variables and size of the system, the greater the error. This is also expected since, with the number of equations and coefficients of the affine forms increasing, the truncation errors associated with non-affine operations increase.

4.5 Summary

A novel method for voltage stability assessment of power systems with intermittent sources of generation such as wind and solar power has been presented in this chapter. Specifically, the proposed methodology computes the bounds of the PV curves and associated static load margins when the system presents uncertainties due to operating conditions, without any assumption on their pdfs. The results depict a reasonable good accuracy at significantly lower computational costs when compared to those obtained using simulation based techniques. Comparisons also show that the lower bound of the maximum loadability obtained using the AA-based approach is pessimistic, while it is optimistic in some cases for the SF approach, thus making the AA-based approach more appropriate for practical applications.

The proposed AA-based method takes into account the correlations among variables, which is not possible with other self-validated methods such as IA-based methods. The accuracy of the proposed method is mainly attributed to this characteristic. However, as the number of uncertain variables, size of the system, and size of the uncertainty intervals increase, the accuracy of the method decreases. This should not be a significant problem for the practical application of the proposed technique, since the number and sizes of uncertain generation sources in real systems is not expected to be more than 30% of the total system generation.

Chapter 5

Affine Arithmetic Based Transient Stability Assessment

5.1 Introduction

In this chapter, the proposed AA-based method for transient stability assessment of power systems considering uncertainties associated with operating conditions is presented and discussed. This method is based on the solution of the DAEs that describe the system dynamic behavior using a trapezoidal integration approach, which is described in detail. Two test cases are discussed: first, a Single Machine Infinite Bus (SMIB) test system with simplified models is used to illustrate the proposed technique in detail; thereafter, a two-area test system, using detailed synchronous generator models, and wind turbines based on Doubly Fed Induction Generators (DFIGs) is used to demonstrate its more practical application. The results are compared with those obtained using simple MCS to verify the accuracy of the proposed AA-based method. The computational burden of the AA-based technique, and its possible application to large systems are also discussed.

5.2 Problem Formulation

The set of DAEs (2.17) and (2.18) describing a power system can be formulated in affine form as follows [122]:

$$\dot{\widehat{x}}_D(t) = f_D\left(\widehat{x}_D, \widehat{y}, \widehat{p}_D, \widehat{\lambda}\right) \quad \text{for} \quad \widehat{x}_D(0) = \widehat{x}_{D_{IC}} \tag{5.1}$$

$$0 = g(\widehat{x}_D, \widehat{y}, \widehat{p}_D, \widehat{\lambda}) \quad \text{for} \quad \widehat{y}(0) = \widehat{y}_{IC} \tag{5.2}$$

The purpose of this formulation is to compute the hull of the system response due to system uncertainties such as intermittent sources of power, to examine the effect of large disturbances on the system. To achieve this goal, the set of AA DAEs (5.1) and (5.2) are solved using the trapezoidal integration approach, resulting in the following formulation for the DAE system:

$$\widehat{x}_{D_n} - \widehat{x}_{D_{n-1}} - (\Delta t/2)\left(f_D\left(\widehat{x}_{D_{n-1}}, \widehat{y}_{n-1}, \widehat{p}_D, \widehat{\lambda}, t_{n-1}\right) + f_D\left(\widehat{x}_{D_n}, \widehat{y}_n, \widehat{p}_D, \widehat{\lambda}, t_n\right)\right) = 0 \tag{5.3}$$

$$g(\widehat{x}_{D_n}, \widehat{y}_n, \widehat{p}_D, \widehat{\lambda}) = 0 \tag{5.4}$$

Based on a similar representation of the affine forms for voltages and angles used in [14] and [121], the initial affine forms of the state and algebraic variables are computed using the following affine relations:

$$\widehat{x_D} = x_{D_o} + \sum_{m \in N_{IG}} \left.\frac{\partial x_D}{\partial P_{G_{A_m}}}\right|_o \Delta P_{G_{A_m}} \varepsilon_{IG_m} \tag{5.5}$$

$$\widehat{y} = y_o + \sum_{m \in N_{IG}} \left.\frac{\partial y}{\partial P_{G_{A_m}}}\right|_o \Delta P_{G_{A_m}} \varepsilon_{IG_m} \tag{5.6}$$

which represent the impact of the various uncertain sources ΔP_G in the corresponding variables. The load admittances are then modeled as:

$$\widehat{Y} = Y_o + \sum_{m \in N_{IG}} \left.\frac{\partial Y}{\partial P_{G_{A_m}}}\right|_o \Delta P_{G_{A_m}} \varepsilon_{IG_m} \tag{5.7}$$

The central values in (5.5)-(5.7) are computed by solving the following set of steady-state equations:

$$f_D\left(x_{D_o}, y_o, p_{D_o}, \delta_o\right) = 0 \tag{5.8}$$

$$g\left(x_{D_o}, y_o, p_{D_o}, \delta_o\right) = 0 \tag{5.9}$$

The affine forms of the intermittent sources of power are modeled as in (4.8), and the central values of the intermittent sources of power are computed using (3.31). For a different period of time, a different affine interval for the uncertain power injections may be needed; for instance, ΔP_{G_A} may be chosen according to the forecasting error associated with the operating horizon of interest. The partial derivatives in (5.5)-(5.7) are computed using sensitivity analysis.

The resultant set of algebraic equations (5.3) and (5.4) can be solved using a Newton approach as follows:

$$\widehat{J}\left(\widehat{z}^{r}\right)\left(\widehat{z}^{r+1} - \widehat{z}^{r}\right) = 0 - \widehat{F}_A\left(\widehat{z}^{r}\right) \tag{5.10}$$

or equivalently,

$$\Delta\widehat{F}_A = \widehat{J}\Delta\widehat{z} \tag{5.11}$$

This linear system of equations is solved iteratively, updating the state and algebraic variables until convergence is attained. The set of DAEs are simultaneously solved, achieving better numerical stability than partitioned techniques. Unlike the Krawczyk's or the Interval Gauss Seidel Iteration approaches used to solve the system of equations in IA [124], the Newton-based approach used in this thesis does not require certain special classes of matrices such as M-matrices and H-matrices to solve the linearized set of equations.

The components of the vector $\Delta\widehat{F}_A$ in (5.11) exhibit the following form after all affine operations and non-affine approximations are carried out:

$$\begin{aligned}\Delta\widehat{F}_{A_s} = \Delta F_{A_{o_s}} + \Delta F_{A_{1_s}}\varepsilon_{IG_1} + \Delta F_{A_{2_s}}\varepsilon_{IG_2} + ... + \Delta F_{A_{m_s}}\varepsilon_{IG_m} \\ + \sum_{h\in Nh}\left|(Fa_{h_s})\right|\varepsilon f_{h_s} = 0 \qquad \forall m \in N_{IG}, \quad s = 1...N_{DA}\end{aligned} \tag{5.12}$$

The last term of this equation, which corresponds to the independent noise symbols resulting from the non-affine operations, can be reduced to a single noise symbol as follows:

$$\Delta F_{H_s} \varepsilon f_{H_s} = \sum_{h \in Nh} \left|(Fa_{h_s})\right| \varepsilon f_{h_s} \quad s = 1...N_{DA} \tag{5.13}$$

Similarly, the components of the Jacobian matrix can be written as:

$$\begin{aligned} \widehat{J}_{s,k} &= J_{o_{s,k}} + J_{1_{s,k}} \varepsilon_{IG_1} + J_{2_{s,k}} \varepsilon_{IG_2} + ... + J_{m_{s,k}} \varepsilon_{IG_m} \\ &+ \sum_{h \in Nh} \left|(Ja_{h_{s,k}})\right| \varepsilon j_{h_{s,k}} \quad \forall m \in N_{IG} \quad s,k = 1...N_{DA} \end{aligned} \tag{5.14}$$

$$J_{H_{s,k}} \varepsilon j_{H_{s,k}} = \sum_{h \in Nh} |(Ja_{h_{s,k}})| \varepsilon j_{h_{s,k}} \quad s,k = 1...N_{DA} \tag{5.15}$$

And the affine forms of the vector $\widehat{\Delta z}$ are:

$$\begin{aligned} \widehat{\Delta z_s} = \Delta z_{o_s} + \Delta z_{1_s} \varepsilon_{IG_1} + ... + \Delta z_{m_s} \varepsilon_{IG_m} + \Delta z_{H_s} \varepsilon_{H_s} \\ s = 1...N_{DA}, \forall m \in N_{IG} \end{aligned} \tag{5.16}$$

This vector is comprised of the state and algebraic variables, and thus has the following form:

$$\widehat{\Delta z} = \begin{bmatrix} \widehat{\Delta x_D} \\ \widehat{\Delta y} \end{bmatrix} \tag{5.17}$$

Applying equation (2.34) to (5.11) yields the following components of the affine form $\widehat{\Delta F}$:

- Central values:

$$\Delta F_{A_{o_s}} = \sum_{k=1}^{N_{DA}} J_{o_{s,k}} \Delta z_{o_k} \quad s = 1...N_{DA} \tag{5.18}$$

- The m-th components:

$$\Delta F_{A_{m_s}} = \sum_{k=1}^{N_{DA}} J_{o_{s,k}} \Delta z_{m_k} + \sum_{k=1}^{N_{DA}} J_{m_{s,k}} \Delta z_{o_k} \qquad s = 1...N_{DA}, \forall m \in N_{IG} \tag{5.19}$$

- Approximation errors:

$$\Delta F_{H_s} = \sum_{k=1}^{N_{DA}} J_{o_{s,k}} \Delta z_{H_k} + \sum_{k=1}^{N_{DA}} J_{H_{s,k}} \Delta z_{o_k} \qquad s = 1..N_{DA}, \forall m \in N_{IG} \tag{5.20}$$

Equations (5.18)-(5.20), stated in matrix form, are used to compute the components of the affine form $\widehat{\Delta z}$ (5.17) as follows:

$$\begin{bmatrix} \Delta F^r_{A_{o_1}} \\ \Delta F^r_{A_{o_2}} \\ \vdots \\ \Delta F^r_{A_{o_{N_{DA}}}} \end{bmatrix} = \begin{bmatrix} J^r_{o_{1,1}} & J^r_{o_{1,2}} & \dots & J^r_{o_{1,N_{DA}}} \\ J^r_{o_{2,1}} & J^r_{o_{2,2}} & \dots & J^r_{o_{2,N_{DA}}} \\ \vdots & \vdots & \dots & \vdots \\ J^r_{o_{N_{DA},1}} & J^r_{o_{N_{DA},2}} & \dots & J^r_{o_{N_{DA},N_{DA}}} \end{bmatrix} \begin{bmatrix} \Delta z^r_{o_1} \\ \Delta z^r_{o_2} \\ \vdots \\ \Delta z^r_{o_{N_{DA}}} \end{bmatrix} \tag{5.21}$$

$$\begin{bmatrix} \Delta F^r_{A_{m_1}} - \Delta z^r_{o_1} J^r_{m_{1,1}} - \dots - \Delta z^r_{o_{N_{DA}}} J^r_{m_{1,N_{DA}}} \\ \Delta F^r_{A_{m_2}} - \Delta z^r_{o_1} J^r_{m_{2,1}} - \dots - \Delta z^r_{o_{N_{DA}}} J^r_{m_{2,N_{DA}}} \\ \Delta F^r_{A_{m_{N_{DA}}}} - \Delta z^r_{o_1} J^r_{m_{N_{DA},1}} - \dots - \Delta z^r_{o_{N_{DA}}} J^r_{m_{N_{DA},N_{DA}}} \end{bmatrix} = A^r_o \begin{bmatrix} \Delta z^r_{m_1} \\ \Delta z^r_{m_2} \\ \vdots \\ \Delta z^r_{m_{N_{DA}}} \end{bmatrix} \quad \forall m \in N_{IG} \tag{5.22}$$

$$\begin{bmatrix} \Delta F^r_{H_1} - \Delta z^r_{o_1} J^r_{H_{1,1}} \ldots - \Delta z^r_{o_{N_{DA}}} J^r_{H_{1,N_{DA}}} \\ \Delta F^r_{H_2} - \Delta z^r_{o_1} J^r_{H_{2,1}} - \ldots - \Delta z^r_{o_{N_{DA}}} J^r_{H_{2,N_{DA}}} \\ \Delta F^r_{H_{N_{DA}}} - \Delta z^r_{o_1} J^r_{H_{N_{DA},1}} - \ldots - \Delta z^r_{o_{N_{DA}}} J^r_{H_{N_{DA},N_{DA}}} \end{bmatrix} = A^r_o \begin{bmatrix} \Delta z^r_{H_1} \\ \Delta z^r_{H_2} \\ \vdots \\ \Delta z^r_{H_{N_{DA}}} \end{bmatrix} \tag{5.23}$$

where:

$$A^r_o = \begin{bmatrix} J^r_{o_{1,1}} & J^r_{o_{1,2}} & \ldots & J^r_{o_{1,N_{DA}}} \\ J^r_{o_{2,1}} & J^r_{o_{2,2}} & \ldots & J^r_{o_{2,N_{DA}}} \\ \vdots & \vdots & \ldots & \vdots \\ J^r_{o_{N_{DA},1}} & J^r_{o_{N_{DA},2}} & \ldots & J^r_{o_{N_{DA},N_{DA}}} \end{bmatrix} \tag{5.24}$$

The state and algebraic variables are iteratively updated as follows until convergence is attained:

$$\widehat{x}^{r+1}_D = \widehat{x}^r_D + \Delta\widehat{x}^r_D \tag{5.25}$$

$$\widehat{y}^{r+1} = \widehat{y}^r + \Delta\widehat{y}^r \tag{5.26}$$

where $\Delta\widehat{y}^r$ and $\Delta\widehat{x}^r_D$ are computed using (5.21)-(5.24). Figure 5.1 illustrates the proposed algorithm for the AA-based transient stability assessment. This algorithm is very similar to the commonly used approach to solve the DAEs for time domain simulations, but in affine form.

5.3 Simulation Results

To test the proposed AA-based methodology for transient stability assessment, three test cases are considered. The first is a Single Machine Infinite Bus (SMIB) test system [94], which allows a thorough test and demonstration of the proposed methodology using simplified models; the second corresponds to a two-area system [99], aimed at testing the proposed method using detailed models for the synchronous generators. In the third study, the two are system is modified to consider wind turbines based on Doubly Fed Induction Generators (DFIGs), allowing

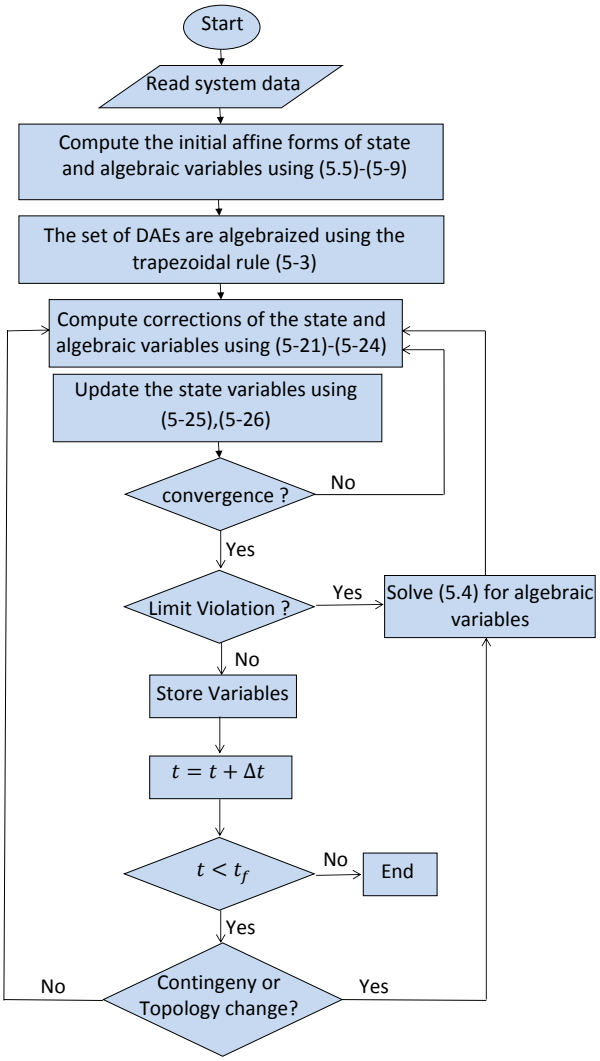

Figure 5.1: AA-based time domain simulation algorithm.

to more realistically test and demonstrate the proposed approach using intermittent sources of power. To validate and compare the results obtained using the proposed AA-based technique, MCS are used as the benchmark, assuming uniform probability distributions of the intermittent sources of power; 3000 samples for the first study case and 5000 samples for the second and third study cases were required for MCS to converge.

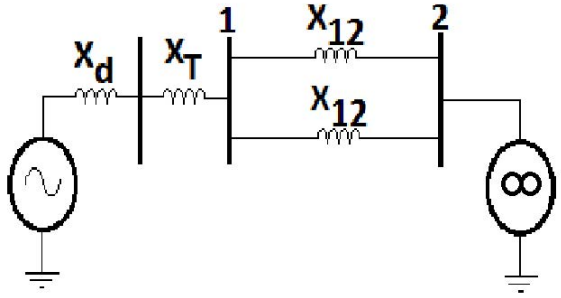

Figure 5.2: SMIB test system [94].

5.3.1 Single Machine Infinite Bus Test System

The system shown in Figure 5.2 comprises a synchronous generator, which is assumed to be intermittent, and connected through a transformer and two parallel lines to an infinite bus. The data for this system is given in Table 5.1. A three phase fault is assumed in the middle of one of the lines connecting Buses 1 and 2, which is subsequently cleared by tripping the faulted line. The initial central values for the affine forms are computed assuming that the infinite bus is drawing 5.5 p.u. of real power at unity power factor.

Table 5.1: SMIB test system data.

H $(p.u. \cdot s)$	D $(p.u)$	X'_d $(p.u.)$	X_T $(p.u.)$	X_{12} $(p.u.)$	V_2 $(p.u)$	p.f.	P_o $(p.u.)$
3.0	0.1	0.025	0.025	0.1	1.0	1	5.5

In this example, the generator was represented using a classical synchronous machine model. However, it is important to point out that the proposed AA-based approach for transient stability assessment is not model-dependent, as demonstrated with the second test system. The set of algebraized DAEs in affine form for this study case is given in Appendix A.

Figure 5.3 shows the upper and lower bounds of the system dynamic response when the intermittent source varies within the interval [522.5, 577.5] MW, i.e. a ±5% variation from the power drawn by the infinite bus. Notice that the bounds obtained using the AA-based approach closely follows the bounds obtained using MCS, with a maximum error of 0.98%.

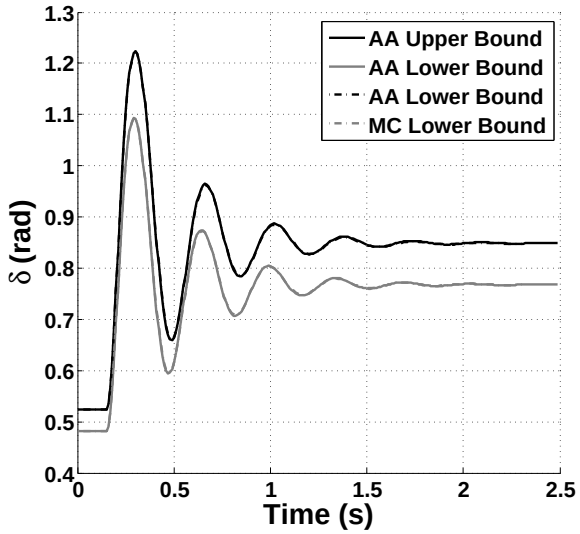

Figure 5.3: SMIB test system: 3-cycle fault with ±5% variation in generation.

Figures 5.4 and 5.5 depict the effect of the size of the interval that models the intermittent source of power on the accuracy of the proposed AA-based technique. In these cases, the intervals considered are [495, 605]MW, i.e. ±10% variation and [440, 660] MW, i.e. ±20%, respectively, resulting in a maximum error of 3.88% for ±10% variation and 8.69% for ±20% variation when compared to MCS. Thus, it can be readily inferred that as the size of the interval, that models the uncertain variables increases, the error increases as well, as expected. Also notice that the AA-based approach is slightly conservative as compared to MCS, which is a desirable feature of the proposed method.

Figure 5.6 illustrates a case where the system becomes unstable for the ±5% range of power variation [522.5, 577.5] MW of the intermittent source. Notice that the AA-based approach is also able to accurately represent unstable cases, with a maximum error of 4.98% for the simulations considered.

Finally, Figure 5.7 illustrates the bounds obtained when stable and unstable cases are contained within the assumed interval of power variation of the intermittent source. Thus, observe that the upper bound is unstable, while the lower bound is stable. It is important to point out that the accuracy of the method, for simulation times beyond 0.45 s, decreases because of the

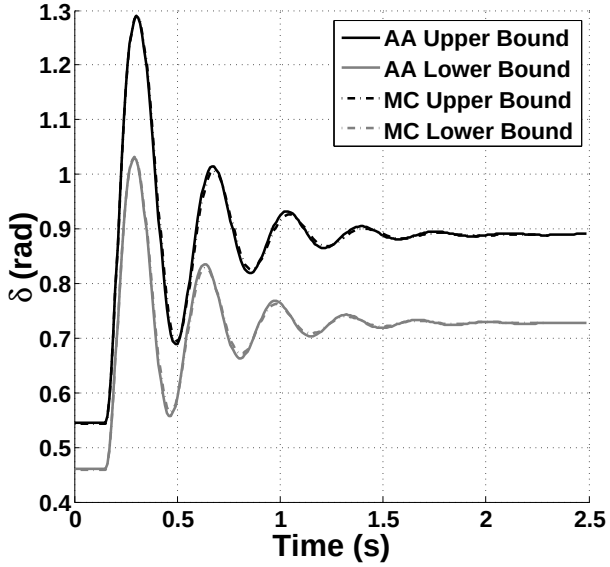

Figure 5.4: SMIB test system: 3-cycle fault with ±10% variation in generation.

significant difference between the curve that bounds unstable cases and the curve that bounds stable cases, as time progresses. Nevertheless, for the simulation time considered, the proposed AA-based approach is able to identify stable and unstable bounds.

The proposed AA approach was computationally more efficient than MCS for all cases, yielding 23 times faster simulations (0.798 s vs 18.36 s) for the results depicted in Figure 5.7.

5.3.2 Two-area Test System with Synchronous Generators

The system shown in Figure 5.11 is comprised of 11 buses and four generators that supply a total base load of 2734 MW [99]. Two of these generators (G2 and G4) are assumed to be intermittent sources of power, and are represented using detailed synchronous generator sub-transient models, as well as fast static excitation systems. The set of algebraized DAEs in affine form for this study case is given in Appendix B. The data for the generators is shown in Table 5.2.

Figure 5.9 illustrates the dynamic response of the system for a three-phase fault in the middle of one of the parallel lines connecting buses 8 and 9; the fault is cleared after 7.1 cycles by

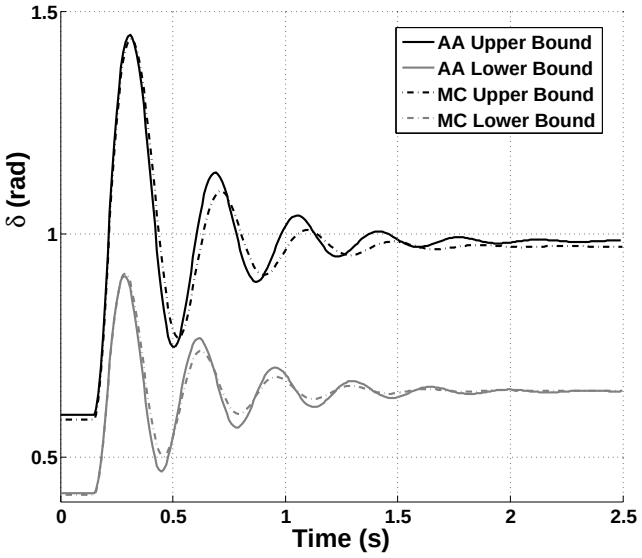

Figure 5.5: SMIB test system: 3-cycle fault with ±20% variation in generation.

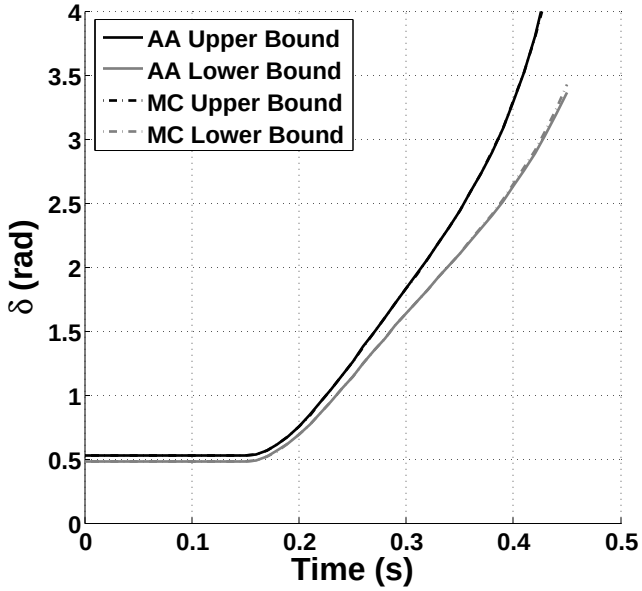

Figure 5.6: SMIB test system: 15-cycle fault with ±5% variation in generation.

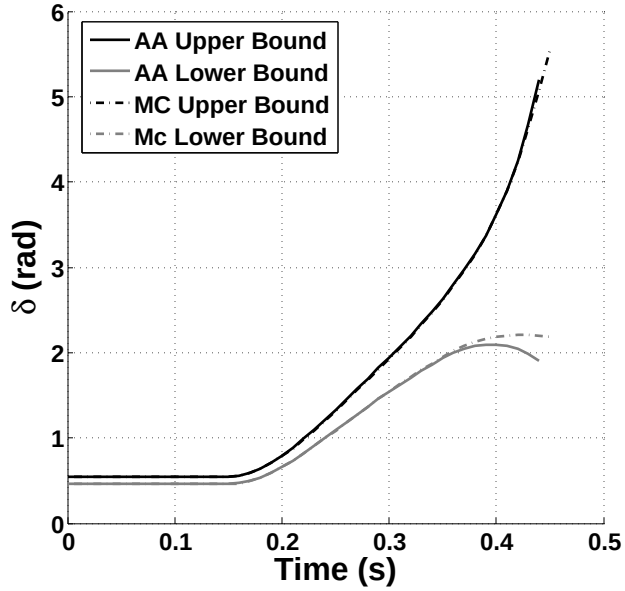

Figure 5.7: SMIB test system: 12-cycle fault with ±10% variation in generation.

Table 5.2: Sub-transient model data for synchronous generators

$X_d(p.u.)$	$X_q(p.u.)$	$X_l(p.u.)$	$X'_d(p.u.)$	$X'_q(p.u.)$	$X''_d(p.u.)$	$X''_q(p.u.)$	$R_a(p.u.)$	$T'_{d0}(s)$	$T'_{q0}(s)$
1.8	1.7	0.2	0.3	0.55	0.25	0.25	0.0025	8	0.4
$T''_{d0}(s.)$	$T''_{q0}(s.)$	$H_{G1}(p.u.\cdot s)$	$H_{G2}(p.u.\cdot s)$	$H_{G3}(p.u.\cdot s)$	$H_{G4}(p.u.\cdot s)$	K_a	$T_{ec}(s.)$	Da	$S_n(MVA)$
0.03	0.05	6.5	6.5	6.175	6.175	200	0.01	0.01	900

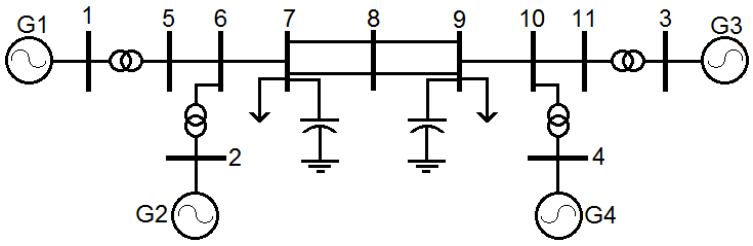

Figure 5.8: Two-area test system with synchronous generators.

tripping the faulted line. Notice that the system is unstable for ±10% variation of power at G2

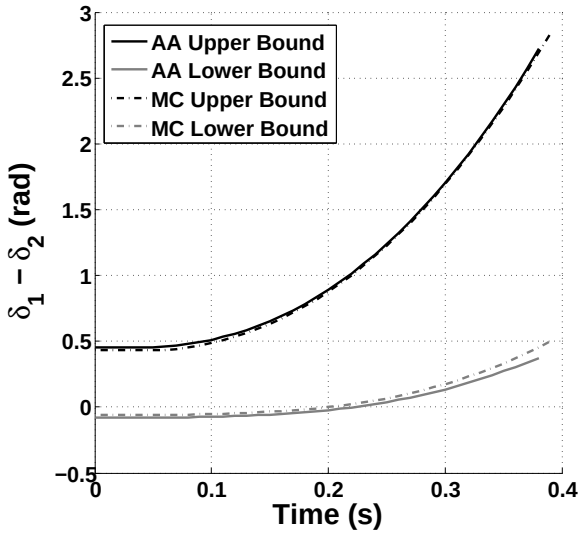

Figure 5.9: Two-area test system with synchronous generators results: 7.1-cycle fault with ±10% variation in generation.

and G4. The AA-based approach closely follows the hull of dynamic curves, with a maximum error of 6.02%, and being 292 times faster (13.48 s vs 3936.33 s) with respect to MCS.

Figure 5.10 depicts the dynamic response of the system for a three-phase fault close to Bus 9. The fault is cleared after 1 cycle by tripping the faulted line. The system is stable for the ±10% range of variation of the assumed intermittent power sources. The AA-based approach closely follows the hull of dynamic curves, with a maximum error of 8.3%.

5.3.3 Two-area Test System with Wind Turbines

In the two-area test system system in Figure (5.11), two of these generators (G2 and G4) are replaced by wind turbines based on DFIG, which are modeled using the dq equations presented in Appendix C. The set of algebraized DAEs in affine form for this study case is also given in Appendix C. Generators G1 and G2 are modeled using a classical representation and the corresponding data is given in Table 5.3. The wind turbine data is shown in Table 5.4.

Figure 5.12 illustrates the dynamic response of the system for a three-phase fault in the middle

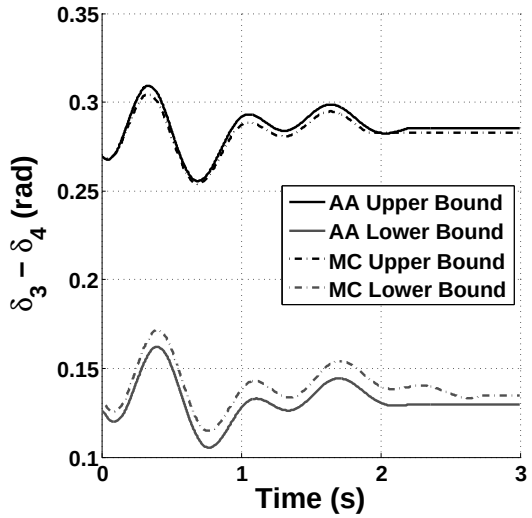

Figure 5.10: Two-area test system results with synchronous generators results: 1-cycle fault with ±10% variation in generation.

Table 5.3: Synchronous generators data.

$x'_d(p.u.)$	$H_{G2}(p.u.\cdot s)$	$H_{G4}(p.u.\cdot s)$	Da
0.3	6.5	6.175	0.1

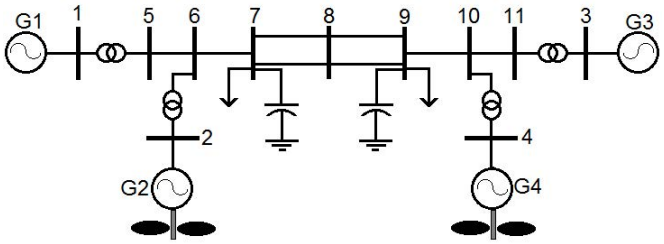

Figure 5.11: Two-area test system with DFIG-based wind turbines.

Table 5.4: DFIG-based wind turbines data.

$x_s(p.u.)$	$x_r(p.u.)$	$x_m(p.u.)$	$r_r(p.u.)$	$r_s(p.u.)$	K_p	K_v	$T_p(s)$	$T_r(s)$	$H_m(kWs/kVa)$
0.10	0.08	3	0.01	0.01	5.0	50	0.01	0.01	3

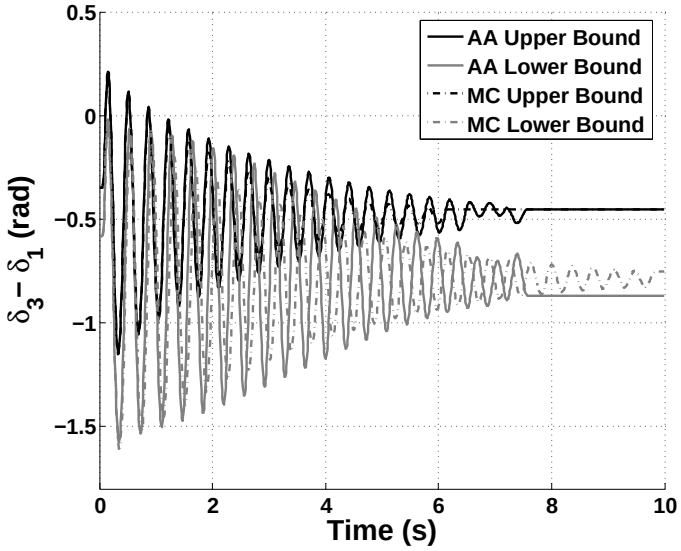

Figure 5.12: Two-area test system with DFIG-based wind turbines results: 3-cycle fault with ±10% variation in generation.

of one of the parallel lines connecting Buses 8 and 9; the fault is cleared after 3 cycles by tripping the faulted line. Notice that the system is stable for ±10% variation of power at G2 and G4. The AA-based approach exhibits a maximum and mean error of 20.67% and 7.67%, respectively, being 238 times faster than MCS. Figure 5.13 depicts the dynamic response of the system for a three-phase fault close to Bus 9, which is cleared after 8 cycles by tripping the faulted line. In this case, the system is unstable for the ±10% range of variation of the assumed intermittent power sources. Notice that the AA-based approach closely follows the hull of dynamic curves, with a maximum error of 5.65%.

The sources of error of the proposed AA-based method are associated with the truncated approximation of non-affine functions such as sinusoidal functions, the size of the intervals of the uncertain variables, and errors due to the number of uncertain variables and size of the system. The greater the number of uncertain variables and size of the system, the greater the error, as demonstrated for the two-area test system. This is expected, since with the number of equations and coefficients of the affine forms increasing, the truncation errors associated with non-affine operations also increase. However, given the limited number of uncertain generators and limited

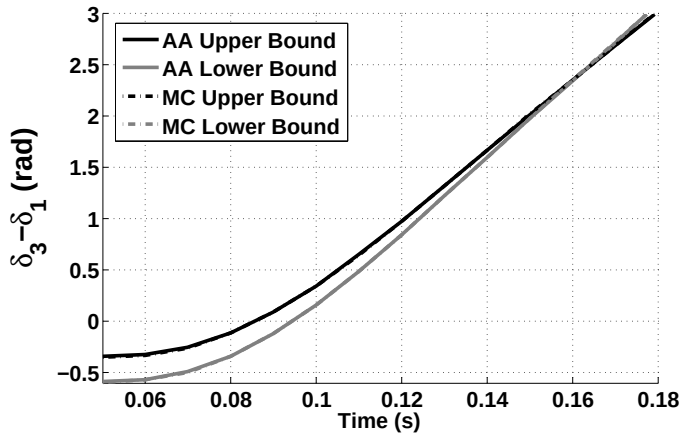

Figure 5.13: Two-area test system with DFIG-based wind turbines results: 8-cycle fault with ±10% variation in generation.

range of variation in real systems, one would expect reasonable results in real-sized systems.

5.4 Summary

This chapter presented a novel AA-based method for transient stability assessment of power systems with intermittent sources of generation such as wind and solar power. Similar to the AA-based methods for power flow analysis and voltage stability assessment discussed in Chapters 3 and 4, respectively, uncertainties were modeled as intervals without any assumptions regarding their probabilities. The proposed AA-based method was able to compute the hull of the system dynamic response when the system presents uncertainties due to operating conditions, based on a trapezoidal integration technique. It was noticed that stable and unstable bounds of the system dynamic response are adequately represented by the AA-based approach, and the results depicted a reasonable good accuracy at significantly lower computational costs when compared to those obtained using simulation based techniques.

Chapter 6

Conclusions, Contributions, and Future Work

6.1 Summary and Main Conclusions

Most of the available techniques for probabilistic stability assessment of power systems are based on analytical and sampling based approaches, which may be computationally demanding and/or rely on assumptions that may be unrealistic in some cases. To overcome these difficulties, novel AA-based methods for voltage and transient stability assessment of power systems with intermittent sources of generation such as wind and solar power were proposed in this thesis.

A new representation of generator reactive power limits was proposed in this thesis, which is a more efficient alternative to the bus type switching strategy adopted in the existing AA-based power flow analysis. This new representation is based on the introduction of additional noise symbols associated with voltage control settings, which allows keeping the generator reactive powers within limits by modifying their terminal voltages.

The proposed AA-based method for voltage stability assessment computes the bounds of the PV curves and associated static load margins when the system presents uncertainties due to operating conditions, without any assumption on their pdfs. This method is based on a parametrization technique which allows obtaining feasible solutions for the whole hull of PV curves. The

results depicted a reasonable good accuracy at significantly lower computational costs when compared to those obtained using simulation based techniques. Comparisons also showed that the lower bound of the maximum loadability, obtained using the AA-based approach is pessimistic, while it was optimistic in some cases for the SF approach, thus making the AA-based approach more appropriate for practical applications.

The proposed AA-based method for transient stability assessment is able to compute the hull of the system dynamic response when the system presents uncertainties in operating conditions. This method is based on a trapezoidal integration approach, which yields a good numerical stability, and is not model-dependent; thus, any model for synchronous generators, wind turbines and PV arrays can be used, as demonstrated in the study cases. Similar to the AA-based method for voltage stability assessment, results depicted a reasonable good accuracy at significantly lower computational costs when compared to those obtained using simulation based techniques. Stable and unstable bounds of the system dynamic response were adequately represented by the AA-based approach.

The proposed AA-based methods represent computationally efficient alternative to the well-known sampling and analytical approaches, and unlike most of these approaches, uncertainties are modeled as intervals without any need for assumptions regarding their probabilities. These intervals reflects the uncertainty of the estimated output power, and avoids the difficulties in properly representing the uncertainties of wind and solar power using pdfs.

6.2 Main Contributions

This thesis conceptualized and proposed new AA-based computing paradigms for PV curve computation and transient stability assessment of power systems considering uncertainties associated with intermittent sources of power. The main contributions are as follows:

- A more efficient representation of generator reactive power limits, which avoids the bus switching strategy used in the existing AA-based power flow analysis method, has been proposed in this thesis. The use of rectangular-coordinate equations in the AA-based power flow problem is also studied, demonstrating to be more efficient and accurate than the polar-coordinate equations approach.

- A novel, computationally efficient and reasonably accurate approach based on AA for voltage stability assessment of power systems with intermittent power sources has been proposed in this thesis, as a better alternative to popular simulation-based tools. This method is also more adequate as compared with a previously proposed technique to estimate the impact of parameter variations in voltage stability assessment.

- Finally, a new, computationally efficient and reasonably accurate AA-based method method for transient stability assessment of power systems with power sources has also been proposed in this thesis. This method is not model-dependent and, as the proposed AA-based voltage stability technique, uncertainties are modeled as intervals without any need for assumptions regarding their probabilities.

The proposed AA-based methods, as well as part of the results of this thesis have been published in [117], [121], and [122], and the journal paper [125] has been submitted for publication.

6.3 Future Work

The following research topics could be considered to improve the proposed AA-based methods:

- In order to efficiently account for system contingencies, the uncertainty associated with equipment outages (i.e. lines and transformers) could be modeled using AA by describing the equipment outages with proper variations of the admittance matrix elements. For instance, the parameters of the equipment equivalent circuits could be defined using the intervals $[X, 1e6]$, where X is the value of the impedance, and 1e6 corresponds to the equipment out of service. This approach needs further research to show its feasibility.

- Code development to facilitate the general handling of model equations in affine form is needed. This code will allow testing the proposed AA-based methods with larger test systems.

Appendix A

AA Model of Single-Machine-Infinite-Bus Test System

Algebraized DAEs in affine form:

$$\widehat{\delta}_n - \widehat{\delta}_{n-1} - \frac{\Delta t}{2}\left(\widehat{\omega}_n - \omega_s + \widehat{\omega}_{n-1} - \omega_s\right) = 0 \tag{A.1}$$

$$\widehat{\omega}_n - \widehat{\omega}_{n-1} - \frac{\Delta t}{2}\left(\widehat{f_{2a}} + \widehat{f_{2b}}\right) = 0 \tag{A.2}$$

where:

$$\widehat{f_{2a}} = \left[\widehat{P}_m - \widehat{P}_e sin(\widehat{\delta}_n - Da(\widehat{\omega}_n - \omega_s)\right] \frac{\omega_s^2}{2H\widehat{\omega}_n} \tag{A.3}$$

$$\widehat{f_{2b}} = \left[\widehat{P}_m - \widehat{P}_e sin(\widehat{\delta}_{n-1} - Da(\widehat{\omega}_{n-1} - \omega_s)\right] \frac{\omega_s^2}{2H\widehat{\omega}_{n-1}} \tag{A.4}$$

where:

- Power delivered before the fault:

$$\widehat{P}_e = \frac{\widehat{E'}V_2}{X'_d + X_T + X_{12}X_{13}/\left(X_{12} + X_{13}\right)} \tag{A.5}$$

- Power delivered during the fault:

$$\widehat{P}_e = \frac{\widehat{E'} V_2 X_{13}/(X_{13} + X_{12})}{X'_d + X_T + X_{12}X_{13}/(X_{12} + X_{13})} \tag{A.6}$$

- Power delivered after the fault:

$$\widehat{P}_e = \frac{\widehat{E'} V_2}{X'_d + X_T + X_{12}} \tag{A.7}$$

Appendix B

AA Model of Two-Area Test System with Synchronous Generators

Algebraized DAEs in affine form:

$$\widehat{E}'_{q_n} - \widehat{E}'_{q_{n-1}} - \frac{\Delta t}{2}\left(\widehat{f}_{1_a} + \widehat{f}_{1_b}\right) = 0 \tag{B.1}$$

where:

$$\widehat{f}_{1_a} = \frac{1}{T''_{do}}\left(\widehat{E}'_{q_n} - \left(X'_d - X''_d\right)\widehat{I}_{d_n} - \widehat{E}''_{q_n}\right) \tag{B.2}$$

$$\widehat{f}_{1_b} = \frac{1}{T''_{do}}\left(\widehat{E}'_{q_{n-1}} - \left(X'_d - X''_d\right)\widehat{I}_{d_{n-1}} - \widehat{E}''_{q_{n-1}}\right) \tag{B.3}$$

$$\widehat{E}'_{d_n} - \widehat{E}'_{d_{n-1}} - \frac{\widehat{\Delta t}}{2}\left(\widehat{f}_{2_a} + \widehat{f}_{2_b}\right) = 0 \tag{B.4}$$

where:

$$\widehat{f}_{2_a} = \frac{1}{T''_{qo}}\left(\widehat{E}'_{d_n} - \left(X'_q - X''_q\right)\widehat{I}_{q_n} - \widehat{E}''_{d_n}\right) \tag{B.5}$$

$$\widehat{f}_{2_b} = \frac{1}{T''_{qo}}\left(\widehat{E}'_{d_{n-1}} - \left(X'_q - X''_q\right)\widehat{I}_{q_{n-1}} - \widehat{E}''_{d_{n-1}}\right) \tag{B.6}$$

$$\widehat{E}'_{q_n} - \widehat{E}'_{q_{n-1}} - \frac{\Delta t}{2}\left(\widehat{f}_{3_a} + \widehat{f}_{3_b}\right) = 0 \tag{B.7}$$

where:

$$\widehat{f_{3_a}} = \frac{1}{T'_{do}}\left(\widehat{E}_{f_n} + \left(X_d - X'_d\right)\widehat{I}_{d_n} - \widehat{E}'_{q_n}\right) \tag{B.8}$$

$$\widehat{f_{3_b}} = \frac{1}{T'_{do}}\left(\widehat{E}_{f_{n-1}} + \left(X_d - X'_d\right)\widehat{I}_{d_{n-1}} - \widehat{E}'_{q_{n-1}}\right) \tag{B.9}$$

$$\widehat{E}'_{d_n} - \widehat{E}'_{d_{n-1}} - \frac{\Delta t}{2}\left(\widehat{f_{4_a}} + \widehat{f_{4_b}}\right) = 0 \tag{B.10}$$

where:

$$\widehat{f_{4_a}} = \frac{1}{T'_{qo}}\left(-\left(X_q - X'_q\right)\widehat{I}_{q_n} - \widehat{E}'_{d_n}\right) \tag{B.11}$$

$$\widehat{f_{4_b}} = \frac{1}{T'_{qo}}\left(-\left(X_q - X'_q\right)\widehat{I}_{q_{n-1}} - \widehat{E}'_{d_{n-1}}\right) \tag{B.12}$$

$$\widehat{\omega}_n - \widehat{\omega}'_n - \frac{\Delta t}{2}\frac{1}{M}\left(2\widehat{P}_m + \widehat{f_{5_a}} + \widehat{f_{5_b}}\right) = 0 \tag{B.13}$$

where:

$$\widehat{f_{5_a}} = -\widehat{I}_{d_n}\widehat{V}_n sin\left(\widehat{\theta}_n - \delta_n\right) - \widehat{I}_{q_n}\widehat{V}_n cos\left(\widehat{\theta}_n - \widehat{\delta}_n\right) - Da\left(\widehat{\omega}_n - \omega_s\right) \tag{B.14}$$

$$\widehat{f_{5_b}} = -\widehat{I}_{d_{n-1}}\widehat{V}_{n-1} sin\left(\widehat{\theta}_{n-1} - \delta_{n-1}\right) - \widehat{I}_{q_{n-1}}\widehat{V}_{n-1} cos\left(\widehat{\theta}_{n-1} - \widehat{\delta}_{n-1}\right) - Da\left(\widehat{\omega}_{n-1} - \omega_s\right) \tag{B.15}$$

$$\widehat{\delta}_n - \widehat{\delta}_{n-1} - \frac{\Delta t}{2}\left(\widehat{\omega}_n - \widehat{\omega}_{n-1}\right) = 0 \tag{B.16}$$

$$\widehat{E}_{f_n} - \widehat{E}_{f_{n-1}} - \frac{\Delta t}{2}\left(\widehat{f_{7_a}} + \widehat{f_{7_b}}\right) = 0 \tag{B.17}$$

where:

$$\widehat{f_{7_a}} = \frac{1}{T_{ec}}\left(K_a(\widehat{V}_{ref} - \widehat{V}_n) - \widehat{E}_{f_n}\right) \tag{B.18}$$

$$\widehat{f_{7_b}} = \frac{1}{T_{ec}}\left(K_a(\widehat{V}_{ref} - \widehat{V}_{n-1}) - \widehat{E}_{f_{n-1}}\right) \tag{B.19}$$

$$\widehat{E}''_q - \left(r_s\widehat{I}_q - X''_d\widehat{I}_d + \widehat{V}_q\right) = 0 \tag{B.20}$$

$$\widehat{E}''_d - \left(r_s\widehat{I}_d - X''_d\widehat{I}_q + \widehat{V}_d\right) = 0 \tag{B.21}$$

$$\widehat{V}_q - \left(\widehat{V} cos\left(\widehat{\theta}_{Ia} - \widehat{\delta}\right)\right) = 0 \tag{B.22}$$

$$\widehat{V}_d - \left(\widehat{V} sin\left(\widehat{\theta}_{Ia} - \widehat{\delta}\right)\right) = 0 \tag{B.23}$$

$$\widehat{I}_q - \left(\widehat{I} cos\left(\widehat{\theta}_{Ia} - \widehat{\delta}\right)\right) = 0 \tag{B.24}$$

$$\widehat{I}_d - \left(\widehat{I} sin\left(\widehat{\theta}_{Ia} - \widehat{\delta}\right)\right) = 0 \tag{B.25}$$

Network equations:

- For generator buses:

$$\widehat{V}_j \widehat{I}_j cos\left(\widehat{\theta}_j - \widehat{\theta}_{Ia_j}\right) - P_{L_j} - \sum_{i=1}^{N} \left(\widehat{V}_j \widehat{V}_i \left(G_{ji} cos\left(\widehat{\theta}_j - \widehat{\theta}_i\right) + B_{ij} sin\left(\widehat{\theta}_j - \widehat{\theta}_i\right)\right)\right) = 0 \tag{B.26}$$

$$\widehat{V}_j \widehat{I}_j sin\left(\widehat{\theta}_j - \widehat{\theta}_{Ia_j}\right) - Q_{L_j} - \sum_{i=1}^{N} \left(\widehat{V}_j \widehat{V}_i \left(G_{ji} sin\left(\widehat{\theta}_j - \widehat{\theta}_i\right) - B_{ij} cos\left(\widehat{\theta}_j - \widehat{\theta}_i\right)\right)\right) = 0 \tag{B.27}$$

- For load buses:

$$\sum_{i=1}^{N} \left(\widehat{V}_j \widehat{V}_i \left(G_{ji} cos\left(\widehat{\theta}_j - \widehat{\theta}_i\right) + B_{ij} sin\left(\widehat{\theta}_j - \widehat{\theta}_i\right)\right)\right) + P_{L_i} = 0 \tag{B.28}$$

$$\sum_{i=1}^{N} \left(\widehat{V}_j \widehat{V}_i \left(G_{ji} sin\left(\widehat{\theta}_j - \widehat{\theta}_i\right) - B_{ij} cos\left(\widehat{\theta}_j - \widehat{\theta}_i\right)\right)\right) + Q_{L_i} = 0 \tag{B.29}$$

Appendix C

AA Model of Two-Area Test System with Wind Turbines

The DFIG generator DAEs are:

$$\dot{\omega}_m = \left(\frac{P_\omega}{\omega_m} - (\Psi_{ds} i_{qs} - \Psi_{qs} i_{ds}) \right) \frac{1}{2H_m} \tag{C.1}$$

$$\dot{i}_{qr} = \left(-\frac{x_s + x_m}{x_m V} \frac{P_\omega^{opt}(\omega_m)}{\omega_m} - i_{qr} \right) \frac{1}{T_r} \tag{C.2}$$

$$\dot{i}_{dr} = K_v \left(V - V_{ref} \right) - \frac{V}{x_m} - i_{dr} \tag{C.3}$$

$$\dot{\theta_p} = \frac{K_p}{T_p} \left(\omega_m - \omega_{ref} \right) \tag{C.4}$$

where:

$$\Psi_{ds} = -((x_s + x_m) i_{ds} + x_m i_{dr}) \tag{C.5}$$

$$\Psi_{qs} = -((x_s + x_m)i_{qs} + x_m i_{qr}) \tag{C.6}$$

$$P_\omega = \frac{\rho}{2} c_p\left(\lambda_p, \theta_p\right) A_r v^3 \tag{C.7}$$

$$c_p = 0.22\left(\frac{116}{\lambda_i} - 0.4 * \theta_p - 5\right) e^{\left(\frac{-12.5}{\lambda_i}\right)} \tag{C.8}$$

$$\frac{1}{\lambda_i} = \frac{1}{\lambda_p + 0.08\theta_p} - \frac{0.035}{\lambda_p^3 + 1} \tag{C.9}$$

and the following algebraic equations:

$$v_{ds} = -r_s i_{ds} + (x_s + x_m)i_{qs} + x_m i_{qr} \tag{C.10}$$

$$v_{qs} = -r_s i_{qs} - (x_s + x_m)i_{ds} - x_m i_{dr} \tag{C.11}$$

$$v_{dr} = -r_r i_{dr} + (1 - \omega_m)((x_r + x_m)i_{qr} + x_m i_{qs}) \tag{C.12}$$

$$v_{qr} = -r_r i_{qr} - (1 - \omega_m)((x_r + x_m)i_{dr} + x_m i_{ds}) \tag{C.13}$$

The algebraized DAEs in affine form are as follows:

- For wind turbines based on DFIGs:

$$\begin{aligned} &\widehat{\omega}_n - \widehat{\omega}_{n-1} - \frac{\Delta t}{2} * \left(\frac{\widehat{P}_\omega}{\widehat{\omega}_{m_n}} - (\widehat{\Psi}_{ds_n}\widehat{i}_{qs_n} - \widehat{\Psi}_{qs_n}\widehat{i}_{ds_n})\frac{1}{2H_m}\right) \\ &+\frac{\Delta t}{2}\left(\frac{\widehat{P}_\omega}{\widehat{\omega}_{m_{n-1}}} - (\widehat{\Psi}_{ds_{n-1}}\widehat{i}_{qs_{n-1}} - \widehat{\Psi}_{qs_{n-1}}\widehat{i}_{ds_{n-1}})\frac{1}{2H_m}\right) = 0 \end{aligned} \tag{C.14}$$

$$\widehat{\Psi}_{ds_n} = -((x_s + x_m)\widehat{i}_{ds_n} + x_m\widehat{i}_{dr_n}) \tag{C.15}$$

$$\widehat{\Psi}_{qs_n} = -((x_s + x_m)\widehat{i}_{qs_n} + x_m\widehat{i}_{qr_n}) \tag{C.16}$$

$$\widehat{i}_{qr_n} - \widehat{i}_{qr_{n-1}} - \frac{\Delta t}{2} * \left(\left(-\frac{x_s + x_m}{x_m V} \frac{\widehat{P}^{opt}_{\widehat{\omega}_n}(\widehat{\omega}_{m_n})}{\widehat{\omega}_{m_n}} - \widehat{i}_{qr_n} \right) \frac{1}{T_r} + \left(-\frac{x_s + x_m}{x_m V} \frac{\widehat{P}^{opt}_{\widehat{\omega}_{n-1}}(\widehat{\omega}_{m_{n-1}})}{\widehat{\omega}_{m_{n-1}}} - \widehat{i}_{qr_{n-1}} \right) \frac{1}{T_r} \right) = 0 \tag{C.17}$$

$$\widehat{i}_{dr_n} - \widehat{i}_{dr_{n-1}} - \frac{\Delta t}{2} \left(K_v \left(\widehat{V}_n - \widehat{V}_{ref} \right) - \frac{\widehat{V}_n}{x_m} - \widehat{i}_{dr_n} + K_v \left(\widehat{V}_{n-1} - \widehat{V}_{ref} \right) - \frac{\widehat{V}_{n-1}}{x_m} - \widehat{i}_{dr_{n-1}} \right) = 0 \tag{C.18}$$

$$\widehat{\theta}_{p_n} - \widehat{\theta}_{p_{n-1}} - \frac{\Delta t}{2} \left(\frac{K_p}{T_p} \left(\omega_{m_n} - \widehat{\omega}_{ref_n} \right) + \frac{K_p}{T_p} \left(\omega_{m_{n-1}} - \widehat{\omega}_{ref} \right) \right) = 0 \tag{C.19}$$

$$\widehat{v}_{ds_n} - \left(-r_s\widehat{i}_{ds_n} + (x_s + x_m)\widehat{i}_{qs_n} + x_m\widehat{i}_{qr_n} \right) = 0 \tag{C.20}$$

$$\widehat{v}_{qs_n} - \left(-r_s\widehat{i}_{qs_n} - (x_s + x_m)\widehat{i}_{ds_n} - x_m\widehat{i}_{dr_n} \right) = 0 \tag{C.21}$$

$$\widehat{v}_{dr_n} - \left(-r^r\widehat{i}_{dr_n} + (1 - \widehat{\omega}_{m_n})((x^r + x_m)\widehat{i}_{qr_n} + x_m\widehat{i}_{qs_n}) \right) = 0 \tag{C.22}$$

$$\widehat{v}_{qr_n} - \left(-r^r\widehat{i}_{qr_n} - (1 - \widehat{\omega}_{m_n})((x^r + x_m)\widehat{i}_{dr_n} + x_m\widehat{i}_{ds_n}) \right) = 0 \tag{C.23}$$

- For Synchronous Generators:

$$\widehat{\omega}_n - \widehat{\omega}_{n-1} - \frac{\Delta t}{2}(\widehat{P}_m - \widehat{E} * \widehat{V}_n * sin(\widehat{\delta}_n - \widehat{\theta}_n) - Da * (\widehat{\omega}_{r_n} - \widehat{\omega}_s) + \widehat{P}_m - \widehat{E} * \widehat{V}_{n-1} * sin(\widehat{\delta}_{n-1} - \widehat{\theta}_{n-1}) - Da * (\widehat{\omega}_{r_{n-1}} - \omega_s)) = 0 \tag{C.24}$$

$$\delta_n - \delta_{n-1} - \frac{\Delta t}{2}(\omega_n - \omega_s + \omega_{n-1} - \omega_s) = 0 \tag{C.25}$$

Bibliography

[1] "Green Energy Act," 2009. [Online]. Available: http://www.e-laws.gov.on.ca/html/source/statutes/english/2009/elaws_src_s09012_e.htm

[2] "Grid Integration of Wind Generation," Working Group C 6.08 CIGRE, 2011.

[3] D. Gautam, V. Vittal, and T. Harbour, "Impact of Increased Penetration of DFIG-Based Wind Turbine Generators on Transient and Small Signal Stability of Power Systems," *IEEE Trans. Power Syst.*, vol. 24, no. 3, pp. 1426–1434, Aug. 2009.

[4] K. Methaprayoon, C. Yingvivatanapong, L. Wei-Jen, and J. Liao, "An Integration of ANN Wind Power Estimation Into Unit Commitment Considering the Forecasting Uncertainty," *IEEE Trans. on Industry Applications*, vol. 43, no. 6, pp. 1441–1448, Nov. 2007.

[5] J. Matevosyan and L. Soder, "Minimization of Imbalance Cost Trading Wind Power on the Short-Term Power Market," *IEEE Trans. on Power Syst.*, vol. 21, no. 3, pp. 1396–1404, Aug. 2006.

[6] H. Bri-Mathias and M. Milligan, "Wind Power Forecasting Error Distributions Over Multiple Timescales," in *Proc. Power and Energy Society General Detroit, Michigan*, 2011, pp. 1–7.

[7] H. Bludszuweit, J. Dominguez-Navarro, and A. Llombart, "Statistical Analysis of Wind Power Forecast Errors," *IEEE Trans. on Power Syst.*, vol. 23, no. 3, pp. 983–991, Aug. 2008.

[8] S. Tewari, C. Geyer, and N. Mohan, "A Statistical Model for Wind Power Forecast Error and its Application to the Estimation of Penalties in Liberalized Markets," *IEEE Trans. on Power Syst.*, vol. 26, no. 4, pp. 2031–2039, Nov. 2011.

[9] [Online]. Available: http://www.energy.gov.on.ca/docs/en/MEI_LTEP_en.pdf

[10] [Online]. Available: http://www.aeso.ca/gridoperations/18286.html

[11] L. Ming-Shun, C. Chung-Liang, L. Wei-Jen, and L. Wang, "Combining the Wind Power Generation System With Energy Storage Equipment," *IEEE Trans. on Industry Applications*, vol. 45, no. 6, pp. 2109–2115, Nov. 2009.

[12] V. Akhmatov, "Analysis of Dynamic Behaviour of Electric Power Systems With Large Amount of Wind Power," Ph.D. Thesis, Technical University of Denmark, Denmark, 2003.

[13] D. Gautam, C. Goel, and D. Villacci, "Control Strategy to Mitigate the Impact of Reduced Inertia Due to Doubly Fed Induction Generators on Large Power Systems," *IEEE Trans. on Power Syst.*, vol. 26, no. 1, pp. 214–224, Feb. 2011.

[14] A. Vaccaro, C. Cañizares, and D. Villacci, "An Affine Arithmetic-Based Method for Reliable Power Flow Analysis in the Presence of Data Uncertainty," *IEEE Trans. on Power Syst.*, vol. 25, no. 2, pp. 624–632, May. 2010.

[15] P. Jorgensen, J. S. Christensen, and J. O. Tande, "Probabilistic Load Flow Calculation Using Monte Carlo Techniques for Distribution Network With Wind Turbines," in *Proc. 8th International Conference on Harmonics and Quality of Power*, 1998, pp. 1146–1151.

[16] R. N. Allan, C. H. Grigg, and M. R. G. Al-Shakarchi, "Numerical Techniques in Probabilistic Load Flow Problems," *International Journal for Numerical Methods in Engineering*, vol. 10, no. 4, pp. 853–860, Mar. 1976.

[17] S. Conti and S. Raiti, "Probabilistic Load Flow Using Monte Carlo Techniques for Distribution Networks With Photovoltaic Generators," *Solar Energy*, vol. 81, no. 12, pp. 1473–1481, Dec. 2007.

[18] P. Chen, Z. Chen, and B. Bak-Jensen, "Probabilistic Load Flow: A Review," in *Proc. 3rd Int. Conf. Electric Utility Deregulation and Restructuring and Power Technologies*, 2008, pp. 1586–1591.

[19] R. Allan and A. Leite da Silva, "Probabilistic Load Flow Using Multilinearisations," *IEE Generation, Transmission and Distribution*, vol. 128, no. 5, pp. 280–287, Sep. 1981.

[20] M. Brucoli, F. Torelli, and R. Napoli, "Quadratic Probabilistic Load Flow With Linearly Modelled Dispatchs," *International Journal of Electrical Power and Energy Systems*, vol. 81, pp. 138–146, Jul. 1985.

[21] D. Dondera, R. Popa, and C. Velicescu, "The Multi-Area Systems Reliability Estimation Using Probabilistic Load Flow by Gramm-Charlier Expansion," in *Proc. EUROCON the International Conference on Computer as a Tool*, 2007, pp. 1470–1474.

[22] P. Zhang and S. T. Lee, "Probabilistic Load Flow Computation Using the Method of Combined Cumulants and Gram-Charlier Expansion," *IEEE Trans. on Power Syst.*, vol. 19, no. 1, pp. 676–682, Feb. 2004.

[23] S. Chun-Lien, "Probabilistic Load-Flow Computation Using Point Estimate Method," *IEEE Trans. on Power Syst.*, vol. 20, no. 4, pp. 1843–1851, Nov. 2005.

[24] P. Caramia, G. Carpinelli, and P. Varilone, "Point Estimate Schemes for Probabilistic Three-Phase Load Flow," *Electr. Power Syst. Res.*, vol. 80, pp. 168–175, Feb. 2010.

[25] G. Verbic and C. Cañizares, "Probabilistic Optimal Power Flow in Electricity Markets Based on a Two-Point Estimate Method," *IEEE Trans. on Power Syst.*, vol. 21, no. 4, pp. 1883–1893, Nov. 2006.

[26] H. Yu, C. Y. Chung, K. P. Wong, H. W. Lee, and J. H. Zhang, "Probabilistic Load Flow Evaluation With Hybrid Latin Hypercube Sampling and Cholesky Decomposition," *IEEE Trans. on Power Syst.*, vol. 24, no. 2, pp. 661–667, May. 2009.

[27] A. M. L. da Silva and V. L. Arienti, "Probabilistic Load Flow by a Multilinear Simulation Algorithm," vol. 137, no. 4, pp. 276–282, Jul. 1990.

[28] P. R. Bijwe and G. K. V. Raju, "Fuzzy Distribution Power Flow for Weakly Meshed Systems," *IEEE Trans. on Power Syst.*, vol. 21, no. 4, pp. 1645–1652, Nov. 2006.

[29] A. Dimitrovski and K. Tomsovic, "Boundary Load Flow Solutions," *IEEE Trans. on Power Syst.*, vol. 19, no. 1, pp. 348–355, Feb. 2004.

[30] M. Cortes-Carmona, R. Palma-Behnke, and G. Jimenez-Estevez, "Fuzzy Arithmetic for the DC Load Flow," *IEEE Trans. on Power Syst.*, vol. 25, no. 1, pp. 206–214, Feb. 2010.

[31] L. Hong, L. Shi, L. Yao, Y. Ni, and M. Bazargan, "Study on Fuzzy Load Flow With Consideration of Wind Generation Uncertainties," in *Proc. Transmission and Distribution Conference and Exposition: Asia and Pacific*, 2009, pp. 1–4.

[32] Z. Wang and F. Alvarado, "Interval Arithmetic in Power Flow Analysis," *IEEE Trans. on Power Syst.*, vol. 7, no. 3, pp. 1341–1349, Aug. 1992.

[33] L. Barboza, G. P. Dimuro, and R. Reiser, "Towards Interval Analysis of the Load Uncertainty in Power Electric Systems," in *Proc. 8th International Conference on Probabilistic Methods Applied to Power Sytems*, 2004, pp. 538–544.

[34] B. Das, "Radial Distribution System Power Flow Using Interval Arithmetic," *Elect. Power Syst.*, vol. 24, no. 10, pp. 827–836, Dec. 2002.

[35] A. Vaccaro and D. Villaci, "Radial Power Flow Tolerance Analysis by Interval Constraint Propagation," *IEEE Trans. on Power Syst.*, vol. 24, no. 1, pp. 28–31, Feb. 2009.

[36] A. Vaccaro, C. Cañizares, and D. Villaci, "A Simple and Reliable Algorithm for Computing Boundaries of Power Flow Solutions due to System Uncertainties," in *Proc. Powertech - Innovative ideas toward the Electrical Grid of the Future*, 2009, pp. 1–6.

[37] A. Rodrigues, R. Prada, and M. Da Guia da Silva, "Voltage Stability Probabilistic Assessment in Composite Systems: Modeling Unsolvability and Controllability Loss," *IEEE Trans. on Power Syst.*, vol. 25, no. 3, pp. 1575–1588, Aug. 2010.

[38] A. Leite da Silva, I. Coutinho, A. C. Zambroni de Souza, R. B. Prada, and A. Rei, "Voltage Collapse Risk Assessments," *Electr. Power Syst. Res.*, vol. 54, no. 3, pp. 221–227, Jun. 2000.

[39] S. Chun-Lien and L. Chan-Nan, "Two-Point Estimate Method for Quantifying Transfer Capability Uncertainty," *IEEE Trans. on Power Syst.*, vol. 20, no. 2, pp. 573–579, May. 2005.

[40] R. Billinton and S. Aboreshaid, "Voltage Stability Considerations in Composite Power System Reliability Evaluation," *IEEE Trans. on Power Syst.*, vol. 13, no. 2, pp. 655–660, May. 1998.

[41] M. Ni, J. D. McCalley, V. Vittal, and T. Tayyib, "Online Risk-Based Security Assessment," *IEEE Trans. Power Syst.*, vol. 18, no. 1, pp. 258–265, Feb. 2003.

[42] J. Zhang, I. Dobson, and F. L. Alvarado, "Quantifying Transmission Reliability Margin," *Int. J. Elect. Power Energy Syst.*, vol. 26, no. 9, pp. 697–702, Nov. 2004.

[43] S. Greene, S. G. Dobson, and F. Alvarado, "Sensitivity of Transfer Capability Margins With a Fast Formula," *IEEE Trans. on Power Syst.*, vol. 17, no. 1, pp. 34–40, Feb. 2002.

[44] ——, "Sensitivity of the Loading Margin to Voltage Collapse With Respect to Arbritary Parameters," *IEEE Trans. on Power Syst.*, vol. 12, no. 1, pp. 262–272, Feb. 1997.

[45] H. Chen, "Security Cost Analysis in Electricity Markets Based on Voltage Security Criteria and Web-Based Implementation," PhD Thesis, University of Waterloo, Waterloo, Canada, 2002.

[46] E. Haesen, C. Bastiaensen, J. Driesen, and R. Belmans, "A Probabilistic Formulation of Load Margins in Power Systems With Stochastic Generation," *IEEE Trans. on Power Syst.*, vol. 24, no. 2, pp. 951–958, May. 2009.

[47] Y. Kataoka, "A Probabilistic Nodal Loading Model and Worst Case Solutions for Electric Power System Voltage Stability Assessment," *IEEE Trans. on Power Syst.*, vol. 18, no. 4, pp. 1507–1514, Nov. 2003.

[48] A. Schellenberg, W. Rosehart, and J. Aguado, "Cumulant-Based Stochastic Nonlinear Programming for Variance Constrained Voltage Stability Analysis of Power Systems," *IEEE Trans. on Power Syst.*, vol. 21, no. 2, pp. 579–585, May. 2006.

[49] S. Senthil Kumar and R. P.Ajay-D-Vimal, "Fuzzy Logic Based Stability Index Power System Voltage Stability Enhancement," *International Journal of Computer and Electrical Engineering*, vol. 2, no. 1, pp. 24–31, Feb. 2010.

[50] Z. Jing, G. Yun-Feng, and M.-H. Y., "Assessment of Voltage Stability for Real-Time Operation," in *Proc. IEEE Power India Conference*, 2006, p. 5.

[51] R. Moore and W. Lodwick, "Interval Analysis and Fuzzy Set Theory," *Fuzzy Sets and Syst.*, vol. 135, no. 1, pp. 5–9, Apr. 2003.

[52] R. Albrecht, "Topological Theory of Fuzziness," in *Proc. Int. Conf. Computational Intelligence, Springer, Heidelberg*, 1999, pp. 1–11.

[53] L. Zadeh, "Some Reflections on Soft Computing, Granular Computing and Their Roles in the Conception, Design and Utilization of Information/Intelligent Systems," *Soft Computing*, vol. 2, no. 1, pp. 23–25, Apr. 1998.

[54] L. Wang and C. Singh, "Population-Based Intelligent Search in Reliability Evaluation of Generation Systems With Wind Power Penetration," *IEEE Trans. on Power Syst.*, vol. 23, no. 3, pp. 1336–1345, Aug. 2008.

[55] Z. Yang, M. Zwolinski, and C. Chalk, "Bootstrap, an Alternative to Monte Carlo Simulation," *Electronics Letters*, vol. 34, no. 12, pp. 1174–1175, Jun. 1998.

[56] M. M. Othman, S. Kasim, N. Salim, and I. Musirin, "Risk Based Uncertainty (RibUt) Assessment of a Power System Using Bootstrap Technique," in *Proc. IEEE International Power Enineering and Optimization Conference (PEDCO) Melaka, Malaysia*, 2012, pp. 460–464.

[57] N. Zhou, J. Pierre, and D. Trudnowski, "A Bootstrap Method for Statistical Power System Mode Estimation and Probing Signal Selection," in *Proc. IEEE PES Power Syst. Conference and Exposition PSCE*, 2006, pp. 172–178.

[58] R. Billinton, H. Chen, and R. Ghajar, "A Sequential Simulation Technique for Adequacy Evaluation of Generating Systems Including Wind Energy," *IEEE Tran. on Power Syst.*, vol. 11, no. 4, pp. 728–734, Dec. 1996.

[59] L. Arya, L. Titare, and D. P. Kothari, "Determination of Probabilistic Risk of Voltage Collapse Using Radial Basis Function (RBF) Network," *Electric Power System Research*, vol. 76, pp. 426–434, Apr. 2006.

[60] ——, "Probabilistic Assessment and Preventive Control of Voltage Security Margins Using Artificial Neural Network," *International Journal of Electrical Power and Energy Systems*, vol. 29, no. 2, pp. 99–105, Feb. 2007.

[61] K. Timko, A. Bose, and P. Anderson, "Monte Carlo Simulation of Power System Stability," *IEEE Trans. Power Apparatus and Syst.*, vol. 102, no. 10, pp. 3453–3459, Oct. 1983.

[62] E. Vaahedi, W. Li, T. Chia, and H. Dommel, "Large Scale Probabilistic Transient Stability Assessment Using BC Hydro's On-Line Tool," *IEEE Trans. Power Syst.*, vol. 15, no. 2, pp. 661–667, May. 2000.

[63] C. Ferreira, J. A. Dias Pinto, and F. P. M. Barbosa, "Dynamic Security Analysis of an Electric Power System Using a Combined Monte Carlo-Hybrid Transient Stability Approach," in *Proc. IEEE Power Tech Proceedings Porto*, 2001.

[64] W. Wangdee and R. Billinton, "Bulk Electric System Well-Being Analysis Using Sequential Monte Carlo Simulation," *IEEE Trans. Power Syst.*, vol. 21, no. 1, pp. 188–193, Feb. 2006.

[65] R. Billinton, P. R. S. Kuruganty, and M. F. Carvalho, "An Approximate Method for Probabilistic Assessment of Transient Stability," *IEEE Trans. Reliability*, vol. 28, no. 3, pp. 255–258, Aug. 1979.

[66] R. Billinton and P. R. S. Kuruganty, "Probabilistic Assessment of Transient Stability in a Practical Multimachine System," *IEEE Trans. Power Apparatus and Syst.*, vol. 100, no. 7, pp. 3634–3641, Jul. 1981.

[67] H. Yuang-Yih and C. Chang, "Probabilistic Transient Stability Studies Using the Conditional Probability Approach," *IEEE Trans. on Power Syst.*, vol. 3, no. 4, pp. 1565–1572, Nov. 1988.

[68] R. Billinton and S. Aboreshaid, "Stochastic Modelling of High-Speed Reclosing in Probabilistic Transient Stability Studies," *IEE Proc. Generation, Transmission and Distribution*, vol. 142, no. 4, pp. 350–354, Jul. 1995.

[69] D. Fang, L. Jing, and T. Chung, "Corrected Transient Energy Function-Based Strategy for Stability Probability Assessment of Power Systems," *IET Proc. Generation, Transmission and Distribution*, vol. 2, no. 3, pp. 424–432, May. 2008.

[70] S. Faried, R. Billinton, and S. Aboreshaid, "Probabilistic Evaluation of Transient Stability of a Power System Incorporating Wind Farms," *IET Proc. Renewable Power Generation*, vol. 4, no. 4, pp. 299–307, Jul. 2010.

[71] H. Kim and C. Singh, "Probabilistic Security Analysis Using SOM and Monte Carlo Simulation," in *Proc. Power Engineering Society Winter Meeting*, 2002, pp. 755–760.

[72] ——, "Power System Probabilistic Security Assessment Using Bayes Classifier," *Electr. Power Syst. Res.*, vol. 74, no. 1, pp. 157–165, Apr. 2005.

[73] A. Dissanayaka, U. Annakkage, B. Jayasekara, and B. Bagen, "Risk-Based Dynamic Security Assessment," *IEEE Trans. Power Syst.*, vol. 26, no. 3, pp. 1302–1308, Dec. 2011.

[74] B. Jayasekara and U. Annakkage, "Derivation of an Accurate Polynomial Representation of the Transient Stability Boundary," *IEEE Trans. Power Syst.*, vol. 21, no. 4, pp. 1856–1863, Aug. 2006.

[75] A. Karimishad and T. Nguyen, "Probabilistic Transient Stability Assessment Using Two-Point Estimate Method," in *Proc. 8th International Conference on Advances in Power System Control, Operation and Management (APSCOM)*, 2009, pp. 1–6.

[76] E. Chiodo, F. Gagliardi, and D. Lauria, "Probabilistic Approach to Transient Stability Evaluation," vol. 141, no. 5, pp. 537–544, Sep. 1994.

[77] F. Allella, E. Chiodo, and D. Lauria, "Transient Stability Probability Assessment and Statistical Estimation," *Electr. Power Syst. Res.*, vol. 67, no. 1, pp. 21–33, Oct. 2003.

[78] S. Ayasun, Y. Liang, and C. O. Nwankpa, "A Sensitivity Approach for Computation of the Probability Density Function of Critical Clearing Time and Probability of Stability in Power System Transient Stability Analysis," *Applied Mathematics and Computation*, vol. 176, no. 2, pp. 563–576, May. 2006.

[79] J. L. Soufis, A. V. Machias, and B. Papadias, "An Application of Fuzzy Concepts to Transient Stability Evaluation of Power Systems," *IEEE Trans. on Power Syst.*, vol. 4, no. 3, pp. 1003–1009, Aug. 1989.

[80] Y. Chen and A. Dominguez-Garcia, "A Method to Study the Effect of Renewable Resource Variability on Power Systems Dynamics," *IEEE Trans. on Power Syst.*, vol. 27, no. 4, pp. 1978–1989, Nov. 2012.

[81] M. Althoff, M. Cvetkovic, and M. Ilic, "Transient Stability Analysis by Reachable Set Computation," in *Proc. 3rd IEEE PES International Conference and Exhibition on Innovative Smart Grids Technologies ISGT Europe*, 2012, pp. 14–17.

[82] H. N. Villegas, D. C. Aliprantis, and E. C. Hoff, "Reachability Analysis of Power System Frequency Dynamics with New High-Capacity HVAC and HVDC Transmission Lines," in *Proc. IREP Symposium-Bulk Power System Dynamics and Control-IX Rethymnon Greece*, 2013, pp. 1–9.

[83] Z. Wang, Sh. Zheng and C. Wang, "Power System Transient Stability Simulation Under Uncertainty Based on Interval Method," in *Proc. International Conference on Power System Technology PowerCon*, 2006, pp. 1–6.

[84] D. Grabowski, M. Olbrich, and E. Barke, "Analog Circuit Simulation Using Range Arithmetic," in *Proc. Asia and South Pacific Design Automation, Seoul, Korea*, 2008, pp. 762–767.

[85] J. Duncan-Glover, S. S. Sarma, and T. Overbye, *Power System Analysis and Design*. USA: CENGAGE Learning, 2008.

[86] J. Avalos-Muñoz, "Analysis and Applications of Optmization Techniques to Power System Electricity Markets," PhD Thesis, University of Waterloo, Waterloo, Canada, 2008.

[87] M. Pirnia, C. Cañizares, and K. Bhattacharya, "Revisiting the Power Flow Problem Based on a Mixed Complementarity Formulation Approach," *IET Proc. Generation, Transmission and Distribution*, vol. 7, no. 11, pp. 1194–1201, Nov. 2013.

[88] P. Kundur, J. Paserba, V. Ajjarapu, A. Bose, C. Canizares, N. Hatziargyriou, D. Hill, A. Stankovic, C. Taylor, T. Van Cutsem, and V. Vittal, "Definition and Classification of Power System Stability IEEE/CIGRE Joint Task Force on Stability Terms and Definitionss," *IEEE Trans. Power Syst.*, vol. 19, no. 3, pp. 1387–1401, Aug. 2004.

[89] T. Van Cutsem and C. Vournas, *Voltage Stability of Electric Power Systems*. New York, USA: Springer, 1998.

[90] "Voltage Stability Assessment: Concepts, Practices and Tools," *IEEE/PES Power System Stability Subcomitte, Tech. Rep.*, Aug. 2002.

[91] V. Ajjarapu and C. Christy, "The Continuation Power Flow: A Tool for Steady State Voltage Stability," *IEEE Trans. on Power Syst.*, vol. 7, no. 1, pp. 406–423, Feb. 1992.

[92] C. Cañizares and F. L. Alvarado, "Point of Collapse and Continuation Methods for Large AC/DC Systems," *IEEE Trans. on Power Syst.*, vol. 8, no. 1, pp. 1–8, Feb. 1993.

[93] H.-D. Chiang, A. J. Flueck, K. Shah, and N. Balu, "CPFLOW: a Practical Tool for Tracing Power System Steady-State Stationary Behavior Due to Load and Generation Variations," *IEEE Trans. on Power Syst.*, vol. 10, no. 2, pp. 623–634, May. 1995.

[94] A. Gomez-Exposito, A. J. Conejo, and C. Cañizares, *Electric Energy Systems: Analysis and Operation Vol. I.* Boca Raton: CRC press, 2009.

[95] C. Vournas, M. Karystianos, and N. Maratos, "Bifurcations Points and Loadability Limits as Solutions of Constrained Optimization Problems," in *Proc. Power Engineering Society Summer Meeting, 2000. IEEE*, vol. 3, 2000, pp. 1883–1888.

[96] R. Avalos, C. Cañizares, and M. Anjos, "A Practical Voltage-Stability-Constrained Optimal Power Flow," in *Proc. Power and Engineering Society Meeting Conversion and Delivery of Electrical Energy in the 21st Century*, vol. 3, Jul. 2008, pp. 1–6.

[97] NERC, "Reliability concepts," 2007. [Online]. Available: http://www.nerc.com/files/concepts_v1.0.2.pdf

[98] ——, "Available Transfer Capability Definitions and Determination," 1996. [Online]. Available: http://www.westgov.org/wieb/wind/06-96NERCate.pdf/

[99] P. Kundur, *Power System Stability and Control*. McGraw-Hill, 1994.

[100] B. Stott, "Power System Dynamic Response Calculations," *Proc. of the IEEE*, vol. 67, no. 2, pp. 219– 241, Feb. 1979.

[101] F. Milano, *Power System Modelling and Scripting*. London: Springer, 2010.

[102] P. Sauer and M. Pai, *Power System Dynamics and Stability*. Prentice Hall, 1998.

[103] T. Noda, K. Takenaka, and T. Inoue, "Numerical Integration by the 2-Stage Diagonally Implicit Runge-Kutta Method for Electromagnetic Transient Simulations," *IEEE Trans. on Power Delivery*, vol. 24, no. 1, pp. 390–399, Jan. 2009.

[104] Y. Cho, J. Park, and G. Jang, "A Novel Tool for Transient Stability Analysis of Large-Scale Power Systems: Its Application to the KEPCO System," *Simulation Modelling Practice and Theory*, vol. 15, pp. 786–800, Aug. 2007.

[105] A. A. Nimje and C. K. Panigrahi, "Transient Stability Analysis Using Modified Euler's Iterative Technique," in *Proc. International Conference on Power Syst. ICPS*, 2009, pp. 1–4.

[106] H. Yi, S. Cheng, Z. Du, L. B. Shi, and Y. Ni, "Modeling and Simulation on Long-Term Dynamics of Interconnected Power System Using Area COI Concept," *Electr. Power Syst. Res.*, vol. 78, no. 8, pp. 1369–1377, Aug. 2008.

[107] L. de Figueiredo and J. Stolfi, "Self-Validated Numerical Methods and Applications," in *Proc. Brazilian Mathematics Colloq. Monograph IMPA Rio de Janeiro Brazil*, 1997, pp. 1–103.

[108] J. Comba and J. Stolfi, "Affine Arithmetic and its Applications to Computer Graphics," in *Proc. Brazilian Symposium on Computer Graphics and Image Processing VI SIBGRAPI*, 1993, pp. 9–18.

[109] E. Hansen, "A generalized interval arithmetic," *Lecture Notes in Computer Science Springer*, vol. 29, pp. 7–18, 1975.

[110] L. Zhang, Y. Zhang, and W. Zhou, "Tradeoff Between Approximation Accuracy and Complexity for Range Analysis Using Affine Arithmetic," *Journal of Signal Processing Systems*, vol. 61, no. 3, pp. 279–291, Dec. 2010. [Online]. Available: http://www.springerlink.com/content/t4445742873p0273/

[111] F. Messine, "Extensions of Affine Arithmetic: Application to Unconstrained Global Optimization," *Journal of Universal Computer Science*, vol. 8, no. 11, pp. 992–1015, 2002. [Online]. Available: http:http//www.citeseerx.ist.psu.edu/

[112] J. Mason and D. Handscomb, *Chebyshev Polynomials*. Florida, USA: Chapman & Hall/CRC, 2002.

[113] J. Gentle, *Random Number Generation and Monte Carlo Methods*. New York, USA: Springer, 2003.

[114] J. A. Bucklew, *Introduction to Rare Event Simulation*. New York, USA: Springer, 2004.

[115] F. Milano, L. Vanfretti, and J. Morataya, "An Open Source Power System Virtual Laboratory: The PSAT Case and Experience," *IEEE Trans. on Education*, vol. 51, no. 1, pp. 17–23, Feb. 2008. [Online]. Available: http://www.power.uwaterloo.ca/~fmilano/

[116] S. Kodsi and C. Cañizares, "Modeling and Simulation of IEEE 14 bus System with FACTS Controllers," *Tech. Rep., Univ. Waterloo, ON, Canada*, 2003.

[117] J. Muñoz and C. Cañizares, "Comparative Stability Analysis of DFIG-Based Wind Farms and Conventional Synchronous Generators," in *Proc. Power Syst. Conference and Exposition*, 2011, pp. 1–7.

[118] M. X. Prabhakar and R. Jiang, *Weibull Model*. New Jersey, USA: Willey-Interscience, 2010.

[119] A. Khosravi and S. Nahavandi, "Combined Nonparametric Prediction Intervals for Wind Power Generation," *IEEE Trans. on Sustainable Energy*, vol. 4, no. 4, pp. 849–856, Oct. 2013.

[120] A. Khosravi, S. Nahavandi, D. Creighton, and D. Srinivasan, "Optimizing the Quality of Bootstrap-Based Prediction Intervals," in *Proc. Joint Conf. Neural Networks (IJCNN)*, 2011, pp. 3072–3078.

[121] J. Muñoz, C. Cañizares, K. Bhattacharya, and A. Vaccaro, "An Affine Arithmetic Based Method for Voltage Stability Assessment of Power Systems with Intermittent Generation Sources," *IEEE Trans. on Power Syst.*, vol. 28, no. 4, pp. 4475–4487, Nov. 2013.

[122] ——, "Affine Arithmetic Based Methods for Voltage and Transient Stability Assessment of Power Systems with Intermittent Generation Sources," in *Proc. IREP Symposium-Bulk Power System Dynamics and Control- IX , Rethymnon Greece*, 2013.

[123] R. Zimmerman, C. Murillo-Sanchez, , and R. Thomas, "Matpower: Steady-State Operations, Planning, and Analysis Tools for Power Systems Research and Education," *IEEE Trans. on Power Syst.*, vol. 26, no. 1, pp. 12–19, Feb. 2011.

[124] F. Alvarado and Z. Wang, "Direct Sparse Interval Hull Computations for Thin Non-M-Matrices," *Interval Computations*, vol. 2, pp. 5–28, 1993.

[125] J. Muñoz, C. Cañizares, K. Bhattacharya, and A. Vaccaro, "Transient Stability Assessment of Power Systems with Intermittent Generation Sources Using Affine Arithmetic," *IEEE Trans. on Power Syst.*, 8 pages, Manuscript submitted for review on October 17, 2013.